LUND UNIVERSITY

Large Eddy Simulation of Turbulent Combustion in PPC and Diesel Engines

Solsjö, Rickard

2014

Large Eddy Simulation of Turbulent Combustion in PPC and Diesel Engines

Rickard Solsjö

Doctoral Thesis

Division of Fluid Mechanics

Department of Energy Sciences

Lund University

December, 2014

LUND

UNIVERSITY

Abstract

This thesis deals with large eddy simulations (LES) of turbulent combustion processes in direct injection internal combustion (IC) engines. Modeling of direct injection IC engine combustion involves modeling of turbulent spray/gas two-phase flow, modeling of chemical reactions of large hydrocarbon fuels and coupling of chemistry with turbulent flows. LES is chosen in this thesis for it capability to resolve the turbulent structures and the fuel and air mixing, and to provide high spatial and temporal resolution of the unsteady fluid motions and the reaction processes. Lagrangian particle tracking (LPT) method is used to model the fuel spray. Finite rate chemistry is employed with a computationally efficient integration method, the chemistry coordinate mapping (CCM) method, which allows the use of large chemical reaction mechanisms with low computational time. The thesis consists of three parts. In part I the feasibility and accuracy of the LES/LPT approach are investigated for simulation of fuel spray injection, evaporation, and mixing with the ambient gas in high-pressure constant volume vessels known as the rigs of the Engine Combustion Network (ECN). The fuel and air mixing, the liquid penetration length and the vapor-phase fuel jet penetration predicted by the LES/LPT model are in good agreement with the experimental data and the importance of stochastic turbulence dispersion (STD) and spray-induced turbulence (SIT) is investigated. In part II the fuel/air mixing, ignition, liftoff and stabilization of diesel flames in modern diesel engines are studied. Diesel engines often employ multiple-hole injectors and inject at high pressures to control the rate of combustion. To deepen the knowledge of the combustion processes in modern diesel engines, LES is used to investigate the effect of inter-jet angles on the auto-ignition, lift-off length, and the wall effect on the mixing and soot formation process. For the three inter-jet angles employed, 45°, 90° and 135°, a clear inter-jet angle effect is captured, with the trends found in previous experiments properly predicted. From the simulations, the effect such as a shortened lift-off length with decreased inter-jet angle and the effect of varying inter-jet angles on the equivalence ratio in the near-wall regions are scrutinized. In part III, LES is employed to simulate the fuel and air mixing process, the onset of low temperature and high temperature ignition in light-duty and heavy-duty partially premixed combustion (PPC) engines. The PPC engine relies on the fuel and air charge stratification to control the combustion event. With LES the effects of umbrella angles, multiple injection strategies, mean swirling flow, and turbulence, on the mixing process and combustion process are simulated. The LES results reveal the detailed mixing process at different injection condition. The results indicate the high sensitivity of the performance of PPC engines to the operating condition and engine configurations, e.g., injection timing, fuel split and injection

directions. The results provide insight into the complex physical and chemical process involved, which helps improving the understanding of the performance of PPC engines.

Descriptors: large eddy simulation (LES), turbulent spray combustion, Lagrangian particle tracking (LPT), diesel engines, partially premixed combustion (PPC) engines.

Populärvetenskaplig sammanfattning

Trots ny fordonsteknik så har koldioxidutsläppen ökat med nästan 40% i Europa sedan 1990-talet. Detta beror främst på en tilltagande transport på våra vägar. Drivmedel som används inom transportsektorn är nästan uteslutande diesel och bensin, vilka härstammar från fossila bränslen. För att hantera konsekvenserna av transportfordons miljöpåverkan så blir lagstiftningen på utsläpp allt hårdare. Europa och USA ligger i framkant, men miljökraven är även på framfart i Asiatiska länder. Regelverket har hittills främst behandlat partikelutsläpp, obrända kolväten samt kväve- och svavelgaser, men har på senare tid också tilltagit för koldioxidutsläpp. Ettt av EUs framtida mål är att begränsa koldioxidutsläppen till mindre än 95g/kWh för personbilar. Samtidigt i Sverige så är utvecklingen på frammarsch med målet att göra sig oberoende av fossilt bränsle inom transportsektorn till år 2030 och att ha ett helt balanserat bidrag av koldioxidutsläpp till år 2050.

För att möta dessa mål måste förståelsen för förbränningsprocesser i personvagnar och lastbilar öka. Hittills har många av utsläppsproblemen kunnat lösas av efterbehandlingssystem, t.ex. katalysatorer och partikelfilter, men kostanden för dessa är höga så det finns en vilja att kunna minska emissionerna ytterligare direkt i motorcylindern. En del av dagens spjutspetsforskning är att undersöka potentialen av att spruta in bensinliknande bränsle i diesel-motorer som självantänder av den höga kompressionen, istället för det klassiska tändstiftet. Denna metod kallas för förbränning av delvis förblandat bränsle, eller partially premixed combustion (PPC). Metoden är komplicerad och kräver en kombination av t.ex. ökad insugstemperatur på luften eller en optimal insprutningsstrategi av bränsle. Experimentell forskning har dock påvisat hög motorverkningsgrad och låga utsläpp av skadliga avgaser under optimala förutsättningar.

För att öka förståelsen för förbränning av delvis förblandat bränsle och för att kunna optimera och designa morgondagens motorer kan man ta till hjälp av datoriserade matematiska beräkningsmetoder, så kallad computational fluid dynamics (CFD). CFD möjliggör tids- och rumsupplöst information om vad som pågår i förbränningsrummet och kan förklara var/hur källorna till utsläppen uppkommer. Den matematiska metoden är byggd på diskretisering av ekvationer som är kända för att kunna hantera typiska flödessituationer och trots att de flesta existerande förbränningsmodeller är

v

förenklingar av verkligheten så har de visat sig kunna reproducera och öka kunskapen för väldigt komplexa förbränningsprocesser.

Avhandlingen består i huvudsak av två delar där den ena delen syftar till att använda CFD för att simulera PPC förbränning. Det huvudsakliga fallet är för en personvagn som arbetar vid låga laster och där flera insprutningstidpunkter av bensinrepresentativt bränsle skapar en delvis förblandad blandning. Modellen simulerar hur det flytande bränslet bryts upp och förångas vid insprutning och sedan blandas med luften, varvid det först insprutade bränslet undergår låg-temperaturreaktioner och sedan självantänder vid sista insprutningstillfället. Denna strategi ger en långsam tryckökning och värmefrigörelse så att knackning undviks, men ändå så pass kort att värmeförlusterna är låga. Genom att låta bränslet blandas med luft under (relativt) lång tid så minskar mängden partikelutsläpp och temperaturen är så pass låg att kväveoxider inte skapas. CFD simuleringarna visar också hur känslig metoden är mot olika insprutningsstrategier.

Den andra delen av avhandlingen undersöker förbränningsförloppet i en klassisk dieselmotor. Påverkan hos avståndet mellan insputningshålen i en injektor har undersökts både nära injektorn och nära cylinderväggen. Det visar sig att när hålen sitter närmare varandra så minskar syreinblandningen i sprayen, vilket kan ha en negativ påföljd, då sotmängden ökar när bränslet brinner under syrefattiga förhållanden. Simuleringarna visar att syreinblandningen påverkas även nära cylinderväggen, där ett minskat avstånd mellan hålen ger bränslerikare återcirkulationszoner. Detta kan också påverka sotbildningen negativt, eftersom syret är viktigt för att oxidera partiklar under expansionsfasen i en dieselmotor.

vi

List of publications

Paper I: R. Solsjö, X.S. Bai, "*Injection of Fuel at High Pressure Conditions: LES Study*", SAE Technical Paper 2011-24-0041, 2011.

Paper II: M. Jangi, R. Solsjö, B. Johansson, X.S. Bai, "*On large eddy simulations of diesel sprays for internal combustion engines*", Submitted to International Journal of Heat and Fluid Flow, 2014.

Paper III: R. Solsjö, M. Jangi, C. Chartier, Ö. Andersson, X.S. Bai, "*Lift-off and stabilization of n-heptane combustion in a diesel engine with a multiple-nozzle injection*",
Proceedings of the Combustion Institute, Volume 34, Issue 2, 2013, pp. 3031–3038.

Paper IV: R. Solsjö, M. Jangi, X.S. Bai, "*Jet-Jet Interaction in Diesel Engine Combustion*", The International Symposium on Diagnostics and Modeling of Combustion in Internal Combustion Engines (COMODIA), 2012, Japan Society of Mechanical Engineering, August 4, 2012.

Paper V: R. Solsjö, M. Jangi, X.S. Bai, "*Effect of Spray Inter-Jet Angle on Auto-Ignition in a Heavy-Duty Diesel Engine*", Eighth Mediterranean Combustion Symposium, Çeşme, Izmir, Turkey, September 8-13, 2013.

Paper VI: R. Solsjö, M. Jangi, C. Chartier, Ö. Andersson, X.S. Bai, "*Mixing in Wall-Jets in a Heavy-Duty Diesel Engine: A LES Study*", SAE Technical Paper 2014-01-1127, 2014.

Paper VII: R. Solsjö, M. Jangi, M. Tuner, X.S. Bai, "*Large Eddy Simulation of Partially Premixed Combustion in an Internal Combustion Engine*", SAE Technical Paper 2012-01-0139, 2012.

Paper VIII: R. Solsjö, M. Jangi, B. Johansson, X.S. Bai, "*The Effect of Umbrella Angle on Mixing and Combustion in a Light Duty PPC Engine - a LES Study*", 6th European Combustion Meeting, Lund, Sweden, June 20, 2013.

Paper IX: R. Solsjö, M. Jangi, B. Johansson, X.S. Bai, "*The role of multiple injections on combustion in a light-duty PPC engine*"- Manuscript prepared for submission to Combustion and Flame, 2014.

Table of Contents

Chapter 1
Introduction and motivation

1.1 Background

Today's reality in the energy utilization of our society is a consumption of natural resources of unsustainable proportions. Fossil fuels are consumed faster than they are naturally formed and the release of greenhouse gases into the atmosphere is occurring at alarming rates. Yesterday's accessible and cheap energy source has become a dangerous convenience and will, regardless of novel technological advancements, likely remain so for at least a century to come. We are depending on fossil fuel as a source of energy for all of our basic needs, such as generation of electricity, heating of houses and industries, as well as for leisure activities.

The main concern with burning fossil fuel is the environmental impact. On a large scale the release of the greenhouse gas carbon dioxide (CO_2) causes global warning and climate change. Experts today agree that the human interference is contributing to the increasing global temperature, melting of the ice caps and rising sea levels. The amount of CO_2 that is released in combustion is directly proportional to the amount of burned fuel and so the only way to reduce CO_2 emission is to use less fossil fuel.

On a regional, or local, scale the main concern is pollution that is formed e.g., due to incomplete combustion or due to impurities in the fuel. During combustion hazardous emissions, such as nitrogen oxides (NO and NO_2), sulfur oxides (SO_2 and SO_3), unburned hydrocarbons (UHC) and particulate matters (PM) as well as carbon monoxide (CO) and earth-bound ozone (O_3), are formed. The direct consequence in nature is, e.g., acid rain and acidification of lakes, rise of smog and contamination, but it is also dangerous concerning health issues.

The transportation sector faces a great challenge to reduce the dependency of fossil fuels. Although the access to easily extracted fossil fuel is diminishing and the cost is steadily increasing, the automotive industry is growing worldwide. Despite improved vehicle efficiency, greenhouse gas emissions have increased by 36% in Europe since 1990, mainly due to increased traffic. Meanwhile, the East Asia region is one of the

fastest growing economies and in 2011 China became the world's largest car market. In the United States, approximately 70% of the daily-consumed oil is put into internal combustion (IC) engines [1]. Continually stricter laws to reduce pollutants are passed in Europe and in the United States, e.g., the Euro V and VI and the US III, IV, and US2010. The focus of the legislation has so far been on nitrous gases, particulate matter sizes and particle quantities as well as unburned hydrocarbon fuel. Drastic reduction of pollutants in Europe, Japan and in the United States has been carried out and the levels of PM, UHC and NOx in the 2010s were only 2%, 6-12% and 3-12% of the 1990s levels, respectively. In Europe, the goal of the new legislation is to reduce the CO_2 emissions from the road traffic, e.g., one of the goals is to reduce the CO_2 emissions for passenger cars with 18% by year 2015 and with 40% by year 2021. Emission legislation comparable to those mentioned is currently passed in China at an accelerating rate [2].

In Sweden the Energy Agency has put up goals to have a zero net release of greenhouse gases from the entire energy sector by 2050 and by 2030 the Swedish transport fleet should be independent of fossil fuels [3]. As other sectors in Sweden are becoming less dependent on fossil fuel combustion, the contribution from the transport sector to the use of fossil fuels is steadily increasing. The energy use in the transport sector has increased by 70% since the 1970s. To meet the goals, the research in Sweden is turned towards environmental friendly propellants and towards vehicle optimization. The suitable propellants are those that can be harvested in large quantities and with minor environmental impact, such as biodiesel, ethanol, CNGs (bio gas and natural gas) and hydrogen, and part of the investment involves to secure the entire fuel chain, from production to consumption. The transportation fleet represents 25% of Sweden's energy consumption market and 40% of the greenhouse gas emissions, where 70% originates in the road transportation. The individual share of the energy use for domestic transport, by the different transport modes, is seen in Fig. 1.1, together with the share of renewable fuels in the road traffic. To improve the fuel efficiency, research is performed on fuel optimization solutions, e.g., improved vehicle aerodynamics and weight-reduction, low-temperature combustion concepts and fuel cells. Although Sweden's contribution to CO_2 emissions and emission of pollutants in a global perspective is marginal, the international exchange of new designs and solutions speeds up the transition process to a future sustainable energy solution.

Significant development in the combustion-oriented area of internal combustion (IC) engine research has been made over the last decades to meet the demands in the car and truck market. Modernization of commercial equipment, such as the high-speed injectors and the exhaust gas treatment systems, and techniques to modify, e.g., the

combustion chamber, have provided new ways to control the combustion process. The market of new and more environmental friendly fuels, e.g., bio-diesel and ethanol, and engine hybridization innovations are constantly growing. Alongside there have been substantial improvements to carry out detailed optical investigations in combustion engine related facilities, to gain visual information of the combustion processes. It has allowed scientists to scale down the complexity of the problems and it has made parameterization of difficult combustion processes possible. This experimental approach is promising; however, the engine combustion process has to be studied in its normal environment to fully optimize it. Combustion itself is a complex chemical process where the fuel undergoes oxidation at low and high temperatures at slow and fast rates, whereby conversion to new chemical species takes place and heat is released. In IC engines this occur under turbulent conditions. The chemical processes interacts with complex flows under different operating conditions and is subject to, for instance, cyclic and transient variations, variation in chamber configuration, radiation and heat-transfer, etc.
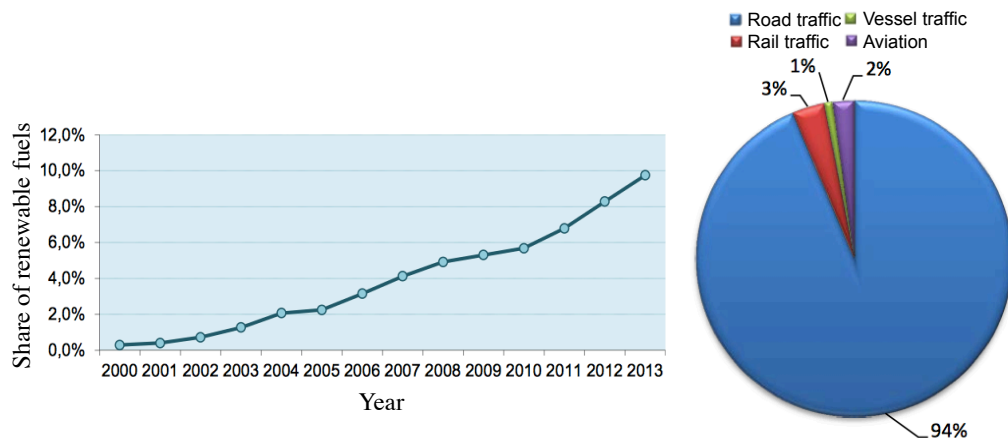
Figure 1.1. The share of renewable fuels in the road traffic (left) and the individual share of the road traffic, the vessel and rail traffic and the aviation traffic in the transportation sector (right). Reproduced from [4].

To improve the knowledge of IC engine combustion, computational fluid dynamics (CFD) offers the possibility to perform mathematical modeling of flow, combustion, and heat-transfer in fundamental as well as practical applications, as a replacement or

support to experimental work. CFD is a method in which the flow and combustion processes are described using the Navier-Stokes, energy and mass conservation equations in a continuous fluid approach. In history CFD has grown with the technological advancements and with the development of computers until today where enormous computational resources have become available [5]. This expansion has made it possible to conduct massive parallel computations of complicated geometrical configurations under extreme flow and combustion conditions to provide predictive and explanatory power. The advancement of CFD has made it possible to work in synergy with experimental work and can be used as a tool in the early development stages of, e.g., designs of new combustion applications. Even though there is a need to develop more general flow and combustion models, CFD has successfully been shown to represent complex combustion behavior under complex geometrical conditions and offers great potential to assist development of new concepts to meet the future legislations on emissions and fuel consumption, e.g., for IC engines.

1.2 Objectives and scope of the work

The main objective of this thesis is to improve and to deepen the understanding of the combustion processes in direct injection (DI) diesel combustion engines and direct injection partially premixed (PPC) combustion engines. In this work large eddy simulations (LES) is coupled with the Lagrangian particle tracking (LPT) approach, LES-LPT, to simulate the fuel breakup, fuel vaporization and fuel and air mixing processes in IC engines. The combustion modeling is carried out with finite-rate chemistry. The numerical simulations are performed using a flow-solver from open source CFD libraries [6].

The feasibility of modeling spray injection employing LES-LPT was investigated with models accounting for spray-induced turbulence (SIT) and stochastic turbulence dispersion (STD). The simulations were carried out for the non-reacting spray-A case, provided by the ECN [7]. The effect of the SIT model was found nearly negligible for the results. However, it was found that including the STD model was necessary to predict, the global behavior of the spray, e.g., the liquid-length and vapor-phase fuel penetration, compared with the experiments. The prediction of the exchange rates of mass, momentum and heat, between the liquid and gas phase improved, when the STD model was included. The results from this study motivated the continued work to perform the LES-LPT simulations in real engine conditions, in particular under diesel engine combustion conditions and DI-PPC engine conditions.

The numerical simulations of the diesel engine combustion processes were performed in close interaction with experimental laser-diagnostics, carried out by the generic diesel engine group (GenDies) at Lund University. The aim of this study was to investigate the processes related to the jet-jet and jet-cylinder wall interaction phenomena and to provide spatial and temporal information at experimentally inaccessible parts of the engine. More specifically, the effect of the inter-jet angle on the lift-off length and the downstream wall-jet mixing process in the recirculation zones was studied. The configuration was an optically accessible Scania D12 engine with two customized injectors; one injector with a 90° inter-jet angle and the other injector with a 45° and a 135° inter-jet angle.

The work on numerical simulations of the PPC engine processes were performed in close interaction with the group for partially premixed combustion engines at the Division of Internal Combustion Engines and the Division of Combustion Physics, at Lund University. The aim of this study was to explore the turbulent fuel and air mixing processes and combustion processes related to PPC engine combustion. This work was performed in a heavy-duty Scania D13 engine and in a light-duty optically accessible VOLVO D5 engine. The effect of, e.g., multiple injection strategies, the swirl level and the spray umbrella angle on the fuel and air mixing process and the combustion behavior was investigated.

The thesis is divided into 7 chapters, and 9 papers listed in the appendix.
Chapter 1 gives the background, objectives and scope of this work. In Chapter 2 a presentation of various classical combustion engine concepts is given followed by a description of novel combustion concepts that have emerged during the last years of engine research. In Chapter 3 a mathematical description of the physical and chemical processes involved in IC engines is given with a detailed list of the equations that govern the flow and combustion. It is followed by a description of turbulence and characterization of the engine combustion processes. Chapter 4 deals with modeling of internal combustion engines, such as the geometry aspects, multiphase flow, turbulence and chemistry modeling. Chapter 5 gives a description of the numerical details utilized in this work, e.g., spatial discretization, temporal integration and mesh generation. Chapter 6 provides highlights of the results, with details of the results given in the 9 papers listed in the appendix. In Chapter 7 conclusions are presented together with suggestions for the future work.

Chapter 2
Towards High Efficiency and Low Emission IC Engines

Internal combustion engines that employ direct injection of fuel can be categorized into different types. If the injected fuel quickly undergoes liquid fuel breakup, vaporization, auto-ignition and the fuel burns as a lifted diesel flame, it is referred to as diesel engine combustion. If the fuel injection process is nearly separated from the start of combustion and if a stratified air and fuel mixture that burns under a low temperature is generated, it is referred to as PPC engine combustion.

This thesis deals with the two processes mentioned above and this section aims to give an overview on the advantages and drawbacks of the classical direct injection diesel combustion, homogeneous charge compression ignition combustion and the partially premixed combustion processes. Homogeneous charge compression ignition is included because of its close connection to the partially premixed combustion engine. A physical description of the combustion process is given, together with a discussion on the main pollutants, as well as a short introduction to the current research and novel development. Expanding the knowledge of low-temperature combustion are motivated by the increasing engine performance and emission requirements over the years. Previously the emission legislation could be met by in-cylinder solutions and improved combustion geometries; however, with the tightening regulations it became necessary to involve more after-treatment. Alas, the accompanying economic cost, e.g., the increased fuel consumption and space requirements, for the vehicles with these advanced after-treatment systems was greater than for the vehicles without these after-treatment systems. For this reason improving the in-cylinder solutions has again become appealing. Therefore, understanding the advantages and limitations of the state-of-the-art combustion concepts is necessary to make progress towards more efficient and cleaner IC engines.

The total engine efficiency that can be extracted from an IC engine is the brake efficiency. The brake efficiency may be divided into the combustion efficiency, the thermal efficiency, the mechanical efficiency and the gas-exchange efficiency.

- The combustion efficiency reflects how much of the introduced fuel that is converted into heat.
- The thermal efficiency reflects the efficiency of converting the released heat into work.
- The mechanical efficiency reflects the influence of, e.g., piston ring friction and other equipment, on the total efficiency.
- The gas-exchange efficiency reflects the efficiency of considering the entire engine cycle including the gas exchange process, with the engine cycle excluding the gas exchange process.

To achieve the highest possible brake efficiency, the product of all of the listed efficiencies must together be optimized. Another indication of engine performance is the net and gross indicated mean effective pressures ($IMEP_n$ and $IMEP_g$), where the former includes the gas-exchange process and the latter excludes the gas-exchange process. The discussion below mainly concerns combustion efficiency and thermal efficiency.

2.1 Conventional direct injection (DI) diesel engine combustion

2.1.1 Characterization of diesel engines

In classical diesel engines the air is inhaled to the engine cylinder during the intake stroke until intake valves closing (IVC) and the air is thereafter compressed until top-dead-center (TDC). The piston compression increases the air pressure and temperature and the combustion process is controlled by direct injection of fuel sprays, which are introduced to the hot and high ambient density environment near TDC. The high-speed sprays promote fuel and air mixing by creating small-scale turbulence that efficiently breaks up and vaporizes the liquid near the nozzle. During this process the necessary amount of hot air to auto-ignite the mixture is entrained. The spray-controlled combustion process, unlike the HCCI process, which is described below, makes the diesel spray combustion event less sensitive to small fluctuations of the ambient temperature, and more sensitive to the injection strategy. Therefore, to understand spray flow and air entrainment is one of the central issues to reduce the accompanying hazardous pollutants related to diesel engine combustion, especially PM or soot and NOx (NO and NO_2). Furthermore, efficient fuel and air mixing is pivotal to avoid wall-wetting, which may lead to augmented emissions of unburned hydrocarbons and oil

7

dilution. The combustion efficiency is, in general, high in diesel engines and the reduction of CO and UHC becomes more important under low-load operating conditions and when high levels of exhaust gas recirculation (EGR) are employed. Typical for the diesel engine compared with the classical spark-ignition (SI) engine is the higher thermal efficiency, because of the high compression ratio, resulting in lower fuel consumption. Diesel engines also exhibit lower pumping losses, higher noise levels and smaller cycle-to-cycle variations (due to the spray controlled combustion), compared with the traditional SI engine.

2.1.2 Conceptual model for a diesel flame

The diesel engine is well adopted in numerous applications and it has proven to deliver high engine efficiencies, however, a detailed description of the structures of diesel spray flames was not available until the 1990s. In 1997, Dec et al. [8,9] proposed a conceptual model for diesel flames, which has now become widely accepted in the spray and engine combustion community. Figure 2.1 shows the proposed conceptual model that clarifies the different regimes of combustion and physical processes present in spray combustion. Liquid fuel spray is introduced (from left to right) into the air at high speed, whereupon the emanating liquid fuel drops quickly vaporize due to rapid fuel and air mixing. The distance from the injector nozzle to the downstream position where the liquid fuel has been vaporized completely is called the liquid length. Liquid vaporization is followed by auto-ignition of the fuel/air mixture and the onset of a fuel-rich, $\Phi > 1$, premixed combustion regime. Downstream the premixed combustion region a diffusion flame is established around the stoichiometric mixture, $\Phi = 1$. The distance from the leading front of the stabilized premixed/diffusion flame to the nozzle is referred to as the lift-off length. Downstream the lift-off position no more air can enter the inner region of the reacting jet and this results in a significant production of soot pre-cursors, such as polycyclic aromatic hydrocarbons (PAH), due to the high equivalence ratio and temperature, $T\sim1600-2000$ K. The soot grows in number and size downstream the premixed combustion region, but it may be oxidized if entering the diffusion flame. Described by the Zel'dovich mechanism large amounts of NOx are expected to form just after the stoichiometric diffusion flame, because of the strong temperature dependence. This structural description of a reacting spray is valid for a wide range of conditions, e.g., with certain EGR dilution, variation in fuel properties, and injection pressure, although the extent and location of the various regions may differ.
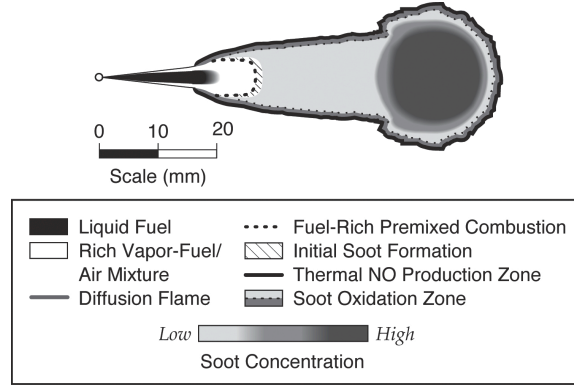
Figure 2.1. Conceptual model of the classical diesel spray combustion. Reproduced from Dec [7].

The description of the diesel flame combustion does not provide information about the lift-off. Global effects, such as ambient conditions and fuel injection properties, which affects the lift-off length have bee explored experimentally in constant-volume chambers. A semi-empirical scaling law to predict the height of a lifted spray flame has been developed [10]

$$H = 7.04 \cdot 10^8 T_a^{-3.74} \rho_a^{-0.85} d^{0.34} U Z_{st}^{-1} \qquad (2.1)$$

where H is the lift-off height, T_a is the mean ambient temperature, ρ_a is the ambient density, d is the nozzle diameter, U is the injection velocity and Z_{st} is the stoichiometric mixture fraction. This empirical law successfully predicts the lift-off length for the more frequently used diesel type fuels. To investigate the lift-off length stabilization mechanism, numerical simulations employing RANS and LES were performed with detailed chemistry under varying fuel types and ambient temperature conditions. Pauls et al. [11] identified both auto-ignition and auto-ignition/flame-front propagation combustion modes close to the lift-off length position for different fuels, employing OH chemiluminescence optical diagnostics and RANS modeling. Gong et al. [12] studied reacting jets at constant ambient densities and varying ambient temperatures, for n-dodecane fuel, employing LES modeling. In the case of a lower ambient temperature, low-temperature ignition (LTI) was found upstream the lift-off position, followed by an auto-ignition flame-front (AIIF) at fuel rich conditions at the lift-off height. Certain levels of heat-release were found between the LTI and the AIIF, suggesting that the LTI affected the AIIF. At the higher ambient temperature, the AIIF

9

disappeared and instead the flame base had a similar structure to a triple-flame, with a fuel-rich premixed flame on the inner side of the diffusion flame. The lift-off length is shorter at the higher ambient temperature, limiting the availability of oxygen to the LTI and thus inhibiting the AIIF. In the study, two mechanisms to control lift-off length stabilization were found for a range of temperatures. In a lower ambient temperature LTI followed by AIIF was shown to control the lift-off height and in a higher ambient temperature the LTI and triple flame propagation was controlling the lift-off height.

In a study by Pickett et al. [13] to expand the stabilization theory, the lift-off mechanism was investigated by igniting a diesel spray upstream of the natural lift-off length before and after natural auto-ignition occurred, using laser plasma ignition. When the fuel jet was ignited prior to natural development of auto-ignition, the transient period to return to the natural lift-off length was longer compared with if the spray was ignited after the natural lift-off had occurred. In the case of an already established lift-off, the location between the plasma ignition and the lift-off height played a role. A shorter distance between the plasma ignition location and the natural lift-off resulted in a quicker return of the ignition kernels to the lift-off height. It was proposed that the re-entrainment of burned products into the fuel jets, from adjacent hot reservoirs, has a stabilizing effect on the lift-off length. This is by, e.g., heating of the incoming jet fuel, which in turn affects to ignition properties. The authors suggested that the role of flame-propagation was to fill the hot reservoirs at the jet edges, which in turn stabilize the flame. Overall, the work was to emphasize the role of auto-ignition upstream the lift-off height and the role of the flame-propagation on the flame-stabilization require more investigation.

2.1.3 Trends of research and development

From the time the conceptual diesel flame description was established until now many semi-empirical models, e.g., liquid length scaling laws and the mixing-limited vaporization model of an idealized fuel jet, have been developed for single sprays in a quiescent environment. This work has mainly been carried out in optically accessible constant-volume chambers by utilizing advanced laser diagnostics techniques [14-19]. For a diesel spray the models, for instance, predict a spray vaporization process limited by the fuel and air mixing, and not by atomization. The empirical models provide insight to understand the impact of global parameters, such as the ambient air density and fuel properties, or nozzle diameter and injection pressure, on the physical and chemical processes that occur in diesel spray combustion. The engine combustion network (ECN) is a current international collaboration with experimental and

numerical simulation work to expand the knowledge of fuel spray combustion and to develop new diagnostic methods and to improve CFD models. The work covers, e.g., new methods to increase the detailed knowledge of the liquid spray structure, in-nozzle cavitation and to validate new combustion and sprays models for flow in controlled environments, e.g. refs. [7,20-23], to name a few.

The flow in constant-volume chambers lacks some of the essential flow and spray-interaction features that are typical for the diesel engine. Because of this, important work to evaluate the validity and range of the empirical models has been conducted in optical-accessible engines to increase the fundamental knowledge of diesel engine combustion and to identify potential sources of emissions [24-29]. The laser diagnostic investigations are carried out in optical engines, despite the difficulty to obtain a strong signal, which is distorted by, e.g., scattered light from the liquid spray and the piston glass. Over the last few years, and at the moment, significant efforts to comprehend the effects of jet-jet, jet-wall and jet-flow interactions on the diesel engine mixing and combustion process are carried out [30-37]. One of the observed differences is, for instance the weaker impact of the global temperature on the lift-off length for reacting jets in diesel engines, compared with the lift-off length model, Eq. (2.1). Furthermore, the inter-jet angle, i.e. the distance between the holes on the injector, has shown to influence the combustion event and it is found that the lift-off length decreases when the inter-jet angle decreases. The opposite trend has been seen for the liquid-length, which increases when the inter-jet angle decreases. The effect of the inter-jet angle on the late cycle mixing and soot oxidation has also been the topic of recent experimental and numerical simulation activities. It is found that the equivalence ratio in the near-wall recirculation zone increases with a narrower inter-jet angle. This may influence the soot oxidation process because of the limited availability to oxygen [26,38]. Part of the work that is carried out in this thesis is to examine and to expand the knowledge of the effect of jet-jet interaction and wall-jet interaction on the mixing and combustion behavior in a heavy-duty diesel engine. The results are summarized in Chapter 6, with more details in Paper III-VI.

2.1.4 Emissions

The future emission and engine performance goals can be met by gaining more knowledge about the important parameters that control the combustion process in diesel engines. The two main concerning pollutants for diesel engines are NOx and soot. Previously, the emission goals of NOx and particulate matters (PM) where met by, e.g., gradual improvements of emission control techniques and improved fuel

11

quality [39]. The reduction of soot and NOx in Europe and the United States between the 1990s and 2010 are displayed in Fig. 2.2. The improvements were done without exhaust gas treatment until 2004.
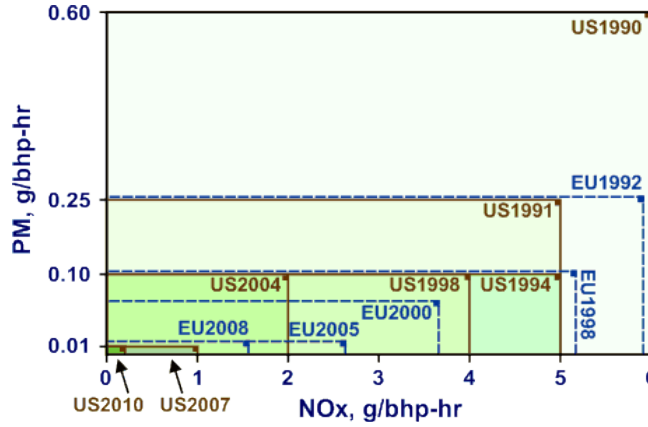
Figure 2.2. Improvements of PM and NOx emission for heavy-duty traffic by tighter pollutants legislation in Europe and in the US. Reproduced from [40].

The challenge of simultaneous reduction of NOx and soot is their inverse relation to temperature and, generally, inhibiting the formation of one would generate more of the other. An increase of the in-cylinder temperature would increase soot oxidation, however, it promotes the formation of thermal NO. On the other hand, a decrease in the in-cylinder temperature would inhibit NOx formation but freeze the soot oxidation process. NOx formation is triggered by the high temperatures that encompasses the diffusion flame [41], as described by the thermal NO Zel'dovich mechanism,

$$O + N_2 \quad \leftrightarrow \quad NO + N \tag{2.2}$$
$$N + O_2 \quad \leftrightarrow \quad NO + O \tag{2.3}$$
$$N + OH \leftrightarrow NO + H \tag{2.4}$$

During the expansion stroke the in-cylinder temperature rapidly decreases and thus freezes the chemical reactions responsible for NOx formation. This means that by retarding the combustion phasing, the combustion temperature decreases and NOx formation can be mitigated, however, at the cost of fuel efficiency. NOx formation can be also be reduced by introducing EGR, which reduces the combustion temperature, or

12

by employing advanced fuel injection profiles [42,43]. Otherwise after-treatment can be employed, such as the selective catalyst reduction (SCR), where a catalytic process forms nitrogen and water from the NOx, or NOx traps, where NO or NO_2 molecules are contained within a medium.

Soot formation is a more complex process; the initial step of soot formation is the pyrolysis of fuel molecules into PAH or pre-cursor species, such as C_2H_2, followed by soot nucleation. Thereafter, the nuclei undergo surface growth where mass is added to the particle. The soot particles coalesce, or combine, and produce primary particles that finally agglomerate into chain-like arrangements [44]. The engine-out soot is a competition between soot formation and soot oxidation, where the former can be reduced by increasing the air-entrainment prior to the lift-off, which is achieved either by decreasing the nozzle diameter or by increasing the injection pressure. A decreased nozzle-hole size increases the air entrainment, which reduces the equivalence ratio at the lift-off, and an increased injection pressure reduces the soot residence time. Soot oxidation can be increased by, e.g., enhancing the late cycle mixing process or by after-treatment solutions, such as diesel particulate filters and late-post injection methods. Over the last years, alternative fuels have been proposed to replace the classical diesel fuels since other chemical compounds are found to produce less soot.

The conventional diesel engine is well established and in 2010, the thermal efficiencies for the heavy-duty engines in the United State were around 43%, with the goal from the US Department of Energy to reach 55% engine efficiency by the year 2015 [45]. Diesel engines generate little UHC and CO emissions, but because of stringent emission legislation the reduction of NOx and soot are necessary yet expensive to compensate for. As a consequence, novel low-temperature combustion concepts to cope with these matters have been, and are, developed and one of these is the homogeneous charge compression ignition engine.

2.2 Homogeneous Charge Compression Ignition (HCCI) Engine Combustion

2.2.1 Characterization of HCCI engines

HCCI is the internal combustion engine concept in which ideally a perfectly homogeneous fuel and air mixture, from either port fuel injection or early direct injection, auto-ignites over the entire cylinder volume simultaneously. The concept of the HCCI engine was already presented in the late 1970s [46] in a two-stroke engine, but it started to attract more attention during the late 1990s. The original idea was to combine the benefits of the SI-engine, such as low soot and NOx emissions, with the benefits of the conventional compression ignition engine, such as high thermal efficiency with high compression ratio operation. Opposite from the diesel engine, the HCCI engine operates at global and local low equivalence ratio conditions, typically $\Phi<0.5$, resulting in low soot and PM emission, and with low combustion temperatures, between 1500 K and 1800 K, resulting in ultra-low NOx formation. The uniform combustion process makes the HCCI combustion close to entirely kinetically controlled and therefore less dependent on the local flow pattern, giving less random cycle-to-cycle variations compared with the classical spark ignition engines. Furthermore, the HCCI IC engine has the potential to deliver high thermal efficiency, comparable to, or even higher than, the diesel engine. On the downside HCCI is found to suffer from incomplete combustion, which gives rise to high CO and UHC levels. This is seen in particular at low-load conditions by, e.g., near-wall combustion quenching, crevice volume fuel trapping and low bulk-gas temperatures [47,48]. At low-loads, large cycle-to-cycle variations and combustion instabilities may appear, which may cause the engine to misfire. For high-load conditions the sharp pressure-rise-rate can give rise to knock and ringing noise, which is the chief limitation.

Another severe problem is the in-direct approach to control the start of combustion and it is found that the control of combustion phasing is sensitive to e.g., variations in gas temperature, whichmay vary between different engine cycles. Adjusting the intake temperature to increase or decrease the reactiveness of the mixture originally controlled the combustion phasing, however, this method was slow in the feedback to the engine control system. Instead methods such as variable compression ratio (VCR), EGR, variable valve timing (VVT) and multi-component fuel were suggested to provide faster feedback to the engine cylinder, e.g., refs. [49-59].

14

2.2.2 Conceptual model for HCCI combustion

Investigations to examine the effects of fuel chemistry and flow processes, such as the wall temperature, the effect of the turbulence generated during the intake process and low-temperature reactions, on the HCCI engine combustion process have been many. Similar to the diesel engine, to come up with a conceptual description to understand and to optimize the HCCI engine, numerical simulations and laser diagnostic methods, such as OH chemiluminescence and planar laser induced fluorescence (PLIF) have been carried out [60-68]. For an HCCI engine working steadily and with controlled combustion phasing, the main combustion event is found to undergo with few random cycle-to-cycle variations, but with the start of ignition occurring in different regions of the combustion chamber for the different cycles. This could be explained by the observation of thermal inhomogeneity of the cylinder gas mixture, with a hotter charge in the central part of the engine with small temperature and fuel concentration stratifications and with a cool boundary layer along the wall. The location of the onset of ignition in the presence of thermal inhomogeneity can vary because of the varying location of a most reactive mixture. The stratification is generated by the large-scale turbulence structures that are generated during the intake flow process. During the intake, the cold fuel and air mixture impinges and interacts with the cylinder walls and is thereafter transported to the other cylinder regions by turbulence transport and by turbulence eddies. A high level of stratification has shown to impact the combustion event and the pressure-rise-rate, and it indicates that a modification of the combustion chamber may promote a slower pressure-rise-rate at high-load conditions, if the fuel and air mixture interaction with the cylinder wall can be controlled.

However, although the start of ignition is found to vary over the combustion for different cycles, the duration of the HCCI combustion is short and without flame propagation, which makes the combustion process significantly faster than the typical SI engine combustion event. It is believed that the high temperatures and pressures that appear during the ignition process quickly spread to the surrounding gases and rapidly ignite the adjacent fuel and air mixtures. The chemistry processes leading to the onset of combustion have been investigated experimentally employing in situ laser diagnostics techniques. Methods such as the PLIF and OH chemiluminescence identified a homogeneous formaldehyde signal prior to onset of main heat-release, which is typically accompanied by ignition chemistry. The drop in formaldehyde signal was followed by the rise of OH signal, which is a species present in the high-temperature reaction zones. OH was only found in the areas where formaldehyde

entirely had been consumed. This revealed the different stages of chemistry that leads up to the HCCI combustion process. From the experiments low-temperature reactions (LTR), or cool flame, became apparent around 10 to 20 CAD before TDC and grew stronger with decreasing fuel octane number. From the natural emission of the cool flame, large inhomogeneity on the small scales were found, which was explained by the spatial variation of species concentration and temperature.

2.2.3 Low-load operation and emissions

The classical diesel engine is found fairly easy to maintain under any load conditions; however, the most suitable operating range for the HCCI engine is at part-load with small pressure-rise-rates during the main combustion event. At these conditions the engine-out emissions are acceptable and it demands less after-treatment of unburned hydrocarbons (UHC) and carbon monoxide (CO) than at e.g., low engine loads.

HCCI operating at idle, low-loads and cold-start conditions experience the risk of exhibiting elevated CO and UHC emissions as well as combustion stability issues. This is mainly because of the low in-cylinder temperature and the multi-modal behavior manifested in cycle-to-cycle combustion behavior. At low-load and high octane number conditions, the high intake temperature that is needed to ignite the fuel and air mixture is not necessarily accessible and the exhaust gas temperature at these operating points is low. Olsson et al. [58] investigated the impact of cooled EGR in a multi-cylinder HCCI engine at low-load and idle conditions. It was found that employing EGR was favorable for CO, UHC and NOx emissions, compared with if EGR was not employed. However, feasible combustion stability at idle conditions could not be achieved unless external inlet air heating was used, since the required heat could not be extracted from the exhaust gas. The overall combustion phasing was difficult to maintain at the investigated conditions and the CO emissions were still unacceptable despite the use of EGR. The improved combustion efficiency was found to be due to the re-introduction of unburned fuel when employing EGR.

Koopmans et al. [69] investigated the effect of cyclic variations on the HCCI combustion process by correlating the combustion event from the previous cycle with the current cycle. It was discovered that a cycle with later combustion phasing and lower combustion peak pressure was followed by a cycle with earlier combustion phasing and higher combustion peak pressure. This was explained by the oxidation of unburned fuel during the gas exchange phase, which increased the initial temperature for the subsequent cycle. This made the fuel and air mixture ignite earlier. It was

concluded that the oscillating behavior of the combustion event made it nearly impossible to continue running in HCCI mode and to decrease the cycle-to-cycle variations would improve the combustion efficiency and enlarge the window for HCCI engine operation. In a study by Hwang et al. [70] the low-load operation could be enlarged by introducing fuel and air stratification and reduction of lean zones for a single stage combustion fuel. Other researchers examined the idea to combine spark ignition combustion with HCCI combustion under difficult operating conditions, known as the spark-assisted compression ignition (SACI).

Dec et al. [47,71] carried out experiments together with numerical simulations of a single-zone combustion model to identify the potential sources of CO and UHC at low-load conditions, with high octane number fuel. By continually decreasing the fueling rate (decreasing equivalence ratio) the numerical simulations predicted that certain levels of the increased CO emissions were due to reduced CO to CO_2 conversion, due to too low bulk-gas temperatures. Previously the sources of CO emissions were believed to be due to wall-quenching effects. The low temperature was believed to be an effect of heat-transfer, crevice trapping of fuel, a decreased temperature due residual components and thermal inhomogeneity of the bulk. The source of UHC was mainly in the near-wall region and in the crevice volume. However, the levels of UHC were significantly increased at very low fueling rates due to a too low combustion temperature, inhibiting the conversion to e.g., CO.

2.3.4 High-load, pressure-rise-rates and emissions

The main problem for the HCCI engine operating at high-load conditions is the sharp pressure-rise-rate, which gives rise to noise, or knock, to increased wall heat-transfer, and to engine wear. Studies to investigate the possibility to run HCCI engines at high loads with high-octane number fuel, in both a single and multi cylinder engine, while mitigating unacceptable pressure-rise-rates, have been carried out. The strategies employed e.g., VCR, high levels of EGR, intake pressure boosting and thermal stratifications [58, 72-75]. It was found possible to achieve stable combustion for a range of fuels between octane number 0-100 with VCR; however, the combustion efficiency decreased as the compression ratio was increased, as the intake temperature had to be reduced to avoid premature onset of combustion. Furthermore, CO emission levels grew as the compression ratio increased, due to a reduced time for the conversion of CO to CO_2. To avoid short combustion durations, sharp pressure-rise-rates and noise for high-octane number fuels at high load conditions, high levels of EGR or inlet preheating (for fuel lean conditions) had to be used. The high levels of

EGR influenced the combustion stability and combustion efficiency and the excessive pre-heating increased the heat-transfer near TDC, and thus reduced the thermal efficiency. Overall, these behaviors along with the sharp-pressure-rise-rates strongly limit the upper load-limit and the engine power-density. Another alternative was to employ supercharging to replace the need for inlet air heating, and is shown to decrease the level of UHC. However, the engine performance may suffer due to pumping losses.

A possible remedy for the sharp pressure-rise-rates was investigated in [76-78]. Here different levels of thermal stratification were compared and it was found that the upper load limit could be extended if the stratification level increased, because of longer combustion durations, when the same combustion phasing was kept. However, to achieve the optimal thermal stratification level was not always realizable in a practical situation. Investigations employing low octane number fuel exhibited advantages in the intake air charge procedure, demanding less inlet preheating. With more cool-flame activity the cylinder pressure, as well as the global cylinder temperature, increased prior to onset of the main heat-release. If a low-octane number fuel was employed, effectively a higher air charge mass could be admitted to the engine and a higher engine efficiency could be obtained. The consequence of a more active cool flame was the requirement of immediate compensation in e.g., fueling rate, because of the complex interaction between the low-temperature reactions with the main heat-release [79]. In later works [79,80], it was potentially shown that the upper load-limit for the HCCI engine could be extended by smoothening the pressure-rise-rate by employing fuels that exhibit two-stage ignition events. In these cases, however, unacceptable NOx levels could easily be attained. Furthermore, if the combustion phasing was excessively retarded, the combustion event could exhibit misfire or partial burn of the fuel. When this occurred the temperature of the recirculated gas had a lower temperature and it became more difficult to initiate the main-stage heat-release, and the combustion event became even further retarded.

Overall, the HCCI engine has a similar, or higher, thermal efficiency compared with the conventional diesel engine and with extremely low NOx and soot emissions. It however suffers from problems with combustion phasing and delivering high power density, along with high levels of UHC and CO emissions. Based on the benefits that were found for the HCCI engine, investigations on low-temperature combustion concepts employing stratification techniques continued. This low-temperature combustion mode with stratified mixtures is sometimes referred to as partially

premixed charge compression ignition (PPCI or PCCI) or partially premixed combustion (PPC) and by some, low-temperature combustion (LTC).

2.3 Partially premixed engine combustion (PPC)

2.3.1 Characterization of the PPC engines

PPC, PCCI or LTC are low-temperature combustion concepts controlled both by direct fuel injection and chemical kinetics and can in some sense be viewed as a combination of the conventional diesel combustion engine and the HCCI combustion engine. By combining the advantages of classical diesel combustion, e.g., the low levels of UHC and CO emissions and the direct control of the fuel delivery, with the advantages of HCCI combustion, e.g., the high thermal efficiency and the low-temperature combustion yielding low NOx, a combustion engine concept that would meet the emission legislation with high-fuel efficiency can be achieved. There are many methods to achieve partially premixed combustion and thus there is no single conceptual model to cover the entire range of low-temperature strategies, yet. However, it is typical that the low-temperature combustion engines involve all, or some, of the following features:

1. A positive dwell time (or positive ignition delay), which means that the end of injection (EOI) occurs prior to the start of main combustion (SOC). This promotes the fuel and air mixing process so as to mitigate the fuel rich zones that may serve as sources for soot formation.
2. Dilution or EGR, to inhibit excessive cool flame activity and to reduce the peak cylinder temperature. This will lead to a slower pressure-rise-rate and to lower rate of formation of NOx. This should also reduce the heat-transfer and the heat-losses to the exhaust.
3. A fuel and air charge stratification, to achieve a sequential heat-release process with slow pressure-rise-rates. This will inhibit noise and knocking and could extend the upper load-limits.

Furthermore, there is a trade-off between a too fast combustion process to consider, which limits the upper load, and a too slow combustion process, which decrease the thermal efficiency due to heat losses.

Because there are currently many strategies to achieve low-temperature combustion that fulfills (1-3), a brief discussion is followed below of an LTC engine concept that

19

employs early and late single injection strategies with high dilution levels. This is discussed together with the advantages that gasoline (or high octane number fuel) partially premixed combustion engines can offer and the relation to the work in this thesis.

2.3.2 Conceptual model for PPC engine combustion

Kimura et al. [81] performed one of the earlier investigations of the low-temperature combustion concept, called modulated kinetics (MK). Kimura et al. achieved low soot emissions, by using a long-ignition delay, and low NOx emission by retarding the injection and reducing the combustion temperature. In this work a low-compression ratio and high levels of EGR were employed. Later, Yanigahara et al. [82] developed a split injection strategy called the uniform bulky combustion system (UNIBUS). This method employed a pilot fuel injection to initiate the low-temperature reactions and the main fuel injection to control the main-stage ignition and the remaining combustion process. This strategy was found to lower the need for EGR.

Musculus et al. [83] proposed a model for a single injection LTC engine with an early or late injection strategy and is briefly recapitulated here. Figure 2.3 illustrate the combustion process of a single injection LTC process in a heavy-duty (HD) engine employing a late fuel injection strategy and in a light-duty (LD) engine employing an early or late fuel injection strategy.

These LTC processes are compared with the described diesel flame combustion model. From the figure it is seen that the fuel is completely vaporized before the onset of main heat-release and it is seen that the first-stage ignition reactions are followed by the second-stage ignition and high-temperature reactions. The regions of soot or soot pre-cursors are significantly smaller when compared with the classical diesel flame and only low levels of second-stage ignition occur at fuel-rich conditions. This clearly depicts the fundamental difference between LTC concepts and classical diesel engine combustion events.

2.3.3 High and low-load operation, emissions and pressure-rise-rates

Noehre et al. [84], characterized single-injection diesel PPC engine combustion at part and high-load in a heavy-duty diesel engine. The study showed that the classical NOx and soot trade-off could be mitigated, when a long ignition delay and approximately

70% EGR was used. However, at such high levels of EGR the combustion efficiency suffered from high penalty of CO and UHC emissions. Furthermore, a low compression ratio had to be used to avoid premature ignition of the diesel fuel, with the consequence of a low thermal efficiency. Therefore, gasoline fuel was investigated as a viable PPC fuel due to its higher resistance to auto-ignition [85]. It was found that a high octane number fuel, in this case reference octane number (RON) 94.7, generated significantly less soot and NOx, as well as higher indicated efficiency, compared with diesel fuel PPC operation. This was carried out at a higher compression ratio and with an EGR level of approximately 32 %.
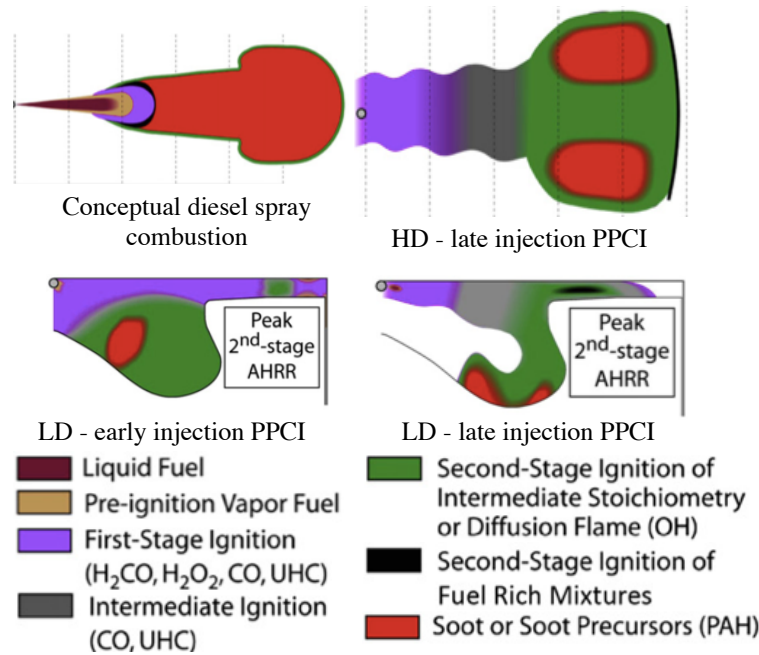
Figure 2.3. Late single-injection LTC for heavy-duty conditions, and early and late single injection LTC for light-duty conditions, compared with the conceptual diesel spray combustion description. Reproduced from [29].

In the work of Klingbeil et al. [86] and Lewander et al. [87], the effects of advancing and retarding the fuel injection on the various emissions, noise and pressure-rise-rates in a PCCI heavy-duty engine and light-duty engine were investigated. These works are believed to represent the general trade-off that appears for low-temperature combustion

DI engines. For a light-duty engine operating with a high level of dilution, ~14% O_2, the fuel injection at a certain early timing resulted in contemporary reduction of all emissions, UHC, PM, CO and NOx but with an excessive pressure-rise-rate exceeding 15 bar/CAD. Increasing the dilution levels gave more CO and UHC emissions, whereas decreasing the dilution levels gave more NOx emissions and steeper pressure-rise-rates. By retarding the fuel injection timing, the CO and UHC emissions were fairly constant until a very retarded injection timing. Thereafter the CO and UHC emissions increased and the levels of NOx, PM emissions and pressure-rise-rate decreased. Operating the heavy-duty engine under similar conditions exhibited similar trends. For LTC engine operation, the main combustion efficiency loss is due to CO emissions that are found mainly in fuel-lean regions, such as in the centerline and squish regions of the engine. Certain levels of UHC and CO emissions are also found near the injector nozzle and from the liquid-fuel film in the wall-regions. For heavy-duty conditions, entrainment waves may generate overly lean regions close to the nozzle and this region thus serves at the main contributor to CO and UHC emissions. With the elimination of the soot and NOx trade-off in LTC engines, other trade-offs may appear [40]:

- Soot and combustion noise – Early injection generates less fuel rich regions but drastic pressure-rise rates appear due to the increased level of pre-mixing.
- NOx and UHC – Reducing NOx by high levels of EGR may decrease the combustion efficiency.
- Exhaust temperature and NOx – The low-temperature combustion reduces the NOx formation, but may be penalized with worse efficiency of the after-treatment systems, because of the lower exhaust gas temperatures.

One of the limiting processes for gasoline PPC engines is the amount of premixed combustion, when the end of injection occurs prior to the start of combustion. With larger portion of premixed combustion, this results in higher pressure-rise-rates and high acoustic noise. To remedy this and to expand the PPC engine load range, Kalghatgi et al. [88] employed a gasoline split fuel injection strategy, which smoothened the heat-release and a higher engine load operation could be achieved. The levels of UHC and CO emissions were, however, higher than for diesel fuel PPC. Manente et al. [89,90] improved the split fuel injection gasoline PPC engine strategy in a heavy-duty engine. Running PCC with approximately 50% EGR it was possible to simultaneously reduce NOx, soot, UHC and CO emission. At the same time a gross indicated efficiency of 57% was achieved. This was accomplished by injecting a considerable amount of fuel in the very early pilot injection and by using the second

fuel injection close to TDC to control the main combustion event of the stratified mixture. In another work, Manente et al. [91] carried out gasoline PPC in a light-duty engine. Gross indicated engine efficiencies, from 45% to 57 %, with low emission levels could be reached by employing an optimized triple-injection strategy.

Hildingsson et al. [92] investigated the auto-ignition properties for gasoline PPC engines at both high and low-load operating conditions. It was found that the optimum fuel should be around the 75-85 RON range for the investigated compression ratios. It was concluded that a lower octane number than this would lose the ignition delay advantage over diesel at high load, while a higher octane number might be difficult to ignite at low-load conditions. In a recent doctoral thesis work, Solaka [93] performed a design of experiments (DoE) and regression analysis, coupling low-temperature reactions with emissions and ignition delay and found that the most suitable fuel octane number over the entire load range was between 65 and 75, with low aromatic concentrations.

The high octane number PPC engine concept has proven to work well for high-load conditions where the fuel can easily be compressed to ignition. At low-load conditions, however, different strategies had to be considered. Strategies to control the combustion process are e.g., residual trapping by negative valve overlap (NVO) to increase the in-cylinder temperature, pre-heating of the intake air or using lower octane number fuels to take the advantage of the cool flame and low-temperature reaction properties. Hence, the possibility to extend the low-load operation limit for gasoline type fuel in light-duty PPC engines has been the target of recent research. Borgqvist et al. [94,95] showed that a low amount of residual trapping is favorable to minimize the gas-exchange losses but the combustion efficiency is low due to the reduced in-cylinder temperature. Sellnau et al. [96,97] employed a triple injection strategy with a fuel octane number of 91. They showed that at low-load conditions, low levels of soot and noise could be obtained with a large amount of exhaust rebreathing.

One part of this thesis is aimed at understanding the role of an injection strategy employing multiple injections to expand the low-load limit for light-duty gasoline PPC combustion engines. In this work the reference injection strategy is a triple fuel-injection event, based on the work by Borgqvist et al. [94,95], in an optical engine configuration with PRF69 fuel. The work serves to explain the trends of pressure-rise-rate and heat-release and the formation of, e.g., CO emissions. The baseline experimental and numerical injection strategy is compared with other injection strategies to investigate the sensitivity to the fuel and air mixing process and the intake temperature.

23

Chapter 3
Turbulent Reacting Flows in IC engines

3.1 Governing equations

Turbulent reactive flows in DI IC engines are described by a set of transport equations derived based on the conservation of mass, momentum and energy.

The first equation is the mass continuity equation, for the gaseous part of the flow,

$$\frac{\partial}{\partial t}\rho + \frac{\partial}{\partial x_i}(\rho u_i) = S_\rho^S \tag{3.1}$$

where ρ is density of the fluid and u_i the velocity component in the i-th direction. The second equations are the momentum, or Navier-Stokes, equations,

$$\frac{\partial}{\partial t}(\rho u_i) + \frac{\partial}{\partial x_j}(\rho u_i u_j) = -\frac{\partial p}{\partial x_i} + \frac{\partial \tau_{ij}}{\partial x_j} + S_{u_i}^S$$

$$\tau_{ij} = \mu\left(\frac{\partial u_i}{\partial x_j} + \frac{\partial u_j}{\partial x_i}\right) - \frac{2}{3}\mu\left(\frac{\partial u_k}{\partial x_k}\delta_{ij}\right) \tag{3.2}$$

where μ is the dynamics viscosity, τ_{ij} is the shear stress tensor for Newtonian fluids and δ_{ij} is the Kronecker delta. The third equation is the species transport equation

$$\frac{\partial}{\partial t}(\rho Y_k) + \frac{\partial}{\partial x_j}(\rho u_j Y_k) = \frac{\partial}{\partial x_j}\left(\rho D_k \frac{\partial Y_k}{\partial x_j}\right) + \dot{\omega}_k + S_{Y_k}^S \tag{3.3}$$

where diffusion is modeled with Fick's Law and Y_k is the mass fraction for species k and $\dot{\omega}_k$ is the reaction rate for species k, k =1,…, N, where N is the number of species in the mixture. The last equation is the enthalpy equation (assuming unity Lewis number and neglecting the radiation term)

24

$$\frac{\partial}{\partial t}(\rho h) + \frac{\partial}{\partial x_j}(\rho u_j h) = \frac{\partial p}{\partial t} + \frac{\partial}{\partial x_j}\left(\rho \alpha \frac{\partial h}{\partial x_j}\right) + S_h^S \qquad (3.4)$$

where

$$h = \sum_{k=1}^{N} Y_k h_k$$

$$h_k = h_{f,k}^0 + \int_{T_0}^{T} C_{p,k}\, dT \qquad (3.5)$$

where α is the thermal diffusion coefficient, $h_{f,k}^0$ is the enthalpy of formation for species k at a reference temperature T_0 and $C_{p,k}$ is the specific heat capacity of species k. The equation of state is used to relate the temperature, species mass fractions and, together with Eq. (3.5), the enthalpy with the thermodynamic pressure

$$P = \rho R_u T \sum_{k=1}^{N} \frac{Y_k}{W_k} \qquad (3.6)$$

where R_u is the universal gas constant, 8.314 J/Kmol, and W_k is the molecular weight of species k. In Eqs. (3.1-3.4), the source terms S_p^S, $S_{u_i}^S$, $S_{Y_i}^S$ and S_h^S account for the exchange rates of mass, momentum, species mass fraction and enthalpy between the gas and the liquid phase.

3.2 Turbulence

In the 1920s L.F. Richardson developed the theory of cascading turbulence energy, where eddies in the energy containing large scales, with characteristic length, velocity and time, l_0, $u(l_0)$, and $\tau(l_0)$ respectively, due to non-viscous forces breaks down into smaller eddies. The perpetually smaller eddies continually break down until they reach the point where viscous forces become dominant and dissipate the energy in the small eddies to heat. In general, the turbulence kinetic energy on the large scales is transferred to the small scales, but reverse cascading can occur and is called backscattering [98]. Kolmogorov proposed three hypotheses to quantify the energy cascade process. He argued that the anisotropy of turbulence loses its way during the eddy breakup process in the energy transfer between scales. Kolmogorov's first hypothesis was related to isotropy,

25

"at sufficiently high Reynolds numbers, the small scale turbulent motions (l<<l$_0$) are statistically isotropic".

In Fig. 3.1, the length scales larger than l$_{EI}$ are considered to be in the energy containing range and l$_{EI}$ is also believed to be the separation between eddies exhibiting anisotropic and isotropic behavior. In the isotropic range,
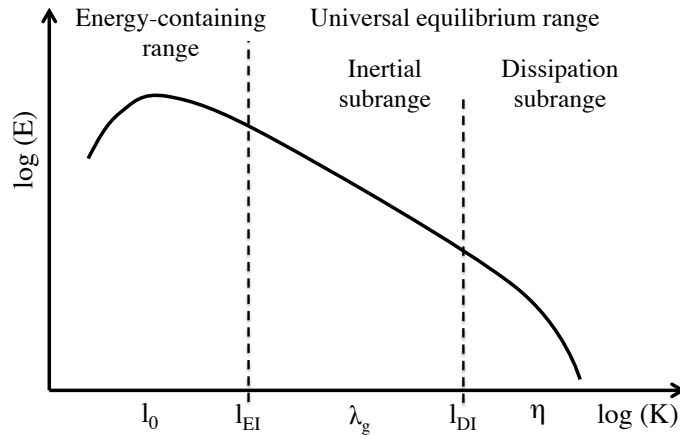
Figure 3.1. Illustration of the energy spectrum of a turbulent flow, as a function of the wavenumber.

Kolmogorov proposed that the statistics of the flow are universally dependent on the viscosity, v and on the dissipation rate of the turbulence kinetic energy, ε. Kolmogorov's second hypothesis was

"in every turbulent flow at sufficiently high Reynolds number, the statistics of the small-scale motions have a universal form, uniquely dependent on v and ε"

This range is called the universal equilibrium range. Furthermore, since it only is the smallest scales that are affected by viscosity, Kolmogorov's third hypothesis reads

"in every turbulent flow at sufficiently high Reynolds number, the statistics of the motions in a range $l_0 >> l >> l_\eta$ are uniquely determined by the kinetic energy dissipation rate ε".

26

The length scale l_{DI} separates the flow structures that are affected by inertia alone, which is called the inertial subrange, and the scales affected by both inertial and viscosity, which is called the energy dissipation range. The length scale η is called the Kolmogorov length scale, which is the smallest scale at which the turbulence kinetic energy is dissipated to heat due to viscosity.

3.2.1 Scales of turbulence

A turbulence Reynolds number based on the characteristic scales of turbulence in the energy-containing range can be expressed as

$$\text{Re}_T = \frac{u_0 l_0}{\upsilon} \tag{3.7}$$

with the corresponding time-scale

$$\tau_0 = \frac{l_0}{u_0} \tag{3.8}$$

The turbulence eddies at the smallest scales are linked to the large scales and by using the hypotheses proposed by Kolmogorov, it is possible to derive the relations between the length scales, time scales and velocity scales. The Kolmogorov scales are

$$l_\eta = \left(\frac{\upsilon^3}{\varepsilon}\right)^{1/4}, \qquad u_\eta = \left(\upsilon\varepsilon\right)^{1/4}, \qquad \tau_\eta = \left(\frac{\upsilon}{\varepsilon}\right)^{1/2} \tag{3.9}$$

and the Kolmogorov scales are related to the large integral scales as

$$\frac{l_\eta}{l_0} \sim \text{Re}_T^{-3/4}, \qquad \frac{u_\eta}{u_0} \sim \text{Re}_T^{-1/4}, \qquad \frac{\tau_\eta}{\tau_0} \sim \text{Re}_T^{-1/2} \tag{3.10}$$

27

3.3 Premixed, non-premixed and partially premixed combustion

In IC engines and many other applications, combustion occurs under premixed, non-premixed or partially premixed conditions. Turbulent premixed combustion is typically found in SI engines whereas the main heat-release from the DI diesel combustion engine comes from a non-premixed flame. Partially premixed combustion is found in situations where both premixed and non-premixed combustion can occur simultaneously, such as in the PPC engine.

In reactive flows, two dimensionless numbers are of practical interest. These are the Damköhler number, Da, and the Karlovitz number, Ka [99]. The Damköhler number is defined as

$$Da = \frac{\tau_0}{\tau_c} \tag{3.11}$$

and it is the ratio between the large eddy turnover time scale τ_0 and the chemical reaction time scale τ_c. The Karlovitz number is defined as

$$Ka = \frac{\tau_c}{\tau_\eta} \tag{3.12}$$

which is the ratio between the chemical time and the smallest eddy time scale.

3.3.1 Turbulent premixed combustion

In premixed combustion the fuel and oxidizer are already well-mixed prior to the onset of combustion. If an added heat-source increases the temperature above the crossover temperature, chain-branching reactions become dominant and high-temperature chemistry starts [99]. In a spark ignition engine, the added heat-source is an electric discharge that generates the turbulent flame, which propagates towards the unburned fuel and air mixture. This premixed combustion is controlled by the chemical kinetics of the fuel as well as the diffusion of heat and mass between the reaction zone and unburned mixture. The flow structures are coupled to the flame across a range of

28

varying energy containing scales, from the large scales determined by e.g. the intake valves and engine bore, down to the small scale structures associated with energy dissipation. Because of a slow laminar flame speed for hydrocarbon fuels, the combustion process in an SI engine is depending on turbulence to increase the flame propagation speed to avoid incomplete combustion. Turbulence wrinkles the instantaneous flame front and hence increases the area of the flame surface facing the unburnt mixture. This leads to a faster fuel consumption, cf. Fig. 3.2.
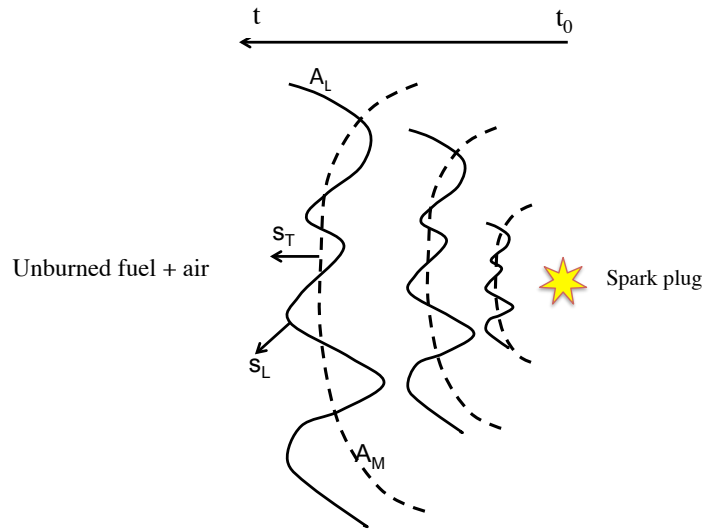

Figure 3.2. A spark ignites the fuel and air mixture at initial time $t=t_0$, thereafter the flame grows and becomes wrinkled by interaction with the surrounding turbulent flow. The turbulent flame propagation speed, s_T, is the propagation speed of the mean flame surface area A_M shown by the dashed line and the local laminar flame speed, s_L, is the instantaneous speed of the wrinkled surface area A_L, the solid line.

When the Karlovitz number is less than 1 it is found that the ratio between the turbulent flame speed, s_T, and the laminar flame speed s_L, is the same as the ratio between the instantaneous flame front area, A_L, and the mean flame front area, A_M, i.e., $s_T / s_L = A_L / A_M$. Since $A_L > A_M$ the turbulent flame speed is larger than the laminar flame speed. If the turbulence mixing time scale becomes small in comparison with the chemical reaction time scales, i.e., in a situation with a very high Karlovitz number, it is possible for fuel pockets to enter the post-flame zone behind the flame front without being oxidized. If sufficiently many fuel pockets make it behind the reaction front, the

29

flame may quench due to the reduced released heat. Detailed numerical modeling to investigate the impact of high Karlovitz number in premixed flames can be found in [100,101].

3.3.2 Turbulent non-premixed combustion

The diesel spray combustion is a classical example of a non-premixed flame. Liquid fuel is injected into a hot ambient air environment. It vaporizes and auto-ignites in multiple locations in the mixing layer [102]. Thereafter a turbulent diffusion flame is formed and the flame is stabilized at stoichiometric mixtures, cf. Fig. 3.3.

The impact of turbulence on the diffusion flame front can be described by the different regimes in the turbulent flame diagram [103]: in the regime of a low Reynolds-number the flame is laminar, in the regime with a Karlovitz number less than unity the chemistry is fast in comparison with the mixing and in the regime with a small Damköhler number and a Karlovitz number above unity, the mixing is fast compared with the chemistry. Generally, since combustion occurs at stoichiometric conditions the chemical time scales are smaller than the time scales of mixing and the flame front becomes thin. This means that combustion occurs as soon as the mixing is finished and it is sometimes referred to as "mixed is burnt".

3.3.3 Partially premixed combustion

In partially premixed combustion both premixed combustion and non-premixed combustion may simultaneously occur in different parts of the mixture. For instance, in the PPC engine the fuel and air charge stratification is generated by the fuel injections. During the combustion process both, e.g., ignition and a diffusion flame may appear in different regions of the engine at the same time. In Figure 3.4 the different regions of fuel and air mixtures in a light-duty PPC engine are shown in a scatter plot of the computational cells in an equivalence ratio and temperature (Φ-T) space. By employing three injections, one in the earlier compression stroke, one at 20 CAD before TDC and one close to TDC, a stratified mixture is obtained. The plot is generated at 5 CAD aTDC, for a non-reacting run, which would correspond to the onset of high temperature ignition. Five zones that are identified for the thermal- and charge stratified mixture as labeled (I)-(V). The mixtures correspond respectively to a thermally stratified air charge without fuel (region I), a thermally stratified charge with the equivalence ratio between 0.15 and 0.3 in the wall vicinity (region II), a mixture near the wall, and cooled by the engine cylinder-wall (region III), a fuel rich mixture

generated in the central part of the engine by the last injection (region IV), and a partially premixed fuel and air mixture generated by the first two injections, at equivalence ratio between 0.15 and 0.35 at around the temperature $800 < T < 970$ K (region V). From the figure, it is seen that with the current injection strategy there is a high probability to find a region in the engine without any fuel, and most of the charge is in the equivalence ratio range below 0.4.
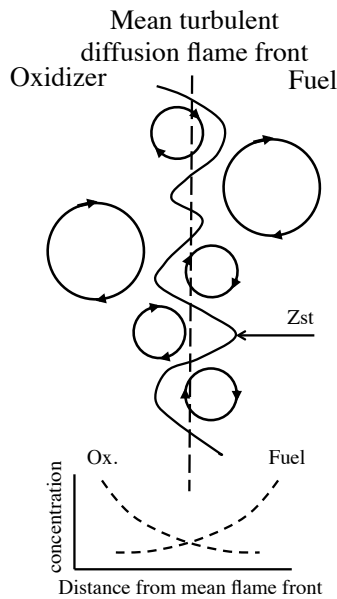
Figure 3.3. Fuel and air ignite around stoichiometric conditions. The combustion is controlled by the fuel and air mixing process. Because of the wrinkling of the flame front at turbulent conditions, when averaging the flame front experimentally it may appear broadened.

3.3.4 Auto-ignition of hydrocarbon fuel

With the modern low-temperature combustion engines, such as the HCCI engine and the PPC engine, it is important to understand the ignition behavior, especially for hydrocarbon fuels under different pressure, temperature and concentrations. The need for accurate, yet sufficiently small and time efficient reaction mechanisms are important to cover the entire width of possible chemical reactions, consider, e.g., the H2-O2 system in [104]. The early studies of kinetic mechanisms identified the

different types of elementary reactions that are present in combustion. These are the chain-initiation reactions, generating the radical species, the chain-branching reactions, increasing the number of radical species, the chain-propagation reactions, a zero net production of radicals and the chain-termination reactions, the reduction of radical species by forming stable molecules.
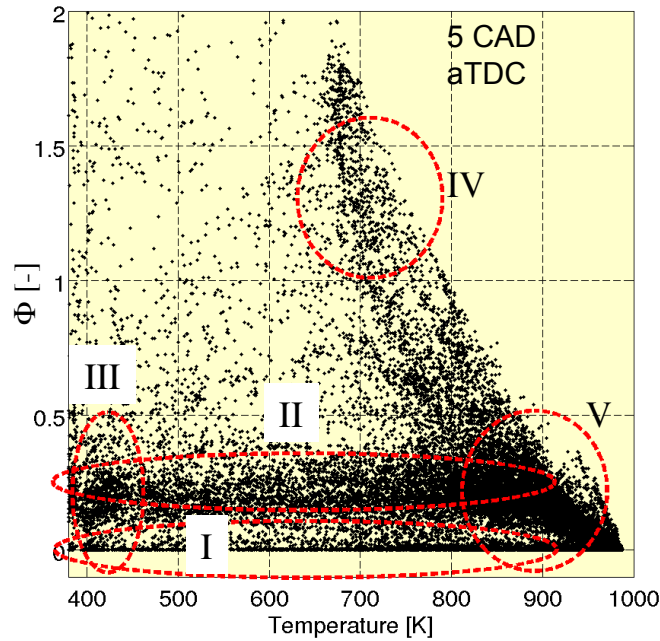
Figure 3.4. Fuel and air charge stratification in the baseline case 1. Five regions are identified as I) an air charge without fuel, II) a thermally stratified charge at constant equivalence ratio, in the wall vicinity, III) a near-wall mixture seen by the low temperature, and IV) a fuel rich mixture in the central part of the engine from the last injection and V) a premixed mixture between equivalence ratio 0.15 and 0.35 at around the ambient mean temperature. Details about the figure is given in Paper IX.

In this thesis, larger hydrocarbons, such as fuel blends of iso-octane and n-heptane, are considered under engine-like conditions. The combustion processes can be divided into three temperature dependent chemical reaction regimes, see e.g., Westbrook [105],

- The low-temperature chemistry regime, T < 850 K
- The mid-temperature chemistry regime, 850 K < T < 1200 K
- The high-temperature chemistry regime, T > 1200 K

where each regime has its own individual key reactions. Two important chain-branching reactions are identified; the first are the reactions around 1000 K, affecting the thermal decomposition of hydrogen peroxide. The second are the reactions above 1200 K, which are mainly governed by the reactions between hydrogen and oxygen, where radicals deplete fuel reactants and the temperature increases.

The most important high-temperature reaction is the radical chain-branching reaction

$$H + O_2 \rightarrow O + OH \tag{3.13}$$

with a net formation of radicals. The OH (hydroxyl) radical decompose the fuel molecules, which will increase the temperature of the system.

In the intermediate temperature regime, reaction (3.13) is too slow to start ignition. The important reactions in the intermediate temperature range are

$$H + O_2 + M \rightarrow HO_2 + M \tag{3.14}$$
$$RH + HO_2 \rightarrow R + H_2O_2 \tag{3.15}$$
$$H_2O_2 + M \rightarrow OH + OH + M \tag{3.16}$$
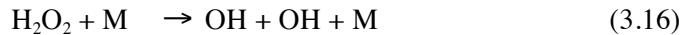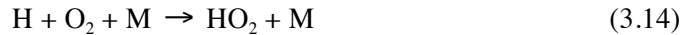
where HO_2 is hydroperoxyl, M is a third body, H_2O_2 is hydrogen peroxide, RH is an alkane (e.g., n-heptane C_7H_{16}) and R is an alkyl radical (e.g., C_7H_{15}).

It is understood that the chain-branching reaction (3.16) becomes important at higher temperatures in the intermedia-temperature chemistry regime, because of the net production of two OH radicals. A common feature in the diesel or HCCI engine is the accumulation of H_2O_2 until a high temperature is reached, where after a rapid decomposition of H_2O_2 occurs and reaction (3.16) becomes dominant. The formed OH will react with the fuel and the temperature of the system increases. Therefore, hydrogen peroxide can be viewed as a precursor for ignition, and OH can be viewed as an indicator for high-temperature heat-release. Anything in the system that would affect the chemical time scales of H_2O_2 would, hence, also affect the combustion ignition delay.

To achieve chain branching at even lower temperatures is more complex. The oxygen in reaction (3.13) does not react with the hydrogen, but instead adds to an alkyl radical

$$R + O_2 + M \rightarrow RO_2 + M \tag{3.17}$$

to form RO_2 (e.g., $C_7H_{15}O_2$). RO_2 is thereafter either decomposed back into $R + O_2$ as the temperature increases above 850 K, or undergo isomerization. The isomerization process is a transfer of an hydrogen molecule from the alkyl radical to the oxygen and breaks the oxygen bond, to become QOOH (where Q is, e.g., C_7H_{14}). The isomerized species reacts and forms ketohydroperoxide (KET). When the temperature is increased and reaches approximately 800 K, the large KET species are decomposed into smaller species where at least two of these are radicals and chain branching is achieved. In Fig. 3.5, the first-stage and second-stage ignition events are shown. The results are from a numerical simulation in a homogeneous reactor at unity equivalence ratio and initial temperature 800 K and pressure 20 bar, with the mechanism from Liu et al. [106]. PRF 90 corresponds to 90% iso-octane and 10% n-heptane; PRF 70 corresponds to 70% iso-octane and 30% n-heptane, etc. It is seen that with an increasing amount of n-heptane, the first-stage ignition grows stronger and the time-lapse until the second-stage ignition starts is seen to decrease

One interesting behavior of two-stage ignition fuels is the negative temperature coefficient (NTC), which is characterized by a longer ignition delay with increased temperature, instead of a shorter ignition delay. It is found that when a certain mixture undergoes reactions at low temperatures, the exothermic process is encompassed by an increase in temperature that is not high enough to initiate the chain branching reactions. After a long ignition delay time, second-stage ignition occurs and the combustion process is governed by the high-temperature reactions [107,108]. If the temperature increase in the first-stage ignition is higher, which is the case at initially lower temperature, then the induction time between the first-stage ignition and second-stage ignition can be shorter. This can result in a shorter overall ignition delay time.
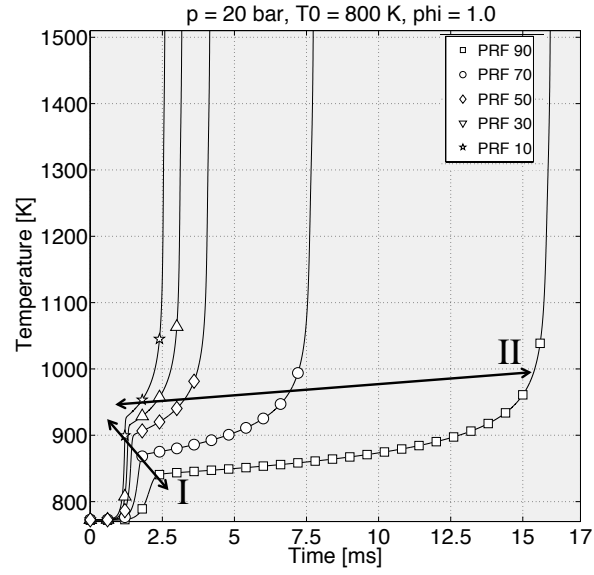
Figure 3.5. A reaction process undergoing first-stage ignition (I) and second-stage ignition (II) is modeled with a PRF mechanism from Liu et al. [106]. The initial conditions were T=800K, p=20 bar and Φ=1. With an increasing amount of n-heptane, the first-stage ignition grows stronger and the time-lapse until the second-stage ignition starts is seen to decrease

.

35

Chapter 4
Modeling of IC Engine Combustion

Modeling of IC engine combustion is a time consuming and a challenging task. Therefore, simplifications must initially be made to meet, e.g., the interest of the research area. Shown in Fig. 4.1, are some of the, according to the author, most important aspects of engine modeling that have to be addressed to provide predictable results and to be useful for understanding IC engine combustion. In this chapter these various aspects are discussed in relation to the work of this thesis.

I. The geometry changes due to valve motion during the intake and gas exchange process and due to the piston motion during the compression and expansion phase.

II. The spray and intake system generate turbulence, the former by rapid spray penetration and spray induced turbulence and the latter by large-scale structures such as swirl and tumble.

III. In direct injection engines the spray is injected into the engine cylinder at high speed and rapid transfer of momentum, heat and mass with the ambient air takes place.

IV. As described in Chapters 2 and 3, chemistry is manifested under a variety of conditions in IC engines and a suitable representation of the chemistry depending on the engine situation is crucial to predict the combustion event.
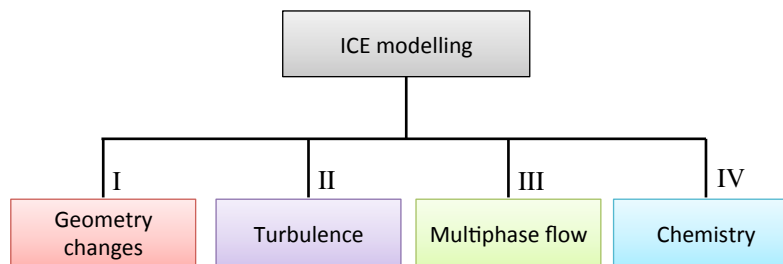
Figure 4.1. Some of the important aspects of ICE modeling that need to be considered for a realistic and physically correct prediction of the combustion processes; changing geometry, turbulence, multiphase flow and chemistry as well as these four constituents' interactions.

4.1 Geometry changes

In the current simulations finite volume (FV) discretization is employed to represent the engine cylinder configuration adequately. The choice of the finite volume approach comes from the standard implementation of the mesh generation in the CFD software [6] and, more importantly, to carefully represent the complex shape of the piston geometry. The complex shape of, e.g., the VOLVO D5 optical engine that is presented in a later chapter requires careful modeling of the complex wall boundary geometry. Different mesh motion methods can account for the piston movement, e.g., a dynamic mesh motion method, where a certain part of the cylinder is compressed by deformation of the cells, or by cell deactivation or cell add/removal layering methods, where cell-layers are removed or added during the simulations. It this work mainly the dynamic deformation approach of the cells is employed, primarily for practical reasons. The description of the deforming mesh motion solver is found in [109] and the description for the add/removal layering technique is found in [110].

The approach used in the present CFD solver is to utilize strictly polyhedral cells in the deformation region of interest. Thereafter the polyhedral faces are split into triangles and a centroid point is introduced. In this way tetrahedral cells are obtained. With identical face decomposition, the cells share an internal face. The mesh motion is described by the following equation

$$\nabla \cdot \left(\gamma \nabla \bar{u} \right) = 0 \tag{4.1}$$

where γ is a diffusion coefficient and $\bar{u}$ is the point velocity field that is used to modify the points position by

$$\bar{x}_{new} = \bar{x}_{old} + \bar{u}\Delta t \tag{4.2}$$

where $\bar{x}_{new}$ and $\bar{x}_{old}$ are the points position before and after the point motion and Δt is the time step. The known piston motion gives the boundary conditions for the engine simulations. This approach has shown to be time efficient and numerically stable. In the dynamic deformation approach of the mesh, a library of engine meshes is generated and the flow field is mapped to the new mesh when the aspect ratio in the deformed region becomes high.

4.2 Turbulence modeling

Turbulent flows involve structures over a wide range of scales in space and time, described in Chapter 3. In CFD simulations there are three main approaches that have emerged; direct numerical simulations (DNS), Reynolds averaged Navier-Stokes (RANS) simulations and large eddy simulations (LES).

4.2.1 Direction numerical simulation (DNS)

In the DNS framework, no modeling, no filtering and no averaging of the governing equations are performed. DNS resolves all of the turbulence scales, down to the smallest Kolmogorov scale, cf. Fig 4.2.
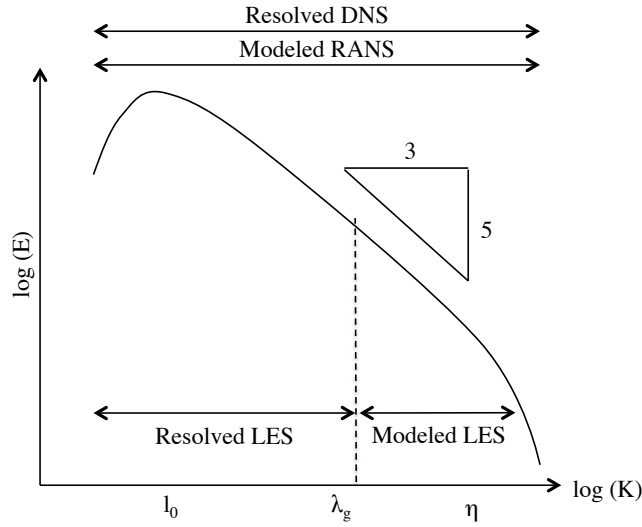
Figure 4.2. Schematic illustration of the resolved and modeled part of the turbulence kinetic energy spectrum in RANS, LES and DNS.

In fact, the grid size should be smaller than the Kolmogorov scale, $\Delta x < \eta$, and the entire computational domain should be of the size at least one integral length scale l_0. However, a larger domain with e.g., 4 integral length scales is preferable to include large-scale motion interactions and to reduce the influence of the boundary conditions.

With increasing turbulence levels the Kolmogorov length-scale decreases and a higher resolution is needed. If the domain is at least one integral scale l_0 of size, the minimum number of grid points n in each direction, so that $l_0 = n\Delta x$ (Eq. (3.10)), can be estimated as

$$n \geq \mathrm{Re}^{3/4} \qquad (4.3)$$

The computational effort scales with Re^3 and it quickly become apparent that DNS is restricted to low Reynolds-number applications. With multiple step chemical reactions, if chemistry is included, DNS is far from suitable in industrial applications.

4.2.2 Reynolds averaged Navier-Stokes (RANS) simulation

If the governing equations, Eqs. (3.1-3.4), are averaged in time, or cycle-averaged, the RANS equations are obtained. This is a more common approach for the modeling of internal combustion engines, as the ensemble results are sometimes more attractive for many problems instead of the turbulent fluctuations. It also turns out that the CPU cost is lower than for other approaches and for these reasons, RANS is the most applied CFD method for industrial use. Assuming a statistically stationary flow, a flow quantity ξ can be decomposed into the time, or ensemble, average, $\tilde{\xi}$ and fluctuation, ξ'', as

$$\xi = \tilde{\xi} + \xi''. \qquad (4.4)$$

The time average is defined as

$$\tilde{\xi} = \lim_{\tau \to \infty} \frac{1}{T} \int_{t_0}^{t_0+T} \rho \xi(t)\,dt \bigg/ \lim_{\tau \to \infty} \frac{1}{T} \int_{t_0}^{t_0+T} \rho\,dt \qquad (4.5)$$

where T is the time period of integration. The period is larger than the turbulence time-scales but smaller than the large-scale variations of the system. If the time average is performed on e.g., Eq. (3.2), the momentum equation, it yields

$$\frac{\partial}{\partial t}\left(\bar{\rho}\tilde{u}_i\right) + \frac{\partial}{\partial x_j}\left(\bar{\rho}\tilde{u}_i\tilde{u}_j\right) = -\frac{\partial \bar{p}}{\partial x_i} + \frac{\partial \bar{\tau}_{ij}}{\partial x_j} - \frac{\partial}{\partial x_j}\left(\overline{\rho u_i'' u_j''}\right) \qquad (4.6)$$

39

In the above formulation overtilde denotes density weighted average whereas overbar denotes standard time-average

$$\bar{\bar{\xi}} = \lim_{\tau \to \infty} \frac{1}{T} \int_{t_o}^{t_0+T} \xi(t) dt \tag{4.7}$$

The last term on the right hand side in Eq. (4.6) is the well-known Reynolds stresses that require closure since the velocity fluctuations are unknown. This term require modeling, which is done by expressing the Reynolds stresses as functions of the averaged flow variables. Solving the RANS equations is straightforward and the main limiting element is the turbulence models themselves and their range of applicability. The models may sometimes be less suitable if they are applied in an area for which they were originally not intended. The most famous turbulence model is the k-ε [111] model that is well practiced in engine simulations.

4.2.3 Large eddy simulations (LES)

In this thesis the large eddy simulations approach is employed. LES has been used recently in simulations of combustion in spark-ignition (SI) engines [112,113] to study the cycle-to-cycle variation in SI engines, in HCCI engines [68,114] and diesel engines [115]. Reviews on LES for ICE combustion can be found in [116,117]. Different from RANS simulations, in LES a spatial filter is applied to the flow field to separate the large scales from the small scales. From the Kolmogorov hypothesis, the large scales contain most of the turbulence kinetic energy and are considered to be the dominant scales of the flow. The small scales are considered universal and isotropic and their behavior is modeled, cf. Fig 4.2. The non-linear term that appears on the right-hand side of Eq. (4.6) when the momentum equation is spatially filtered is called the sub-grid scale (sgs) term, and requires closure.

In the LES framework, applying a spatial filter to the conservation equations, Eq. (3.1-3.4), with the additional spatially filtered mixture fraction equation, the filtered gas phase equations become

$$\frac{\partial}{\partial t} \bar{\rho} + \frac{\partial}{\partial x_i} \left(\bar{\rho} \tilde{u}_i \right) = \bar{S}_\rho^S \tag{4.8}$$

40

$$\frac{\partial}{\partial t}\left(\overline{\rho}\tilde{u}_i\right)+\frac{\partial}{\partial x_j}\left(\overline{\rho}\tilde{u}_i\tilde{u}_j-\overline{\tau}_{ij}+\tau_{ij}^{sgs}\right)=\overline{S}_{u_i}^{S} \tag{4.9}$$

$$\frac{\partial}{\partial t}\left(\overline{\rho}\tilde{Y}_i\right)+\frac{\partial}{\partial x_j}\left(\overline{\rho}\tilde{u}_j\tilde{Y}_i\right)-\frac{\partial}{\partial x_j}\left(\overline{\rho D_i\frac{\partial\tilde{Y}_i}{\partial x_j}}+\Phi_{Y_i}^{sgs}\right)=\overline{S}_{Y_i}^{S}+\dot{\omega}_i \tag{4.10}$$

$$\frac{\partial}{\partial t}\left(\overline{\rho}\tilde{h}\right)+\frac{\partial}{\partial x_j}\left(\overline{\rho}\tilde{u}_j\tilde{h}\right)-\frac{\partial}{\partial x_j}\left(\overline{\rho\alpha\frac{\partial\tilde{h}}{\partial x_j}}+\Phi_{h}^{sgs}\right)=\frac{\partial\overline{p}}{\partial t}+\overline{S}_{h}^{S} \tag{4.11}$$

$$\frac{\partial}{\partial t}\left(\overline{\rho}\tilde{Z}\right)+\frac{\partial}{\partial x_j}\left(\overline{\rho}\tilde{u}_j\tilde{Z}\right)-\frac{\partial}{\partial x_j}\left(\overline{\rho D_i\frac{\partial\tilde{Z}}{\partial x_j}}+\Phi_{Z}^{sgs}\right)=\overline{S}_{Z}^{S} \tag{4.12}$$

where the overbar denotes the spatial filtering

$$\overline{\phi(x,t)}=\int G(r,x)\phi(x-r,t)dr, \tag{4.13}$$

where the integration is over the entire field and the filter function G satisfies the normalization condition, $\int G(r,x)dr=1$. The overtilde denotes the density weighted spatial filtering, $\overline{\rho\phi}=\overline{\rho}\tilde{\phi}$, also called the Favre filtering. In Eqs. (4.8-4.12) ρ is the density; u is velocity, Y_i is the mass fraction of the i-th species; h is the enthalpy; $\dot{\omega}_i$ is the chemical reaction rate for the i-th species; Z is the mixture fraction; α and D are the diffusion coefficients of heat and mass. Superscripts s denotes the spray and sgs denotes the sub-grid scale variables. $\overline{S}_{\rho}^{s},\overline{S}_{u_i}^{s},\overline{S}_{Y_i}^{s},\overline{S}_{h_s}^{s}$ and $\overline{S}_{Z}^{s}$ are the spatial filtered source terms that account for the exchange rate of mass, momentum and energy between the gas and the liquid phases, $\overline{\tau}_{ij}$ is the filtered stress tensor obtained from the resolved strain rate $\tilde{S}_{ij}$ using

$$\overline{\tau}_{ij}=-\overline{p}\delta_{ij}+2\overline{\rho}\upsilon\left(\tilde{S}_{ij}-\frac{1}{3}\tilde{S}_{kk}\delta_{ij}\right). \tag{4.14}$$

where

41

$$\tilde{S}_{ij} = \frac{1}{2}\left(\frac{\partial \tilde{u}_i}{\partial x_j} + \frac{\partial \tilde{u}_j}{\partial x_i}\right). \tag{4.15}$$

The sgs-terms $\tau^{sgs}, \Phi_{Y_i}^{sgs}, \Phi_{h_s}^{sgs}$ and Φ_Z^{sgs} require closure and the latter three are modeled using gradient-diffusion

$$\Phi_{Y_i}^{sgs} = \bar{\rho}\frac{\upsilon^{sgs}}{Sc^{sgs}}\frac{\partial \tilde{Y}_i}{\partial x_j}, \ \Phi_h^{sgs} = \bar{\rho}\frac{\upsilon^{sgs}}{Pr^{sgs}}\frac{\partial \tilde{h}}{\partial x_j}, \ \Phi_Z^{sgs} = \bar{\rho}\frac{\upsilon^{sgs}}{Sc^{sgs}}\frac{\partial \tilde{Z}}{\partial x_j} \tag{4.16}$$

where $Pr^{sgs} = 0.7$ and $Sc^{sgs} = 0.7$ are the sub-grid scale Prandtl number and Schmidt number.

The eddy viscosity concept is historically well employed to close the sub-grid scale tensor τ_{ij}^{sgs}, primarily because of simplicity and due to its analogy with the molecular diffusion. In LES the role of the sub-grid viscosity is to dissipate the turbulence kinetic energy at the small scales and with a high resolution the sgs-stress should only have a minor impact on the results. Three common approaches to consider the dissipation of energy at small scales, one of which is used in this thesis, are described below.

4.2.3.1 Smagorinsky model

The Smagorinsky model adopts the eddy-viscosity concept

$$\tau_{ij}^{sgs} = 2\bar{\rho}\upsilon^{sgs}\left(\tilde{S}_{ij} - \frac{1}{3}\tilde{S}_{kk}\delta_{ij}\right) + \frac{1}{3}\tau_{kk}^{sgs}\delta_{ij} \tag{4.17}$$

where the effect on the resolved scales by the small-scales is considered as eddy viscosity. The eddy viscosity is written as

$$\upsilon_{sgs} = l_s^2\tilde{S} = \left(C_S\Delta\right)^2\tilde{S} \tag{4.18}$$

where $\tilde{S} = \left(2\tilde{S}_{ij}\tilde{S}_{ij}\right)^{1/2}$ and Δ is the filter width. The coefficient C_s is varied depending on the flow situation, e.g., $C_S = 0.17$ in high Reynolds-number turbulence in the inertial subrange [98].

4.2.3.2 Implicit LES (ILES)

The role of the eddy-viscosity sub-grid model is to dissipate energy, mostly at the smallest scales and with ILES it is argued that the numerical scheme could carry out this task. If the discretization scheme is of odd order, e.g., first order

$$\frac{\partial u}{\partial x} = \frac{u_{n+1} - u_n}{\Delta x} + \frac{\Delta x}{2} \frac{\partial^2 u}{\partial x^2} + hot \tag{4.19}$$

where the sub-script n is the cell number in the x-direction, Δx is the cell spacing and *hot* is the higher order terms. The lowest order term in the truncation error behaves as a dissipating diffusion term [5]. In ILES, such low order term resulted from the numerical scheme acts as an "artificial" viscosity.

4.2.3.3 One-equation eddy model

In pursuit of more accurate models that are able to capture non-local effects, the transport equations for the relevant variables are sometimes incorporated. In this work the sub-grid stress tensor is modeled with a one-equation eddy model

$$\tau^{sgs} = 2\bar{\rho}\upsilon^{sgs}\left(\tilde{S}_{ij} - 1/3\tilde{S}_{kk}\delta_{ij}\right) - 2/3\bar{\rho}k^{sgs}\delta_{ij} \tag{4.20}$$

with the sub-grid eddy viscosity modeled as $\upsilon^{sgs} = C_\upsilon \sqrt{k^{sgs}}\bar{\Delta}$ and the filter size $\Delta = V_{cell}^{1/3}$, where V_{cell} is the volume of the local cell. The advantage of the model is that it captures the effect of non-equilibrium between production/dissipation of kinetic energy in the sub-grid scales. This is important when high-Reynolds number flows have to be simulated using a relatively coarse grid resolution. The sub-grid scale kinetic energy k^{sgs} is obtained from a transport equation [118],

$$\frac{\partial}{\partial t}\left(\bar{\rho}k_{sgs}\right) + \frac{\partial}{\partial x_j}\left(\bar{\rho}\tilde{u}_j k^{sgs}\right) = \tau_{ij}^{sgs}\frac{\partial}{\partial x_j}\tilde{u}_i - D^{sgs} + \frac{\partial}{\partial x_j}\left[\bar{\rho}\frac{\upsilon^{sgs}}{Pr^{sgs}}\frac{\partial k^{sgs}}{\partial x_j}\right] + \dot{W}^S \tag{4.21}$$

43

where $D^{sgs} = C_\varepsilon (k^{sgs})^{3/2}/\overline{\Delta}$, $C_v = 0.05$ and $C_\varepsilon = 0.3$. $\dot{W}_s$ is the spray induced turbulence source term [119], which will be discussed below.

4.3 Multiphase flow and spray modeling

The spray breakup and vaporization processes undergo several steps. In Fig. 4.3 the classical description of the many regions of a disintegrating liquid spray discharging into an ambient environment is shown. Prior to the fuel injection discharge, the liquid experiences cavitation and bubble formation, which then collapses when exiting the nozzle, thus speeding up the disintegration process [120,121]. An intact liquid potential core exists only close to the nozzle, un-influenced by the shear layer, for a few nozzle diameters length [122].
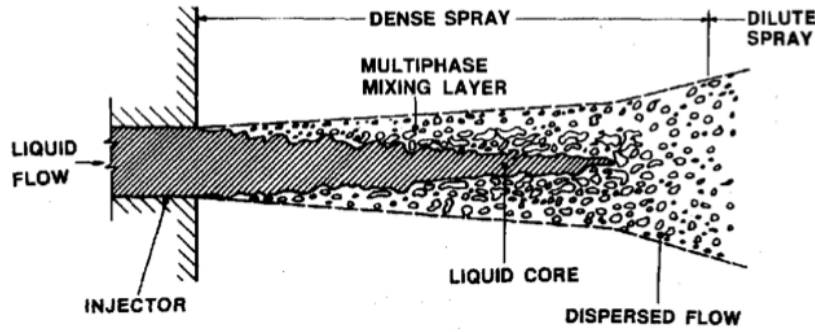

Figure 4.3. The illustration shows the different regions in a spray. The fuel is injected from the left, with a high liquid volume fraction for a few nozzle diameters downstream. Thereafter the liquid core breaks down due to instabilities and larger liquid ligaments are formed. The liquid ligaments further disintegrate into small liquid droplets and fully vaporize, as they are mixed with the ambient air. Reproduced from [123].

Whether an intact liquid core attached to the nozzle exists for the high-pressure injectors is still a question of research, but the extent of the dense spray region and multiphase mixing layer is believed to be limited. Downstream the region close to the nozzle is the so-called primary breakup region where large liquid ligaments are formed from the disintegration of the liquid fuel. Thereafter is the secondary breakup region where the liquid ligaments are broken up into small liquid droplets. The earlier

mentioned semi-empirical model of an equivalent gaseous jet has been compared with the liquid-length in diesel engine-type conditions and it is found that fuel vaporization is limited by the fuel and air mixing and air entrainment [14], and
not by the atomization process itself. However, the description may still be valid for certain pressure conditions.

In this work only the secondary breakup is taken into account to model the breakup process of the spray and the liquid fuel is represented using the Lagrangian particle tracking (LPT) approach. In LPT, a massive amount of individual droplets are modeled using a single parcel. Depending on the size-group of the droplets different parcels are tracked in the flow field. The parcels do not have a physical presence in the physical domain and are considered as mathematical source points. The parcels contain identical droplets, characterizing, e.g., the liquid fuel density and temperature. The equation of motion for a single parcel is

$$\frac{d}{dt}\bar{x}_p = \bar{u}_p \tag{4.22}$$

$$\frac{d}{dt}\bar{u}_p = \frac{C_D \operatorname{Re}_p}{\tau_p 24}\left(\bar{u}_g - \bar{u}_p\right) = \frac{C_D \operatorname{Re}_p}{\tau_p 24}\left(\bar{u}_{rel}\right). \tag{4.23}$$

Here $\bar{x}_p$ is the position vector of the parcel, $\bar{u}_p$ is the parcel velocity, $\bar{u}_g$ is the gas velocity, C_D is the drag coefficient acting on the fuel droplets, $\tau_p = d_p^2/18\bar{\upsilon}$ is the parcel characteristic time, where d_p is the diameter of the parcel and $\bar{\upsilon}$ is the gas-phase kinematic viscosity. The parcel Reynolds number is defined as $\operatorname{Re}_p = \left|\bar{u}_{rel}\right| d_p/\bar{\upsilon}, \bar{u}_{rel} = \bar{u}_g - \bar{u}_p$. The drag coefficient is obtained from

$$C_D = \begin{cases} \dfrac{24}{\operatorname{Re}_p}\left(1 + \dfrac{1}{6}\operatorname{Re}_p^{2/3}\right), \operatorname{Re}_p \le 1000 \\ 0.426, \qquad\qquad \operatorname{Re}_p > 1000 \end{cases} \tag{4.24}$$

The other forces acting on the droplet, the Basset force, the Magnus force, the Saffman force, the pressure and buoyancy force, are neglected. The breakup models are based on WAVE theory, e.g., Reitz and Bracco [124,125]. The models for heat and mass transfer are described in detail in [126] and are used to close the source terms,

45

$\bar{S}_{\rho}^{s}, \bar{S}_{u_{i}}^{s}, \bar{S}_{Y_{i}}^{s}, \bar{S}_{h_{s}}^{s}$ and $\bar{S}_{Z}^{s}$, on the right-hand sides in Eqs. (4.8-4.12). The spray modeling in the current simulations considers the coupling between the gas-phase and liquid-phase and not the interactions between the liquid droplets. Aside the LPT approach, there exists advanced Euler-Euler and multiphase surface tracking methods to represent the interaction between fluid and gas in an continuous description, such as the volume of fluid (VOF) method. These methods have been used for spray and cavitation modeling; however, they are time consuming and require more effort on the closure terms. These methods are not yet the common practice in spray modeling in IC engines.

An inherent problem with the LPT approach is the grid dependency. The numerical solution of the governing equations for the gaseous flow requires a fine resolution to reduce the discretization error and to resolve the flow, but the volume fraction of the particle in a certain cell must be small compared with the volume occupied by the gas phase. In the numerical simulations of a spray, the biggest error introduced in the LPT approach is in the very close nozzle region where the droplets have a large liquid volume fraction in a computational cell.

Jangi and Bai [127] studied the spray-induced turbulence in the LES spray framework. From Eq. (4.21) the spray-induced turbulence, SIT, $\dot{W}_s$ is modeled as

$$\dot{W}_S = \frac{1}{V_{cell}} \sum_p \left(m_p \frac{d}{dt} \bar{u}_p \right) \cdot \bar{u}^{sgs}, \qquad (4.25)$$

where the dot-sign denotes the inner product and $\bar{u}^{sgs}$ is the subgrid scale velocity vector, which is approximated as

$$\bar{u}^{sgs} = 2\tilde{\bar{u}} - 3\tilde{\tilde{\bar{u}}} + \tilde{\tilde{\tilde{\bar{u}}}} \qquad (4.26)$$

where $\tilde{\bar{u}}$, $\tilde{\tilde{\bar{u}}}$ and $\tilde{\tilde{\tilde{\bar{u}}}}$ are the Favre filtered velocity obtained from the solution of Eq. (4.8), and the double and triple Favre-filtered velocity vector, respectively. In Eq. (4.23) the relative velocity is not known and requires closure and in the same paper by Jangi and Bai [127], the O'Rourke model [128] to estimate $\bar{u}_{rel}$ was employed. The relative velocity is then written as

$$\bar{u}_{rel} = \tilde{\bar{u}} + \bar{u}'_p - \bar{u}_p \qquad (4.27)$$

46

where $\vec{u}'_p$ is a stochastic velocity vector accounting for turbulence dispersion of parcels via interaction with the surrounding gases. The velocity $\vec{u}'_p$ is assumed to follow a Gaussian distribution with standard deviation $\sigma = \sqrt{2k^{sgs}/3}$ and mean zero. Each component of $\vec{u}'_p$ is chosen randomly from a Gaussian distribution

$$G\left(\vec{u}_{p,i}\right) = \frac{1}{\sigma\sqrt{2\pi}} \exp\left(-\frac{\vec{u}_{p,i}^2}{2\sigma^2}\right),$$ (4.28)

where $\vec{u}'_p$ is chosen once per Eulerian time step. The model is referred to as the stochastic turbulence dispersion model, STD.

In a joint paper, the effect of the models on the fuel and air mixing process and on the liquid fuel behavior in a PPC engine was investigated. The PPC engine conditions were generated by a triple injection strategy during the end part of the compression stroke, between 50 and 5 CAD before TDC. The summary of the results in this investigation is presented in Chapter 6. It is found that when the STD model is excluded from the simulations, the prediction of the liquid fuel wall-wetting is higher compared with when STD is included. The effect of spray-induced turbulence, SIT, was found nearly negligible [129].

4.4 Modeling of turbulence and chemistry interaction

A challenge for LES and RANS of turbulent combustion is how to treat the right-most term in Eq. (4.10) namely, the chemical source term $\dot{\bar{\omega}}$. Different combustion models have been suggested depending on the flow situation and the scientific question of interest; such as the finite rate chemistry approach, the flamelet or progress variable approach or the mixing controlled combustion approach, the probability density function or conditional momentum closure methods, among others. The concept for some of the models is discussed here.

4.4.1 Combustion models

4.4.1.1 Finite rate chemistry modeling

The study of elementary reactions and their rates is the central task of chemical kinetics. In nearly all combustion processes chemical kinetics determines the pollutant formation and destruction. Adopting the notation from [104] the global reaction mechanism of a mole of fuel reacting with *a* moles of oxidizer forming *b* moles of products can be expressed as

$$F + a\text{Ox} \rightarrow b\text{Pr} \tag{4.29}$$

and occurs at a rate

$$\frac{d[X_F]}{dt} = -k[X_F]^n [X_{Ox}]^m \tag{4.30}$$

where [] denotes the mole concentration, m and n relate to the reaction order and k is the rate coefficient. Every global, or elementary, reaction has its own rate coefficient. The rate coefficient is strongly dependent on the temperature and the rate coefficient is expressed in the empirical Arrhenius form. The rate coefficient can be written as

$$k = k(T) = AT^b \exp\left(-E_A / R_u T\right) \tag{4.31}$$

where A is a constant pre-exponential factor, E_A the activation energy for the reaction, R_u is the universal gas constant, which is 8.314 J/Kmol, and T is the temperature. The activation energy and the pre-exponential factor are empirical parameters. It is useful to estimate the chemical time scale to compare with the mixing time scale in a practical application. Consider the elementary reaction,

$$A + B \rightarrow C + D \tag{4.32}$$

$$\frac{d[A]}{dt} = -k[A][B] \tag{4.33}$$

48

and choose t = τ_c to be the characteristic chemical time for the concentration A to be consumed and to reach the concentration A_0, which is 1/e of the initial value A. The characteristic time scale can then be expressed as [104],

$$\tau_c = \frac{\ln\left[e + (1-e)[A_0]/[B_0]\right]}{k\left([B_0]-[A_0]\right)}.$$

(4.34)

If the effect of turbulence is not included in the combustion modeling, apart from the filtered variables from the resolved flow, the chemistry source term is the same as the rate coefficient and in a single-step reaction becomes

$$\bar{\omega}_F = A\tilde{T}^b\left[\tilde{X}_F\right]^n\left[\tilde{X}_{Ox}\right]^m \exp\left(-E_A/R_u\tilde{T}\right)$$

(4.35)

This model is referred to as the kinetics only model (KOM). A drawback of the model is the lack of consideration of turbulence effect and the fine reaction layers that are unresolved.

The underlining assumption of KOM is that in a computational cell the species and temperature are assumed to be homogeneous so that there is no spatial variation of these quantities within the cell. For this reason sometimes KOM is also referred to as the well-stirred reactor model. This model is likely acceptable if the reactions are spread to wider regions in space. Several authors have compared the predicted ignition delay times of the engine combustion network (ECN) Spray A diesel flames using the KOM/well-stirred reactor model, transported probability density function (PDF) model, and interactive flamelet model [130-132]. It was found that the ignition delay times computed from the various models are in reasonable agreement with one another. This is likely due to that low temperature reactions during the ignition process are spread in wide region in the ECN spray A cases, as such KOM/well-stirred reactor model can be useful to predict the ignition process.

In most of the combustion process chemical reactions occur in thin layers, e.g., in flamelet combustion the thickness of the reaction layers is of the Kolmogorov length scale or less, which is much thinner than a typical CFD cell (except those in direct numerical simulations). This means that in the cell the volume of the reaction layer is only a fraction of the volume of cell. Thus, in the well-stirred reactor model or KOM the volume of the reaction layers is overestimated. On the other hand, in the thin reaction zones within the cell the species mass fraction and temperature are different

49

from those of the cell averaged ones, e.g., the cell averaged temperature is lower than that in the actual reaction layers. This will lead to an underestimation of the reaction rates in KOM.

There are various attempts to consider the fine reaction layers in the computational cells. Mathematically, one may write that

$$\bar{\omega}_F = \kappa \omega_F \left(\tilde{X}_F, \tilde{X}_{Ox}, \tilde{T} \right) \tag{4.36}$$

where $\omega_F \left(\tilde{X}_F, \tilde{X}_{Ox}, \tilde{T} \right)$ is the right hand term of Eq. (4.35) and κ is a segregation factor that expresses the influence of the fine reaction layers on the overall reaction rate in the computation cell [133]. The challenge lies now in the modeling of the segregation factor κ.

Eddy Dissipation Concept model is one of models of this type [134]. Chomiak and Karlsson [135] considered the segregation factor the volume fraction of the reaction layer in the cell. They assumed that κ is proportional to the ratio of the chemical reaction time (τ_c) to the total conversion time in the reactor, i.e., the sum of micromixing (eddy break-up) time (τ_m) and reaction time (τ_c), as given by

$$\kappa = \frac{\tau_c}{\tau_m + \tau_c} . \tag{4.37}$$

A recent development of this type of models is the work of Sabelnikov and Fureby [136], who used a multi-phase analogy to develop equations for computing the volume fraction of the reaction layers and the composition and temperature in the reaction layers.

The three-zone model of Colin and Benkenida [137] is another example that attempts to consider the inhomogeneity of composition and temperature in a computational cell. In the three-zone model the composition inhomogeneity in the computational cell is represented by three mixing zones: a pure fuel zone, a pure air plus possible residual gases zone and a mixed zone in which chemical reactions occur. A mixing model is presented which allows progressive mixing of the initially unmixed fuel and air. This model has been used to study diesel flames.

A different view of the existence of fine reaction layers is the following. The fine reaction layer is a result of inhomogeneity of composition and temperature in a coarse computation cell. Owing to the inhomogeneity, the hot products and reactive radicals in certain part of the cell would first be transported to the cold fuel/air mixture and then the fuel/air mixture would be ignited. The process can be simplified by introducing two time scales, one is the mixing time of the hot products/reactive radicals with the fuel/air mixture tm, and another is the time of chemical reactions tc. Kong and Reitz [138] used the following model to compute the mean reaction rate

$$\kappa = \frac{\tau_c}{f\tau_m + \tau_c}$$

(4.38)

where f is a parameter indicating the importance of the effect of the mixing time scale. With f=0 the model becomes KOM/well-stirred reactor. With f=1 the model becomes identical to the model of Chomiak and Karlsson [135].

4.4.1.2 Mixing-controlled combustion models

In certain situations the combustion process is limited by the mixing process. The eddy breakup model (EBU) and eddy dissipation model (EDM) are mixing-limited combustion models. The eddy breakup model was first proposed for premixed combustion by Spalding [139], based on the Kolmogorov energy cascade breakdown of turbulence eddies. In the model, a mixing time scale is estimated and the rate of consumption becomes

$$\bar{\omega}_p = -\rho C_{EBU} \left(\bar{Y}_F''^2 \right) / \tau_T$$

(4.39)

where C_{EBU} is a flow-specific constant, τ_T is the eddy turn over time and $\bar{Y}_F''^2$ is the variance of the fluctuations of the fuel mass fraction.

A similar model for non-premixed combustion proposed by Magnussen and Hjertager [140], is the eddy dissipation model (EDM). Here, the fluctuations are not required and as for the EBU model, the combustion rates are controlled by mixing between the fuel and oxidizer, i.e., the mixing time scales of the large eddies. Fuel and air appear intermittently and fluctuates and the rate-controlling species is the one in deficit, e.g., oxygen if the mixture is fuel rich. The rate of fuel consumption then becomes

$$\bar{\omega}_F \sim C_{EDC} \min\left(Y_F, Y_{O_2}/\gamma_{O_2}\right)/\tau_T \qquad (4.40)$$

where τ_T in Eq. (4.39) and (4.40) can be estimated as $\tau_T \sim k/\varepsilon,$ by using e.g., the k-ε model. The restriction here is the sensitivity to the modeling coefficient, which is varied depending on the flow situation.

4.4.1.3 The flamelet concept

If the reaction front in a turbulent flame is considered thin and the time scales of combustion is smaller than the time-scales for the smallest eddies in the turbulent flow, i.e. Ka < 1, an ensemble average of instantaneous laminar flame structures, known as flamelets, can be used to represent the mean turbulent flame. To track the flame front, an iso-surface, e.g., level-set G, or reaction progress variable in a premixed case and mixture fraction in a non-premixed case can be employed. Across the reaction front flamelet equations can be used. The flamelet equations describe the reactive and diffusive processes that occur near the flame front and once the location of the flame is known, the flame structures as described by using a pre-tabulated library. The reactions are tabulated from 1-D laminar flame simulations and therefore a very extensive reaction mechanism can be used at a very low cost [99]. The downsides of the model is that the flame chemistry is not dynamically coupled to the flow, the flamelet is restricted to low Karlovitz number flow situations and some considerations need to be done to calculate the correct turbulent flame speed. Despite this, different flamelet models, e.g., for turbulent premixed combustion the level-set G-equation flamelet model has successfully been validated in a range of conditions and in applications such as modeling of low-swirl lean premixed flames [141].

4.4.1.4 Thickened flame model (TFM)

A fundamental problem for LES and premixed combustion is the too coarse grid resolution used to resolve the flame front, hence the laminar flame speed and the rate of heat-release rate may become over or under-predicted. To circumvent this problem, Butler and O'Rourke [142], suggested that the reaction front could be resolved by spreading the flame over many cells by using a thickening factor, F, as long as the integrated heat-release and the ignition delay time were kept. In the approach, the

flame front wrinkling by the turbulent flow is reduced, i.e., the Damköhler and Karlovitz number changes, as the flame thickens. This is remedied by including an efficiency factor in the equations, [143], which is obtained, e.g., in DNS simulations to isolate the impact by flow vortices on flame speed and flame front curvature. The chemistry is represented by integration of the reactions rates and the final expression for the species transport equation fuel mass fraction, c, becomes

$$\frac{\partial \overline{\rho}\tilde{c}}{\partial t} + \frac{\partial}{\partial x_j}\left(\overline{\rho}\tilde{u}_j\tilde{c}\right) = \frac{\partial}{\partial x_j}\left(\overline{\rho}DF\Xi_\Delta\frac{\partial \tilde{c}}{\partial x_j}\right) + \frac{A}{F}\Xi_\Delta\rho\left(1-\tilde{c}\right)\cdot\exp\left(-E_A/R\tilde{T}\right) \qquad (4.41)$$

where Ξ_Δ is a wrinkling factor, D is the diffusion coefficient and F is the thickening factor.

4.4.2 On reaction mechanisms

Auto-ignition of hydrocarbon/air mixture is a complex chemical process, where a large number of species and reactions need to be solved for over a wide range of parameters, e.g., temperature and pressure. Numerical simulations of PRF-fuel employing 990 chemical species and 4060 elementary reactions have been carried out in constant-pressure and constant-volume conditions, e.g. [144,145], to capture ignition delay and the formation of important engine-related species, such as CO and UHC. The use of such detailed mechanisms in applied three-dimensional CFD simulations is too computationally costly, since each species requires a transport equation and the chemistry integration needs to be performed within each computational cell. Furthermore, if the intermediate species have a short lifetime, a restriction on the mathematical stiff solver can appear.

For this reason, three-dimensional CFD simulations resorts to reduced the reaction mechanisms. In particular, the reduced mechanisms are valuable for IC engine combustion modeling where large hydrocarbon fuels generally are employed. Mechanism reduction decreases the computational effort for the numerical simulations, and it becomes possible to study the few number of important kinetic parameters that influence the global properties of a flame, such as the burning velocity [146]. Automatic mechanism reduction and kinetic chemistry lumping is a field of its own [147]; however, the risk of too reduced mechanisms is the application window; which is usually restricted to a certain interval of, for instance, temperature, equivalence ratio and pressure.

In this thesis, primarily two mechanisms have been used to simulate the diesel engine and PPC engine combustion. For the diesel engine combustion the n-heptane mechanism of Rente et al. [148] has been employed and for the PPC engine combustion, the reduced PRF mechanism of Liu et al. [106] is used.

Comparison between the ignition delay time in shock tube measurement with the mechanism provided by Rente, 44 species and 174 reactions, exhibited good agreement for engine type conditions, p=41 bar and temperature ranging from approximately 600 K to 1500 K and equivalence ratio between 0.5 and 2.0. The mechanism furthermore agreed well with the ignition delay for the extensive n-heptane mechanism provided by [149], which consisted of 544 species and 2446 reactions. The PRF mechanism was developed for a range of conditions, with temperature ranging from 650 to 1250 K, pressure from 1 to 40 bar and equivalence ratio between 0.5 to 2, with specific emphasize on laminar flame speed prediction. The model was validated towards shock-tube, jet-stirred reactor, flow-reactor and HCCI experiments. In this work, the mechanism is employed for low-load conditions with equivalence ratios below 2 during combustion and with maximum cylinder pressure of 50 bar, which makes the mechanism suitable for its application. One of the biggest flaws of the mechanism is a consistent over-prediction of the CO-CO2 conversion [106].

4.4.3 Chemistry coordinate mapping (CCM)

As discussed above, there is a need for detailed kinetic mechanisms to properly predict the ignition delay by capturing the low, intermediate and high-temperature reaction chemistry for hydrocarbon fuel. Using extensive mechanisms is at a high cost and therefore in this thesis, a computational acceleration method, the so-called chemistry coordinate mapping (CCM) method is used [150-152]. The idea is to map the thermo-chemistry identical points/mesh cells in the physical space to a multidimensional phase space made up of temperature $\tilde{T}$, mass fraction of H-atom, J_H, and a logarithm function of the scalar dissipation rate, $\alpha_H = \log_{10}\left(\nabla J_H \cdot \nabla J_H + 1\right)$. The mass fraction of H-atom is defined as

$$J_H = \sum_{k=1}^{N} \frac{W_H}{W_k} \beta_{H,K} \tilde{Y}_k,$$ (4.42)

54

where W_H and W_k are the atomic and molecular weighs of hydrogen in the k-th species. The variable $\beta_{H,k}$ is the number of H-atoms in the k-th species and N is the total number of species in the mixture. The phase space intervals $\left(J_H, \tilde{T}, \alpha_H \right)$ is discretized uniformly into N_J, N_T and N_{α_H}, respectively. The (i,j,k) cell in the physical domain is mapped to the (l,m,q) zone into the $\left(J_H, \tilde{T}, \alpha_H \right)$ space. In the simulations carried out in this thesis, the resolution in phase-space is typically $N_J = 1000$, $N_T = 1000$ and $N_{\alpha_H} = 100$. The mean values of the variables in each phase space zone are determined and used as the initial condition for integrating the reaction rate at time t_n, i.e.,

$$\hat{Y}_k \left(l,m,q,t_n \right) = \frac{1}{N_c} \sum_{(i,j,k) \to (l,m,q)} \tilde{Y}_k \left(i,j,k,t_n \right), \tag{4.43}$$

where N_c is the total number of cells in the physical space that are mapped to the (l,m,q) zone. The error that arise from mapping the (i,j,k) cell is

$$\tilde{\varepsilon}_{\tilde{Y}_k (i,j,k,t_n)} = \frac{\left| \tilde{Y}_k \left(i,j,k,t_n \right) - \hat{Y}_k \left(l,m,q,t_n \right) \right|}{\hat{Y}_k \left(l,m,q,t_n \right)} . \tag{4.44}$$

The cells with an error $\tilde{\varepsilon}_{\tilde{Y}_k (i,j,k,t_n)} > \varepsilon_{acp}$, are treated separately in the phase space to ensure accuracy, where ε_{acp} is the largest acceptable error. In the simulations ε_{acp} is set as 10^{-4}. The mean reactions rates are then obtained by integration of the reactions rates in each phase space cell, which are thereafter mapped back to physical space.

In general, there are many cells in the physical space that can be mapped to a single cell in the phase space, which speed up the chemical reaction rate integration. The method has been applied to DNS simulations of premixed and partially premixed combustion [150], RANS spray simulations [22], LES of diesel engine combustion [115] and recently with a transport PDF method [153].

4.5 Strategy of this thesis

In summary, in this thesis the engine simulations are carried out using finite volume discretization of the engine geometry, employing Lagrangian particle tracking of the

liquid fuel, which considers the effect stochastic turbulence dispersion and spray-induced turbulence. The simulations are carried out with the chemistry CCM acceleration approach, employing extensive reactions mechanisms.

The finite volume approach is chosen for its flexibility to resolve complex piston curvatures and the LPT approach for its generally good approximation of the multiphase representation of the liquid fuel. The need of a well predicting model for the spray fuel is also indirectly coupled to chemistry, as chemical reactions proceed in the gaseous boundary layer surrounding the liquid fuel and between the liquid-length and the region for the onset of combustion.

LES is chosen instead of other methods for its predictability of fuel and air mixing, which is crucial especially when modeling partially premixed combustion engines. To predict the low-temperature, mid-temperature and high-temperature reactions, controlling ignition of direct injection and partially premixed combustion, well-defined chemistry reaction mechanisms must be employed. To the authors' knowledge, it is still not computationally affordable to employ detailed turbulence chemistry interaction model, such as the PDF method, in the LES framework with large reaction mechanisms. The combustion modeling approach chosen in this thesis is shown to function reasonable well to predict the onset of ignition and to capture all of the chemistry related phenomena prior to combustion.

56

Chapter 5
Numerical Method and Experimental Diagnostics Techniques

The governing equations mathematically describe the motions of fluids and are made up of a set of partial differential equations (PDEs). To solve the differential equations for 3-D spatial and time-dependent conditions one has to resort to numerical modeling using computers. The equations are discretized into algebraic equations and are solved on discrete points in space and time on a grid. When the equations are solved on a grid, they no longer have the exact solution as the original PDEs have, but the numerical solution should converge towards the exact solution when the grid resolution increases. Commonly the discretization is carried out with the finite difference (FD) or finite volume (FV) methodology and use polynomials to express the continuous variables. The finite difference approach is common for simple geometries and it provides high accuracy; however, the finite volume method can handle complex geometrical situations but at the cost of accuracy [5]. The finite volume method is also known as the control-volume method to which the conservation law is applied and it is the most common method in commercial software. In this work the open source CFD libraries of OpenFOAM [6] are used to carry out the flow simulations. The libraries offer compressible and incompressible flow solvers as well as reacting and non-reacting and multiphase flow solvers. The code written in a high level C++ language, and is open in the sense that users can manipulate and implement new solvers and models at their own will. Some of the mentioned models, such as the CCM model and stochastic turbulence dispersion models are not the standard implementation.

The mesh is generated using *blockMesh*, which is the standard grid-generation utility in OpenFOAM. The additional utility *snappyHexMesh* is used to extract complex shapes from the input surface file, of *stereolithographic* (STL) format. The initial surface file was typically a CAD-drawing of the engine and the STL-file was extracted by the software *Art of Illusion* [154]. A detailed procedure of the grid-generation method using snappyHexMesh is explained in [155].

57

5.1 Spatial discretization and temporal integration

The conservation laws of mass, momentum and energy are formulated in a control volume and the ensemble of all the control volumes makes up the computational domain. The computational nodes are located in the center of each control volume and this is where the flow variables, e.g., velocity and viscosity are defined. The transport equation for an arbitrary variable ξ as discussed in Chapter 4 can be written in conservative and vector form

$$\frac{\partial}{\partial t}\rho\xi + \nabla\cdot\left(\rho\tilde{u}\xi\right) = \nabla\cdot\left(\rho\upsilon\nabla\xi\right) + S_{\xi},\tag{5.1}$$

with ρ and $\tilde{u}$ the spatially filtered density and velocity vector, respectively, and υ the diffusion coefficient of ξ. The first three components in Eq. (5.1) corresponds to the time-derivative, the convective term and the diffusion term, and the term S_{ξ} can for instance represent a source term for spray evaporation. Integration of Eq. (5.1) in each control volume yields

$$\frac{\partial}{\partial t}\int_{V}\rho\xi\,dV + \int_{V}\nabla\cdot\left(\rho\tilde{\tilde{u}}\xi\right)dV = \int_{V}\nabla\cdot\left(\rho\upsilon\nabla\xi\right)dV + \int_{V}S_{\xi}dV\tag{5.2}$$

where V is the cell volume. Using Gauss theorem the integration can be written as

$$\frac{\partial}{\partial t}\int_{V}\rho\xi dV = \int_{S}\rho\xi\left(\tilde{\tilde{u}}\cdot\bar{n}\right)dS = \int_{S}\rho\upsilon\nabla\xi\cdot\bar{n}dS + \int_{V}S_{\xi}dV\tag{5.3}$$

where S are the faces, or surfaces, of each cell and $\bar{n}$ is the unit vector of the faces pointing outwards from the cell. The volume integration is carried out in the cell center point, C,

$$\frac{\partial}{\partial t}\int_{V}\rho\xi dV \approx \rho_{C}\xi_{C}\delta V, \quad \int_{V}S_{\xi}dV \approx S_{\xi,C}\delta V\tag{5.4}$$

where C denotes the cell center and δV is the volume of the cell. The surface integration for the convective fluxes becomes

$$\int_S \rho\xi\left(\tilde{\bar{u}}\cdot\bar{n}\right)dS \approx \sum_f \left(\rho\xi\tilde{\bar{u}}\cdot\bar{n}\right)_f \delta S_f \tag{5.5}$$

where f indicates that the quantities are evaluated at the cell face f and δS_f is the area of the face. In the same way the diffusion term becomes

$$\int_S \rho\upsilon\nabla\xi\cdot\bar{n}dS \approx \sum_f \left(\rho\upsilon\nabla\xi\cdot\bar{n}\right)_f \delta S_f \tag{5.6}$$

To calculate the variables and the gradient of the variables on the cell faces, interpolation from the dependent variables in the cell centers that share the face is needed. In the OpenFOAM libraries for unstructured grids, two cells only share one face.

5.1.1 Numerical schemes for the convective term

As an example, the discretization of the convection term Eq. (5.5) becomes

$$\int_S \rho\xi\left(\tilde{\bar{u}}\cdot\bar{n}\right)dS \approx \sum_f \left(\rho\xi\tilde{\bar{u}}\cdot\bar{n}\right)_f \delta S_f = \sum_f F\xi_f \tag{5.7}$$

where $F = \left(\tilde{\bar{u}}\cdot\bar{n}\right)_f \delta S_f$ is the mass-flux through the face. Now, the face field ξ_f is evaluated employing different schemes. For instance, assuming a linear relation for ξ and that two cells with cell center P and N share a face, a central difference scheme can be used

$$\xi_f = f_x\xi_P + \left(1-f_x\right)\xi_N, \tag{5.8}$$

where $f_x = \overline{fN}/\overline{PN}$ and $\overline{fN}$ is the distance between f and cell center N and $\overline{PN}$ the distance between P and N, cf. Fig. 5.1, which gives 2nd order accuracy. If the scheme is numerically unstable, some first order upwind can be blended with the 2nd order expression (at the cost of accuracy)

$$\xi_f = \xi_P \text{ if } F \geq 0 ; \xi_f = \xi_N \text{ if } F < 0 \tag{5.9}$$

59

such that the blended expression becomes

$$\xi_f = (1-\gamma)\xi_{f,upwind} + \xi_{f,central}$$ (5.10)

where γ is a weight factor between 0, more upwind, and 1, more central difference. In this work a blended-scheme, between 2nd order central difference and 1st order upwind in the spatial discretization is employed, weighted more towards 2nd order.
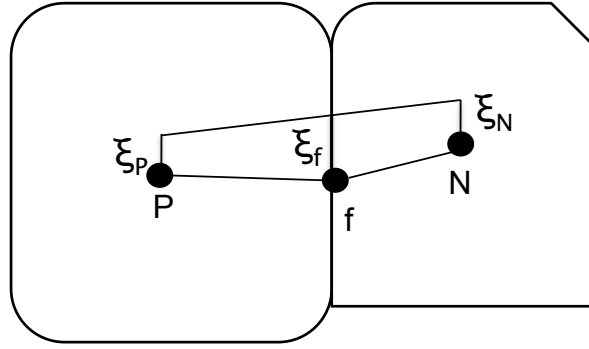

Figure 5.1. Sketch for the linear scheme.

A total variation diminishing (TVD) to calculate γ is used

$$\gamma = \max(\min(\beta r,1),0),$$ (5.11)

where r is the function

$$r = 2\frac{d_f \cdot (\nabla \xi)_i}{\xi_N - \xi_P} - 1.$$ (5.12)

with i=P for $F_f > 0$ and i=N for $F_f \leq 0$. The variable $\beta = 2/k$, where k is the user specified variable, $0 < k \leq 1$. If k=1, the discretization has a 1st order accuracy and if k=0, the discretization has a 2nd order accuracy. In this work, k was set to 0.1.

5.1.2 Numerical schemes for the temporal evolution term

In OpenFOAM the 1st order accurate time scheme is

$$\frac{\partial}{\partial t}\int_{V}\rho\xi\,dV \approx \delta V\frac{\partial\rho_C\xi_C}{\partial t} \approx \delta V\frac{\left(\rho_C\xi_C\right)^{n}-\left(\rho_C\xi_C\right)^{0}}{\Delta t} \tag{5.13}$$

and the 2nd order accurate backwards differencing scheme

$$\frac{\partial}{\partial t}\int_{V}\rho\xi\,dV \approx \delta V\frac{\partial\rho_C\xi_C}{\partial t} \approx \delta V\frac{\frac{3}{2}\left(\rho\xi\right)_C^{n+1}-2\left(\rho\xi\right)_C^{n}+\frac{1}{2}\left(\rho\xi\right)_C^{n-1}}{\Delta t} \tag{5.14}$$

where Δt is the time step; n+1, n and n-1 corresponds to variables in the future, the current and the past time, where the former is unknown and solved for. The 2nd order or 1st order temporal integration scheme is employed in this work, depending on the numerical stability of the simulations.

5.1.3 Pressure-velocity coupling

In OpenFOAM the pressure implicit with splitting of operators (PISO) algorithm has been used for the pressure-velocity coupling. If the semi-discretized form of the Navier-Stokes equations are considered one gets

$$a_P u_P = H(u) - \nabla p \tag{5.15}$$

where

$$H(u) = -\sum_{N}a_N u_N + \frac{1}{\Delta t}u_P^0 \quad . \tag{5.16}$$

Interpolating the velocity to the faces, with e.g., Eq. (5.15) one get

$$u_f = \left(\frac{H(u)}{a_P}\right)_f - \left(\frac{1}{a_P}\right)_f\left(\nabla p\right)_f \tag{5.17}$$

and the flux becomes

$$F_f = S_f \cdot u_f = S_f \left[\left(\frac{H(u)}{a_P} \right)_f - \left(\frac{1}{a_P} \right)_f (\nabla p)_f \right].$$ (5.18)

Thereafter it the follows from the continuity equation that

$$\sum_f S_f \cdot \left[\left(\frac{1}{a_P} \right)_f (\nabla p)_f \right] = \sum_f S_f \cdot \left(\frac{H(u)}{a_P} \right)_f.$$ (5.19)

The steps in the PISO algorithm are found in Issa [156]

1. Predictor step: Eq. (5.15) is solved for an estimate of the velocity field, using the previous time pressure field.
2. H(u) is recalculated with the new velocity field in Eq. (5.16).
3. Eq. (5.19) is used to solve the pressure field.
4. The fluxes in Eq. (5.18) are updated and u_P is updated using Eq. (5.15)
5. Possibly repeat step 2.

5.2 Initial and boundary conditions

IC engine modeling requires some specific initial and boundary conditions. Certain initial and boundary conditions that are typical for engines are,

- intake temperature
- intake pressure
- wall-temperatures
- swirl-level and turbulence field
- EGR level
- temperature and the species constituents of the recirculated gas
- hot-burnt residual products levels
- temperature and constituents of the hot-burnt residual products

62

and typical conditions for DI engine simulations are e.g.,

- amount of the injected fuel
- temperature of the injected fuel
- timing of the injected fuel and
- the mass-flow rate profiles of the injected fuel.

Most of the simulated cases in this thesis have been carried out in optical engines; without EGR for the HD diesel engine simulations and with some dilution for the optical LD PPC engine. The HD PPC engine simulations employed EGR.

In performing the simulations, one of the assumptions was how to treat the wall-temperatures for the optical piston glass, which are known to behave differently from the engine metal walls. The different behavior is manifested in e.g., different heat-conductivities and adiabatic behavior of the quartz glass. Also, the compression ratio is different from the metal engines and the crevice volumes are sometimes larger, e.g., for the VOLVO D5 engine.

The second assumption concerns the fuel mass-flows rate profiles. For the HD diesel engine experimental investigations, which are summarized in the next chapter and found among the published papers, the mass-flow rate profile was measured and used as the inflow condition. For the LD PPC engine configuration, however, the duration of the injection pulses were on the order of 2-3 CAD, at a 500 bar injection pressure. The fuel injection rates for these conditions were not known and were assumed to follow a top-hat function or a triangle function.

The geometrical compression ratio from the experiments and the actual compression ratio during combustion can differ and to account for this, one approach in ICE modeling is to adapt the squish volume or the crevice volume to get the right compression ratio. Another approach is to keep a constant squish height and instead vary the intake pressure or intake temperature. In this work effort has been to have an as correct as possible thermochemical condition at the relevant instances, e.g., during the injection and combustion event.

In this work the intake and exhaust valves are not considered. To account for the large-scale motions that are generated during the intake process, e.g., the swirling flow, a solid body rotational motion is set at 180 CAD before TDC, or at IVC. The swirl is turned to comply with the experimental condition. In this work mainly diesel engines

63

are used and the swirl is considered to be the main large-scale motion. The swirl velocity is modeled with a Bessel function across the bore with non-slip conditions on the cylinder-wall. The swirl level is related to the engine RPM.

The HD PPC engine simulation was carried out with 50% EGR. The constituents of the EGR were calculated assuming 100% combustion efficiency and residual gas constituents of water, carbon dioxide and nitrogen. In case of the optical LD PPC engine, 10% hot-burned products were considered in the initial gas composition, consisting of N_2, O_2, CO_2 and H_2O. This was a result of 60 CAD NVO. In all other situations, air or nitrogen was used as the ambient gas.

5.3 Laser diagnostic methods

With the use of optical laser diagnostic techniques, non-intrusive measurements can be performed to study the mixing and combustion processes in the IC engines. Some of the methods to visualize the IC engine processes are the structured laser illumination planar imaging (SLIPI), fuel-tracer planar laser induced fluorescence (PLIF) and OH-chemiluminescence. A brief description of the methods is given below.

5.3.1 PLIF

Planar LIF is used to measure the fuel distribution in an IC engine and it is a 2D optical diagnostic technique to visualize certain species in a flow. The idea of LIF is that every species have a unique spectral fingerprint that can absorb and re-emit photons (fluoresce) at a chosen wavelength. The photons are recorded with a specific band-pass filter for the camera to reduce interference from e.g. soot luminescence and scattered light. Most commercial fuels contain several species that can fluoresce upon UV excitation and can thus be used for LIF measurements to investigate the fuel distribution. However, with several species affecting the signal, quantitative results of the flow variables, e.g., the local equivalence ratio, becomes difficult. For quantitative measurements a fluorescent tracer with well-known optical characteristics can be added to the fuel. More information on PLIF and fuel-tracer PLIF can be found in [157].

64

5.3.2 SLIPI

Quantitative fuel-tracer LIF experiments are difficult to carry out in IC engines, due to, e.g., background scatter that will give rise to secondary fluorescence and thus inaccuracy of the results. With SLIPI, the effect of background scattering is removed by using laser sheets modulated with some pattern, e.g., a sinusoidal pattern. By using three measurements with different phases, it is possible to reconstruct the original image while removing the background noise. More information about SLIPI can be found in [158].

5.3.2 OH-chemiluminescence

Using only an intensified CCD camera with a filter over a selected wavelength, e.g., 310 nm for OH, photon emissions are detected. The detected species are those excited by heat, which emit a photon in the return from the excited state to the ground state. OH-chemiluminescence is significantly weaker than PLIF and SLIPI. The source of the chemiluminescence is spread throughout the domain and the obtained signal is the integrated signal from the entire axis of observation, opposite from SLIPI and LIF where the signal is from a two-dimensional laser sheet. The straightforward approach of the technique is an advantage and it is relatively cheap compared with other methods.

Chapter 6
Summary of Results and Publications

The first part of this chapter gives a summary of the spray modeling in a constant-volume chamber. Thereafter the models are used to investigate mixing processes in a light-duty PPC engine, under non-reacting conditions. The second part deals with diesel engine modeling, employing both non-reacting and reacting simulations to investigate e.g., the effect of the inter-jet angle on the fuel and air mixing process and the lift-off length. In the third part, the structure of partially premixed combustion is studied in a light-duty PPC engine. The behavior of the PPC combustion process and the sensitivity to injection strategies and temperature are discussed. In the chapter the papers listed in the appendix are briefly discussed, where the author's contribution to the papers are stated

6.1 Spray modeling

Spray modeling is a challenging task since the liquid breakup process involves a range of time-scale and length-scales. The simulated spray is generally compared with the global experimental features, such as the liquid-length and the vapor-phase fuel distribution surrounding the spray; however, the inner structures of the spray are not known in the experiments. Therefore, even if the model captures the global behavior of the spray, it does not necessarily mean that the model assumptions are correct. It therefore becomes important to have a spray model that behaves consistently under varying injection conditions. One common approach for spray modeling in IC engines is the LPT approach, discussed in Chapter 4. The LPT model gives a simplified description of the spray and has shown to work well under many simulated flow and combustion conditions.

In the LES-LPT framework, one must consider that LES require a high resolution, whereas LPT was developed for dilute conditions. This means that the LPT approach is not consistent when the volume fraction of a liquid particle is large in comparison with the gas-phase volume fraction, in a computational cell. The biggest error from the LPT model in spray-simulations appears near the nozzle, where the liquid volume fraction is high. The error decreases downstream the nozzle due to the efficient fuel and air

66

mixing, which breaks up and evaporates the liquid fuel and the liquid-volume fraction decreases.

Motivated by theses issues, the importance of the spray-induced turbulence model (SIT) and the stochastic turbulence dispersion (STD) model has been investigated for spray simulations employing the LES-LPT method. Furthermore, the feasibility of a consistent Eulerian-Lagrangian approach with improved results as the grid resolution increases was examined. For this purpose, the impact of the models and the grid resolution was investigated for constant-volume non-reacting spray conditions. Thereafter, the performance of the models were investigated in non-reacting spray simulations of a light-duty PPC engine, operating with a triple-injection strategy. The details of this work are found in Paper II and the SIT and STD models are described in Chapter 4.

The constant-volume simulations were based on the ECN spray-A conditions, see ref. [7]. The STD and SIT modes were tested for three grid resolutions; $0.5, 0.25$ and 0.125 mm.

Overall, including the SIT model was found to hardly affect the vapor-phase fuel distribution, or the prediction of the vapor-phase fuel penetration and liquid-length, cf. Figs. 2 and 5, in Paper II. Furthermore, the SIT model does not significantly affect the exchange rate of momentum, heat and mass between the gas and liquid-phase, seen by the axial mass-flow rate in Fig. 6.1.1. In the figure, the slope of the curve indicates the rate of air entrainment. In the figure the impact of the SIT model is seen to be small.

In comparison, the effect of the STD model is distinctly seen for the prediction of the vapor-phase fuel penetration and liquid-length compared with the experiments, cf. Fig. 7 in Paper II. Furthermore, the exchange rate is seen to be significantly affected when the STD model is not included, which impacts the rate of air entrainment. This is presented in Fig 6.1.1. As a consequence of the erroneous prediction of the exchange rates between droplets and gas phase, the vapor-phase fuel distribution becomes different compared with when STD is included. This is seen by a plateau shape of the mixture fraction distribution, cf. Fig 9d, in Paper II.

The results were found to be fairly sensitive to the grid resolutions, however, comparable for the 0.25 mm and 0.125 mm resolutions. A resolution of 0.5 mm was found to be too coarse to capture the structure and behavior of the flow, e.g., the

prediction of axial mass flow, cf. Fig 6.1.2, regardless if the SIT and STD models were included.
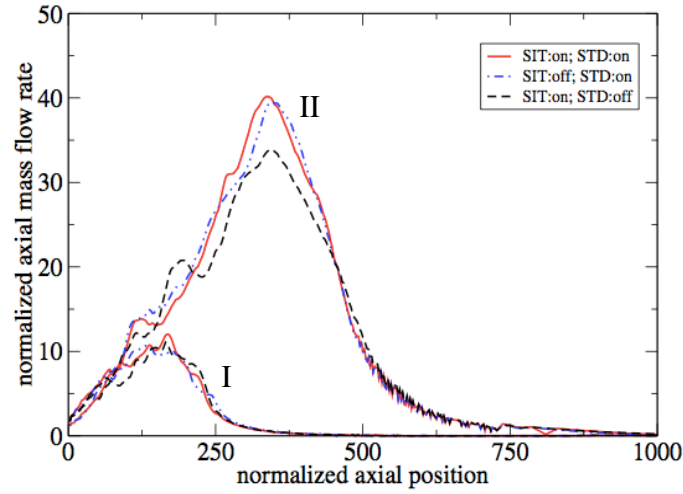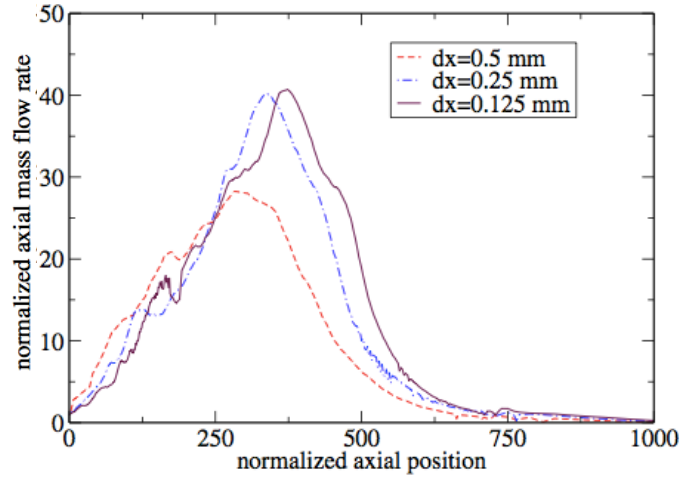

Figure 6.1.1. Axial gas-phase mass flow rate along the axial positions normalized with the nozzle diameter d=0.09 mm, at 0.3 ms (I) and 1.5 ms (II). The red lines correspond to when both the SIT and STD models are "on", the blue lines correspond to when SIT is "off" and STD is "on", and the black lines correspond to when SIT is "on" and STD is "off".

Case	STD	SIT
1	On	On
2	On	Off
3	Off	On

Table 6.1.1. Simulated cases in the light-duty PPC engine.

These conclusions were used to perform simulations of a VOLVO D5 light-duty PPC engine with a triple injection strategy. The studied cases are shown in Table 6.1.1 and the specifics are found in Paper II.

Figure 6.1.2. Axial gas-phase mass flow rate along the axial positions normalized with the nozzle diameter d=0.09 mm, at 1.5 ms, for the three grid resolutions.

The fuel injector has five holes and employed a 140° umbrella angle. The simulations were done in a sector mesh resolving one injector, which was 72° of the entire cylinder geometry, cf. Fig 6.1.3. The aim of this work was to investigate the effect of the STD and SIT models on the liquid fuel behavior and the in-cylinder fuel and air mixing process. The injection strategy is similar to the one described in Paper VIII.

In Fig. 6.1.4 an image sequence of the morphology of the liquid-fuel injection processes is shown with the engine geometry for the three cases:

- When the STD model is not included, the fuel spray from the first injection is dense in the tail and does not convey small particles surrounding the tip of the spray near the wall, compared with when the STD model is included. Furthermore, after the end of injection, liquid particles reside in the vicinity of the impingement zone longer than for case 1 and case 2. A clear difference for the liquid behavior between case 1 and case 2 is not discernable.

- The effect of the STD model becomes even more apparent for the second injection. A large portion of the liquid fuel impinges the wall when the STD model is not included and can still be seen at the start of the third injection. A

69

clear difference for the liquid behavior between case 1 and case 2 is not seen for the second injection.

- The same trend is seen for the last injection as for the first two injections, when the STD model is not included. The injected fuel quickly evaporates for case 1 and case 2.
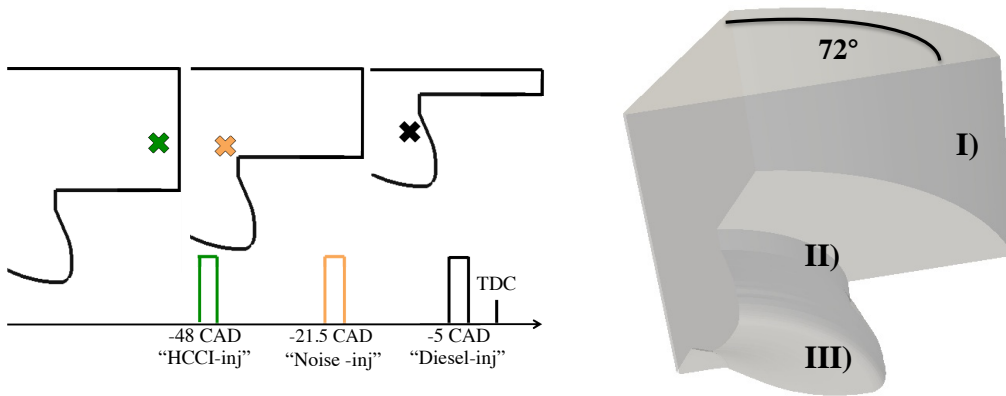
Figure 6.1.3. The triple-injection strategy (left) and the sector mesh geometry (right)

The effect of the SIT and STD models on the fuel and air mixing process is represented by a probability plot of mixture fraction, shown in Fig. 6.1.5, at 5 CAD aTDC. Small variations of the mixture distributions are seen when SIT is not included compared with when SIT included, however, obvious differences are observed between the distributions when the STD model is not included. In the plot is it not possible to trace the fuel to each individual injection. It is, however, reasonable to believe that the rate of air entrainment is slower when the STD model is off, as predicted by the simulations in the constant-volume chamber. In such case, the fuel spray reaches the wall faster and impinges to the wall at a greater speed. When the STD model instead is included, the fuel and air mixing occurs faster, thus leading to a faster decelerating fuel spray

and to forming richer fuel mixtures.

STD/SIT on/on   STD/SIT on/off   STD/SIT off/on

21 CAD before TDC

47 CAD before TDC

46 CAD before TDC

20 CAD before TDC

45 CAD before TDC

19 CAD before TDC

4 CAD before TDC

44 CAD before TDC

3 CAD before TDC

40 CAD before TDC

2 CAD before TDC

5 CAD after TDC
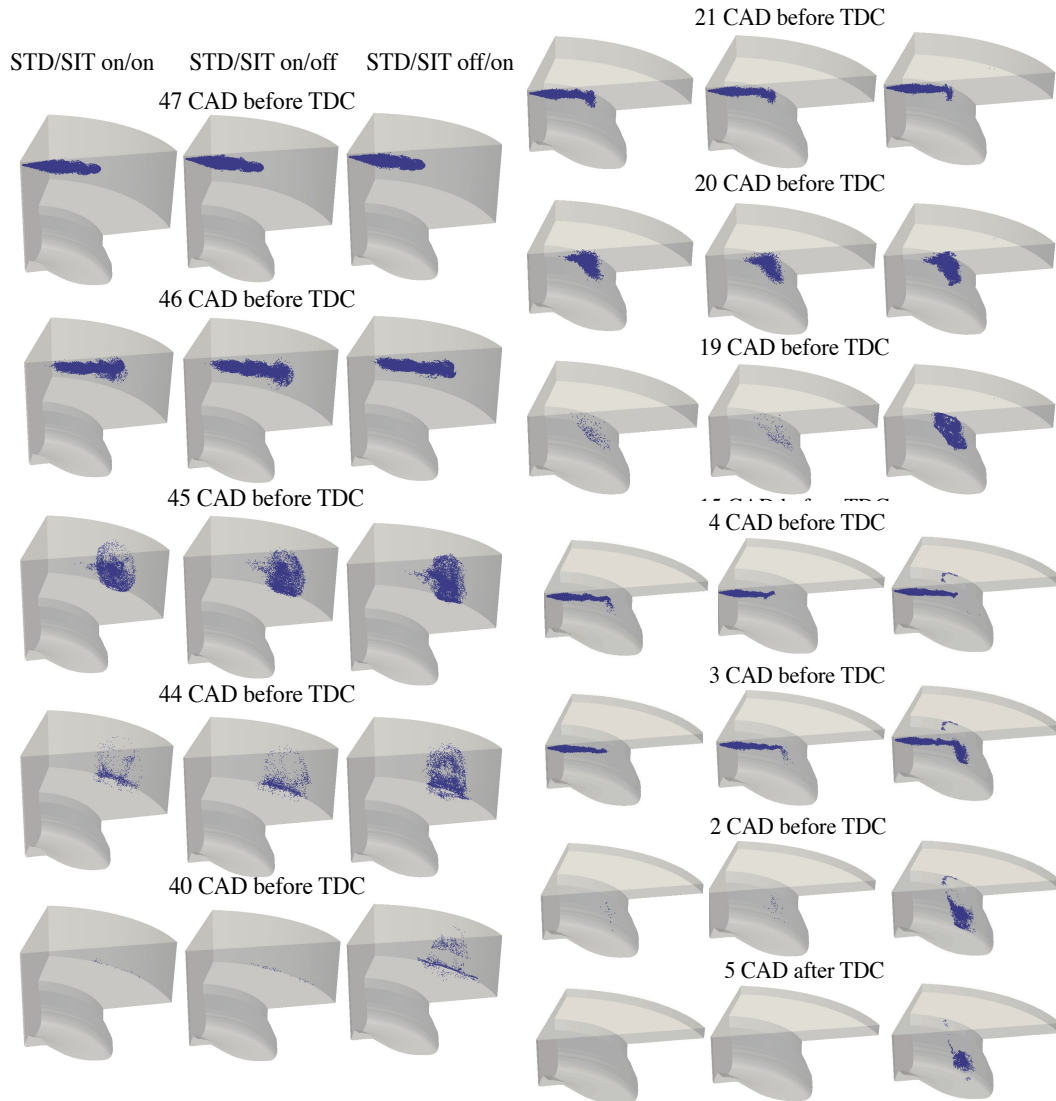
Figure 6.1.4. Liquid particles, shown in blue, are seen to impinge the engine bowl. The results appear independent of the (SIT) model; however, it is very sensitive to the (STD) model.

71

Fig. 11 in Paper II shows the pressure-trace comparison between experiments and numerical simulations for a reacting condition. From the comparison of the probability distribution when STD is off and on, it is reasonable to believe that neglecting the STD model under reacting conditions would fail to predict the combustion phasing for the employed strategy.
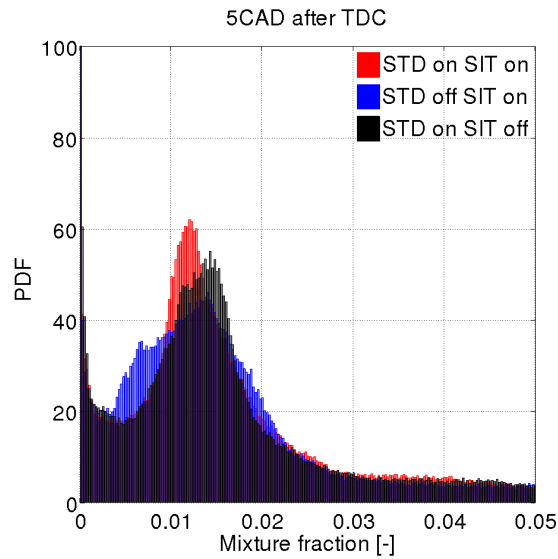
Figure 6.1.5. Fuel and air mixture distributions for case 1-3, at 5 CAD aTDC. The instance corresponds to the combustion phasing in the experimental engine

The results of the engine test case may be summarized as follows: The simulations show a low sensitivity to the SIT model, however, a high sensitivity to the STD model, with respect to the liquid-fuel behavior and mixture distribution. When STD is not included in the simulations, liquid fuel impinges and resides in the wall region during the rest of the compression stroke. This is likely due to an under-prediction of the rate of air entrainment, causing a main portion of the fuel to remain non-vaporized. This leads to a fuel and air mixture distribution different from when STD is considered in the simulations, since the fuel that is yet to evaporate does not participate in the mixing process. At the instance of combustion phasing a higher probability of fuel lean mixture and lower probability of fuel rich mixture is obtained when STD is not included, compared with when STD is considered. This indicates that the combustion phasing may be hard to predict if the STD model is not included.

72

The results of the spray modeling can be summarized:

The results are sensitive to the grid resolution despite the SIT and STD model; however, the liquid-length, vapor-penetration distance and vapor-phase fuel distributions are similar for the 0.25 mm 0.125 mm resolution, when the STD model is included. A resolution of 0.5 mm was found to be too coarse to resolve the structures of the flow and to capture the exchange rates of momentum, heat and mass. This was regardless if the STD and SIT models were included

The SIT model was found to hardly affect the results, neither in the constant-volume simulations nor in the PPC engine simulations.

It is found that the STD model is necessary to predict the exchange rate of momentum mass and heat near the nozzle. If the STD model is not included, the predicted fuel and air mixture distribution drastically changes. Furthermore, if the STD model is excluded in the PPC engine simulations, considerably higher spray is found near the wall. This may lead to an incorrect prediction of the fuel and air mixture distribution for simulations under reaction conditions. In conclusion, the STD model should be included in the simulations of fuel spray injection.

6.2 Diesel engine simulations

Non-reacting conditions

In one part of the diesel engine simulations of this work, the effect of the diesel injection inter-jet angle, i.e. the distance between the holes on the injector, on the equivalence ratio in the near-wall recirculation zone has been investigated. The equivalence ratio in the recirculation zone is believed to impact the soot oxidation and it has thus been the focus of recent experimental activities.

One of the controlling mechanisms to reduce soot emissions is the late-cycle oxidation. To enhance soot oxidation, oxygen must be readily available to the fuel-rich zones during the piston expansion phase. Owing to this, an experimental study to examine the equivalence ratio in the near-wall recirculation zone under different injection pressures and inter-jet angles was conducted. In the work, two mechanisms were suggested to determine the equivalence ratio in the near-wall recirculation zones; either the jet momentum that was generated by the spray that affects the jet-wall impingement, or

the injector nozzle-configuration. For three different injection pressures, a negligible impact on the equivalence ratio in the recirculation zone was found. This suggested that the effect of the nozzle-configuration had a larger impact on the leaning-out process of the fuel wall-jets, compared with the injection pressure. A thorough description of the background of this work can be found in Paper VI.
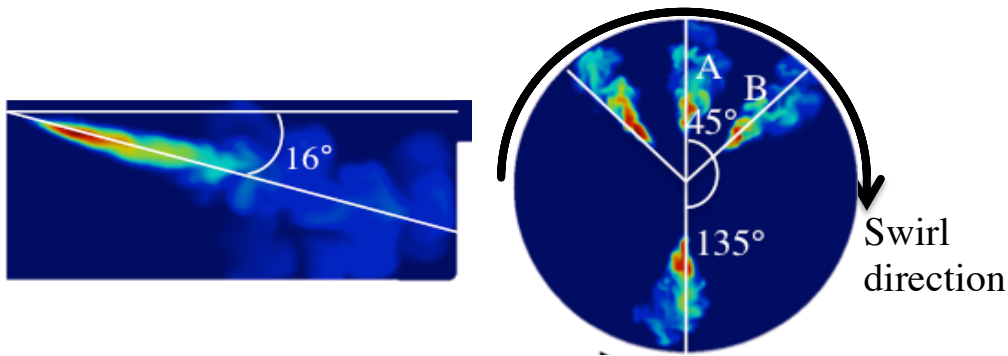

Figure 6.2.1. Instantaneous snapshot of the mixture fraction field with the nozzle configuration together with the swirl-direction and injection angle to fire-deck.

To further investigate this effect, LES was performed to look into more details about the physics of the fuel spray-injection and wall-jet mixing processes. Specially, the equivalence ratio and rms of the velocity fluctuations in the jet impingement region and the near-wall recirculation region were investigated, using statistical analysis of the LES data. The effect of the mass-flow rates and the air entrainment prior to the wall impingement were also analyzed. Two fuel injection pressures, 2000 bar and 2500 bar were studied for a constant swirl level, 0.5, and with the inter-jet angles, 45° and 135, cf. Fig 6.2.1.

The LES of the equivalence ratio is performed in the near-wall region of jet A and in the recirculation zone between jet A and jet B, cf. Fig. 6.2.2. With the LES, the same levels of the equivalence ratio were observed in the jet-wall impingement region for the different injection pressures. The jet velocity is higher when the injection pressure increases, and thus also the rate of air entrainment is increased. To have the same injection duration, more fuel mass is injected for the case with a higher injection pressure. In the experiments the equivalence ratio in the recirculation zone was found to be independent of the injection pressure. This trend is captured by the LES, shown

74

in Fig. 6.2.2. From the LES, the rms-values of the velocity-fluctuations in the recirculation zone were seen to be larger for the higher injection pressure, however, compared with the lower injection pressure.

Similar analysis was performed to examine the effect of the injection pressure on the equivalence ratio in the impingement point and recirculation zone for jet C, cf. Fig 6.2.1. The equivalence ratio of jet C prior to wall-impingement was found independent of the injection pressure and yielded equivalence ratios similar to jet A. However, a higher injection pressure exhibited a lower equivalence ratio in the recirculation zone, compared with a lower injection pressure, seen in Fig. 6.2.3.

The two observations described above can be further discussed.

First, the equivalence ratios are found to be the same for the two injection pressures at the impingement point. This is explained by the more injected fuel mass from the higher injection pressure and a higher rate of air entrainment, compared with the low injection pressure.

Second, the equivalence ratio in the recirculation zone for jet A and B is the same for the two injection pressures. This is due to the nozzle-configuration, which limits the availability of the fresh air for the incoming fuel-jet to mix with. For jet C, a higher injection pressure yields a lower equivalence ratio in the recirculation zone. For the higher injection pressure case, the rms-fluctuations were found higher and the mixing process with the fresh air is not interfered by an adjacent jet.
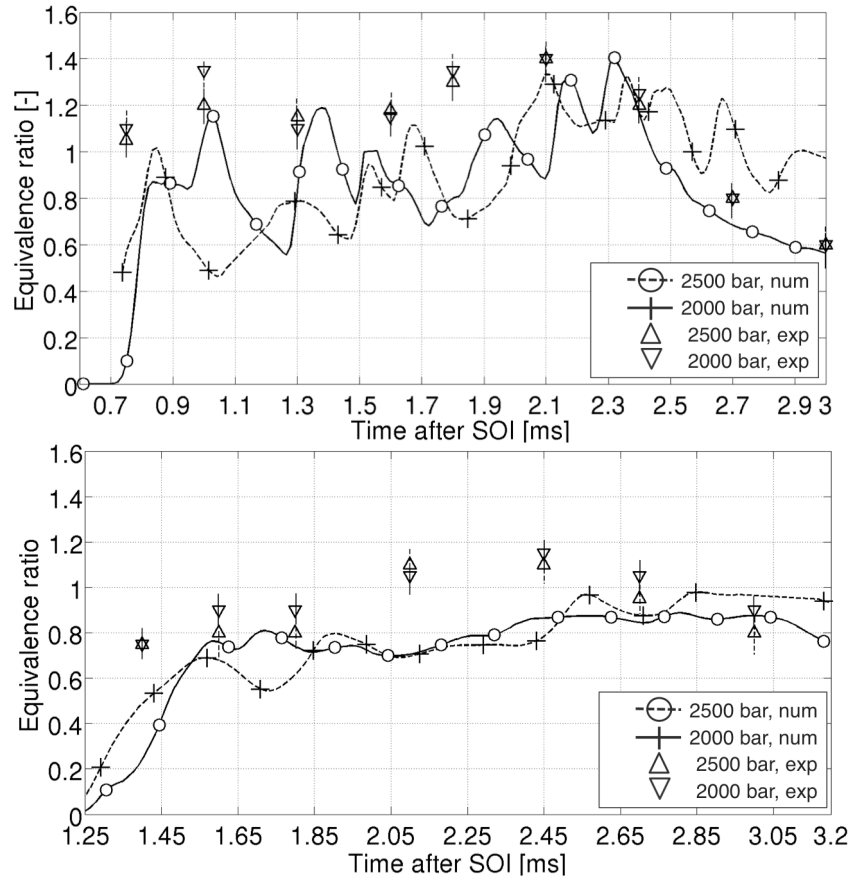
Figure 6.2.2. Predicted equivalence ratio from the LES in the impingement region for the jets A and B, injected at 2000 and 2500 bar (above) in comparison with the experimental data. The same injection conditions are compared with experimental data in the recirculation zone data (below).
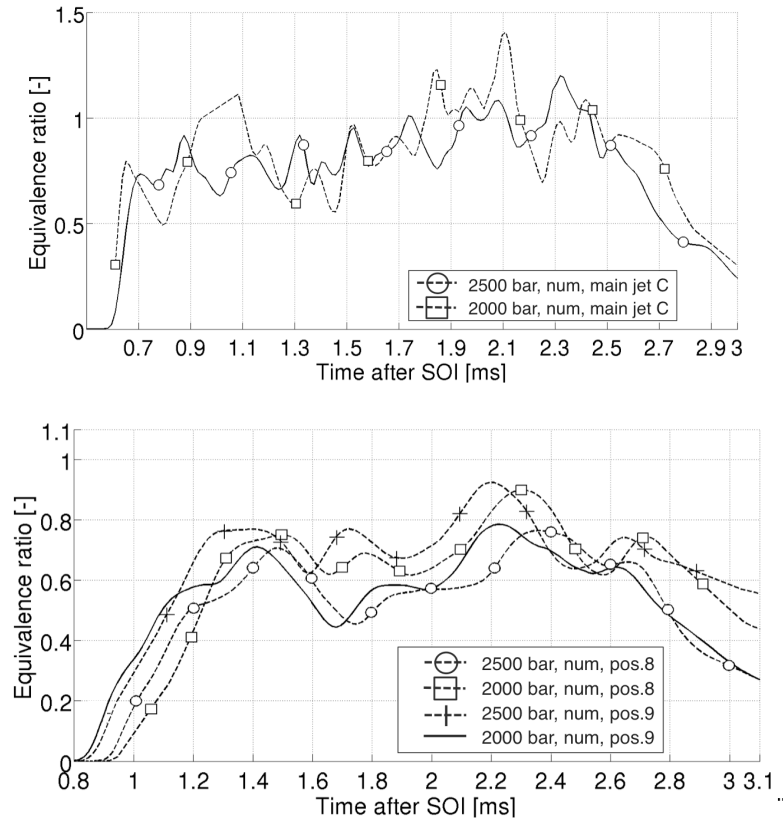
Figure 6.2.3. Predicted equivalence ratio from the LES in the impingement region for the jet C injected at 2000 and 2500 bar in the main jet (above) and in the recirculation zone (below).

Reacting conditions

In the second part of the work on diesel engines simulations, the effect of the inter-jet angle on the lift-off length is examined. In a recent experimental study, the lift-off has been shown to decrease with decreasing inter-jet angle. This may influence the air-entrainment into the fuel jet and therefore also the soot formation downstream the lift-off location.

For this reason, a joint study with the aim to investigate the effect of the inter-jet angle and the engine swirling flow on the auto-ignition and lift-off behavior for multiple fuel jets was performed. The goal of this study was to improve the knowledge of the fundamental processes that occur in diesel combustion engines, which cannot be studied in constant-volume chamber quiescent conditions.
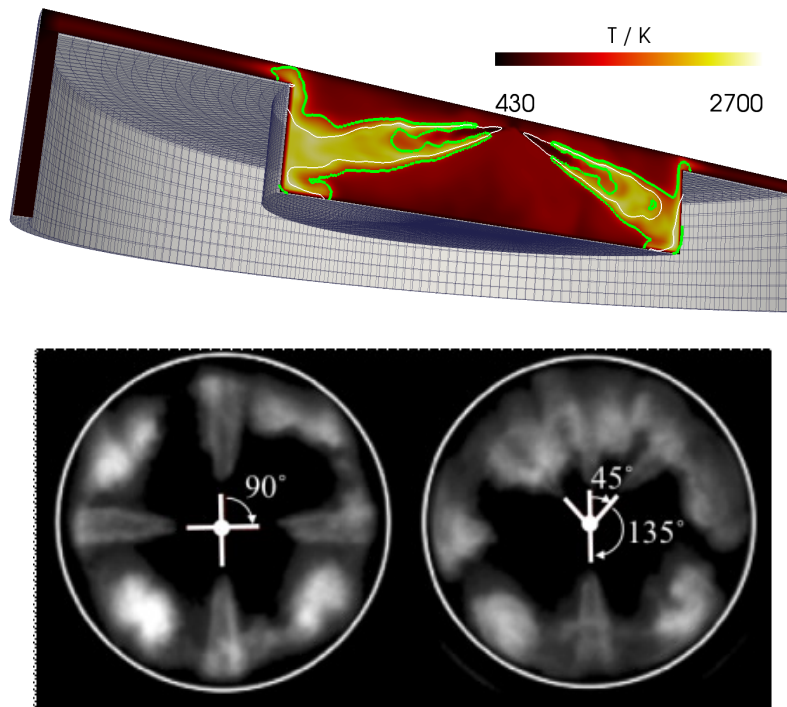
Figure 6.2.4. To the top is the cross-section showing the piston shape and two-reacting jets superimposed by the iso-line of unity equivalence ratio, during the injection process. To the bottom are the employed nozzle-configurations, shown with OH chemiluminescence images during the injection event.

In this work OH chemiluminescence imaging and LES were carried out to analyze the behavior of the lift-off length, in the presence of adjacent jets and swirling flow. The work was conducted in a Scania D12 engine, modified for optical use. The effect of three inter-jet angles, 45°, 90° and 135°, with two different customized common-rail injectors were examined. Shown in Fig. 6.2.4, is the engine geometry used in the

simulations with two-reacting jets superimposed by a unity equivalence ratio iso-line, along with chemiluminescence images of the two different nozzle configurations.

Before the lift-off stabilization and impact of the inter-jet angles were studied in the LES, first the auto-ignition process was examined. Shown in Fig. 6.2.5 is a time sequence of the fuel injection and auto-ignition processes for one of the studied cases. The fuel is initially injected with a 16° angle to firedeck and seen at 2.5 CAD bTDC is the first indication of high-temperature regions, marked with A. Meanwhile, downstream the nozzle there is significant low-temperature reaction activity, seen by the presence of low-temperature reaction species $C_7H_{15}O_2$. As the injection continues, the high-temperature zones at the base of the reacting jet are moving upstream. At the same time, the region of low-temperature reaction is retreating towards the nozzle.
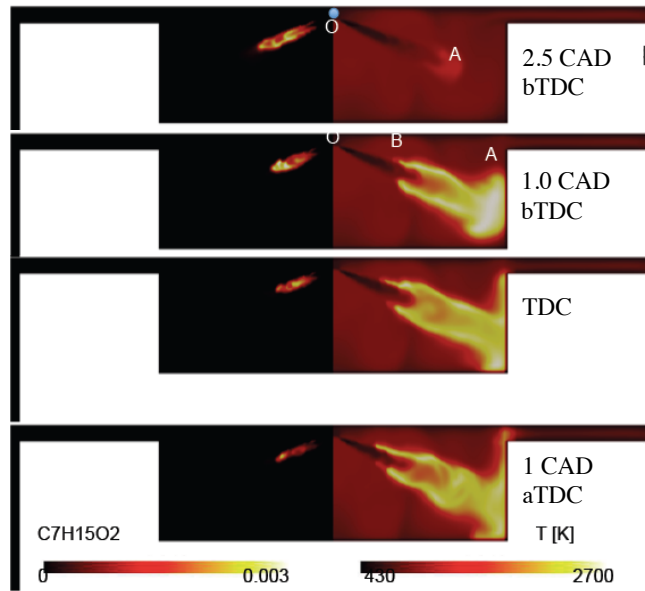
Figure 6.2.5. Cross-section in the z-direction of the engine domain, showing four different times of temperature (right) and the low-temperature reaction species $C_7H_{15}O_2$ (left), during the injection and auto-ignition event.

Figure 6.2.6 shows a scatter plot of OH and $C_7H_{15}O_2$, HO_2 and C_2H_2 during the auto-ignition process. HO_2 typically appear prior to ignition and OH is found in the high

temperature reaction zone. Acetylene, C_2H_2, is a fuel species and is sometimes considered as pre-cursor to soot. At 2.5 CAD bTDC high-temperature combustion has started for one of the jets, seen by OH and the lean manifold arm of HO_2. The presence of low-temperature reactions is seen over a wide range of equivalence ratio, staying below 1000 K. Thereafter HO_2 appears prior to the main-stage heat-release. The species C_2H_2 is initially found in the inner part of the fuel jet, likely close to the location of auto-ignition and is thereafter transported downstream with the high jet flow velocities.

2.5 CAD bTDC
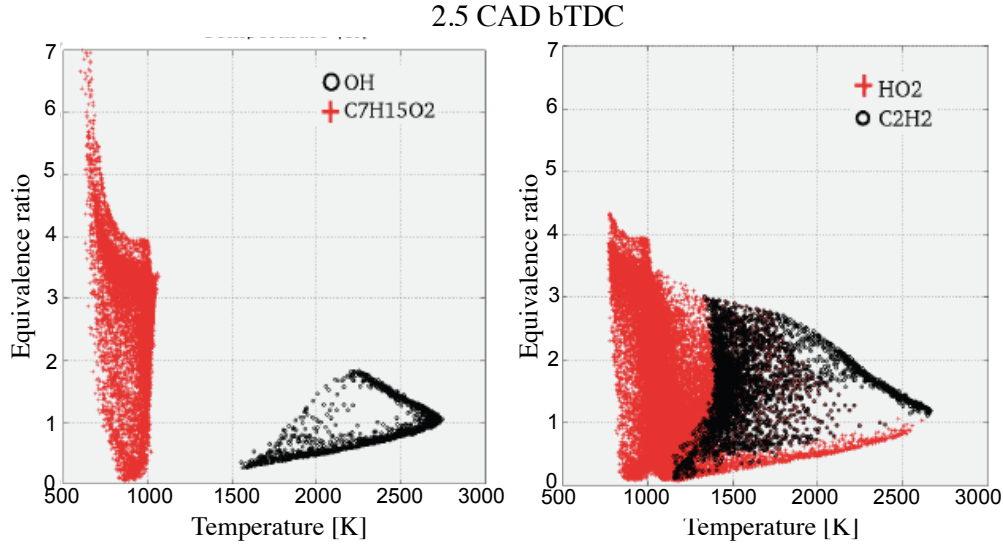
Figure 6.2.6. Scatter plot of the $C_7H_{15}O_2$, HO_2, OH and C_2H_2 during auto-ignition, in the equivalence ratio-temperature space.

From the experiments a decreasing lift-off length was found for a decreasing inter-jet angle, i.e., a shorter lift-off with the 45° inter-jet angle compared with the 135° inter-jet angle. Using the lift-off length scaling law discussed in Chapter 2 (Eq. 2.1),

$$T = 7.04 \cdot 10^8 T_a^{-3.74} \rho_a^{-0.85} d^{0.34} U Z_{st}^{-1} \tag{6.2.1}$$

where H is the lift-off height, T_a is the mean ambient temperature, ρ_a is the ambient density, d is the nozzle diameter, U is the injection velocity and Z_{st} is the stoichiometric mixture fraction, a similar lift-off length for all of the jets is yielded.

80

By employing LES, the temperatures near the lift-off are seen to increase close to the reacting jets, compared with the global engine temperature. For the long injection events employed in this work, the increase of the local temperature is attributed to the swirling flow. The swirling flow is believed to transport the hot-burned products from the neighboring reacting jets in the swirling direction. This influences the lift-off stabilization process and the lift-off position is seen to exhibit a faster retreat towards the nozzle, as the inter-jet distance decreases, cf. Fig. 6.2.7. The figure shows a shorter lift-off length for the 45° inter-jet angle, compared with the other two studied angles. It is reasonable to believe that the low-temperature reactions, shown in Fig. 6.2.5, are rapidly decreasing because of the increasing temperature near the nozzle. The elevated temperature would speed up the chemical rates and the consumption of $C_7H_{15}O_2$ would increase. The 90° inter-jet angle exhibits similar lift-off compared with the lift-off for the 135° inter-jet angle, which may be due to the under-prediction of the lift-off by the LES compared with the experiments.
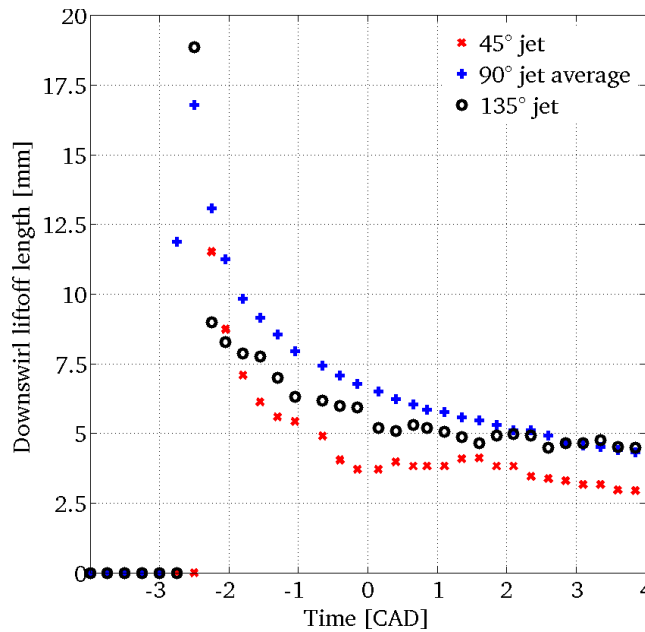
Figure 6.2.7. Lift-off length predicted by LES for the three employed inter-jet angles.

The comparison between the predicted lift-off length from simulations and the experimental lift-off length is seen in Fig 6.2.8, together with the predicted lift-off length from Eq. (6.2.1), for different ambient temperatures. The comparison between the experimental lift-off and the prediction by Eq. (6.2.1) yields that the local temperatures surrounding the reacting jets impact the lift-off length. The LES is seen to predict the trends of the lift-off length, however, underestimates the absolute values compared with experiments. The possible reasons for the under-prediction are discussed in Paper III.
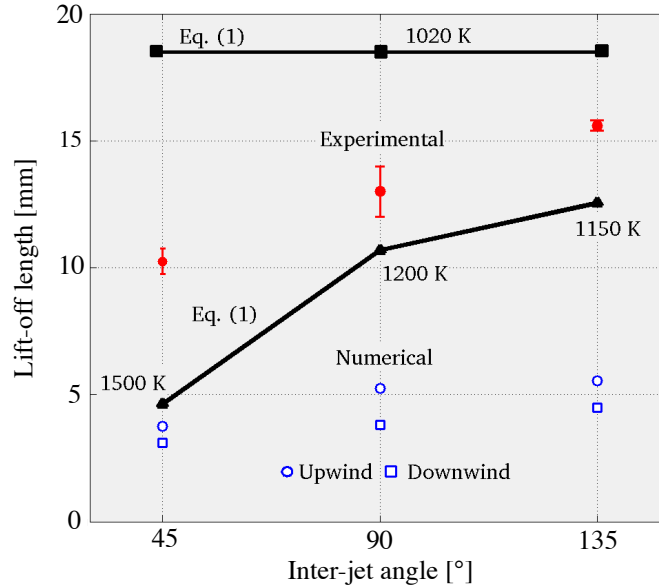
Figure 6.2.8 Lift-off length for the down-swirl side of the reacting jets for the experimental and numerical simulations, together with the predicted lift-off length from the scaling law Eq. (6.2.1).

Furthermore, from the experimental investigations an asymmetrical lift-off length is found for the lifted flames. The lift-off length was longer on the upwind side of the jet, i.e. the side facing the swirling flow, compared with the downwind side. This effect is captured by the LES and is attributed to the swirling flow. The swirl flow transports the burned products in the swirling direction towards the downwind side, but also

transport the burned products from one side of the reacting jet to the other. The observed asymmetrical lift-off height corresponds well with that from the experiments, for all of the inter-jet angles.

Shown in Fig. 6.2.9 is a scatter plot of OH and $C_7H_{15}O_2$, HO_2 and C_2H_2 after the lift-off has stabilized. At this point, a diffusion flame has formed around stoichiometric mixtures, and a fuel rich mixture is burning in the inner region of the fuel jet, cf. Paper IV. High levels of C_2H_2 are formed in the inner region of the fuel jets, explained by lack of oxygen, seen distinctly in Fig. 6.2.9, at around temperature 1500 K and $\Phi=5$. When the lift-off has stabilized near the nozzle, it inhibits further air-entrainment into the fuel jet. The high-temperature species OH is formed in different regions of the reacting jets; around the stoichiometric mixtures close to the diffusion flame and at the outer edges in the fuel rich region in the center of the jet.

2 CAD aTDC
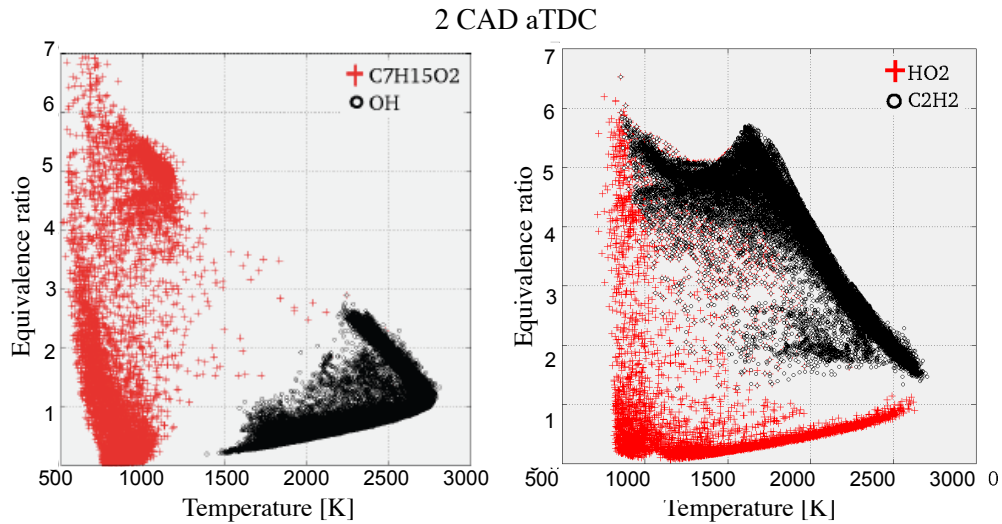
Figure 6.2.9. Scatter plot of the $C_7H_{15}O_2$, HO_2, OH and C_2H_2 when a stabilized lift-off is developed.

In a similar follow-up work the effect of the inter-jet angle on the auto-ignition process for the asymmetrical nozzle configuration, in the presence of swirl, was investigated. The results showed that onset of auto-ignition was found at a far downstream position for all jets, however, the ignition delay was relatively longer for the downswirl jet. By evaluating the average oxygen content and temperature surrounding the fuel jets, it was

found that the low- and intermediate temperature reactions were less active for the downswirl jet. This was explained by a flow effect, where the entrainment of upstream cold gases into the jet delayed the reactions and thus also the ignition delay.

In summary, the various effects of the inter-jet angle and the flow on the lift-off stabilization and auto-ignition processes have been investigated. LES captures and explains the experimentally observed trends, such as the shorter lift-off length for a smaller inter-jet angle. As the lift-off length decreases, the LES predicts a smaller region of low-temperature reactions. This suggests that the higher temperatures from the shortened lift-off length increase the chemical rates and consumption of the low-temperature species. With a shortened lift-off the availability to oxygen decreases, due to the shorter time period to entrain air into the fuel jet. In the LES, high levels of C_2H_2 were predicted, which suggests that more soot may be formed downstream the lift-off location.

6.3 PPC engine simulations

A deep understanding of the fuel and air mixing and the combustion processes is necessary to improve the performance of the PPC engines. It has been observed that small modifications of the injection strategy can alter the entire combustion event significantly. For this reason, LES is employed in this work to investigate the effect of the spray umbrella angle and, mainly, multiple injection strategies on the fuel and air mixing and combustion processes in an optically accessible light-duty PPC engine, modified for optical measurements.

The effect of injection strategies on the mixing and combustion process was studied in the optical light-duty PPC engine, employing a multiple injection strategy with three short injection events of fuel pulses is presented here. The effect of umbrella angle on the mixing is found in Paper VIII. The following results the umbrella angle was fixed. The injection strategy is very similar to the one in Fig. 6.1.3. In addition to this baseline injection, three alternative injection strategies are studied, including a split-fuel two-injection strategy and modified triple-injection strategies, cf. Table 6.3.1. The details about the reaction mechanism and computational models are found in Paper IX. Furthermore, a discussion on the changes in tempeature and fuel mass to account for the uncertainties in the experimental setup is given in Paper IX.

Case	Injection	1	2	3
1	(CAD bTDC/mg fuel per hole)	48 / 0.5	22 / 0.5	5 / 0.56
2	(CAD bTDC/mg fuel per hole)	48 / 0.5	17 / 0.5	5 / 0.56
3	(CAD bTDC/mg fuel per hole)	48 / 0.765	-	5 / 0.815
4	(CAD bTDC/mg fuel per hole)	48 / 0.5	27 / 0.5	5 / 0.56

Table 6.3.1. Simulated cases. Case 1 corresponds to the experimental case, whereas the cases 2-4 are performed to investigate the effect of injection strategies on the PPC engine performance.

The baseline case, case 1, corresponds to the experimental injection strategy and the in-cylinder pressure predicted by the LES is in good agreement with the experiments, as shown in Fig. 6.3.1.
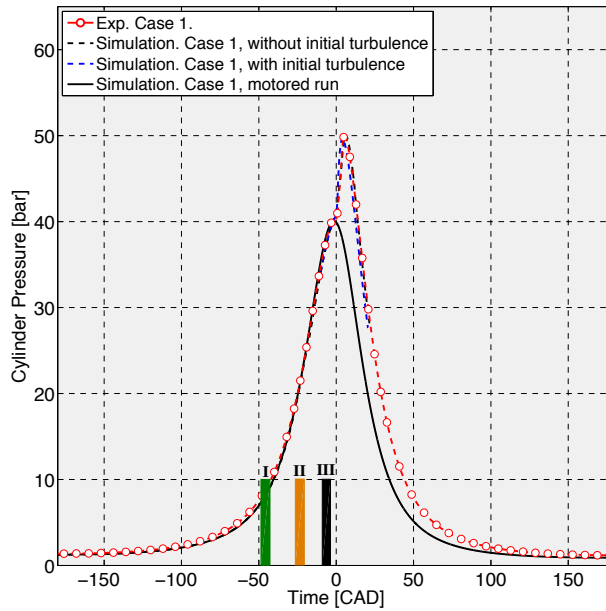
Figure 6.3.1. Experimental pressure trace and LES pressure trace, with the first, second and third injection events, which are indicated as II, II and III, for the baseline case 1.

The intake valves are not considered in this work and the impact of turbulence fluctuations are discussed in Paper IX. The main conclusion was that the effect of the background turbulence, in this case, could be compensated by a slight increase of intake temperature and this approach is considered in the following sensitivity studies.

The details of the mixing and combustion characteristics are explored and are shown in Fig. 6.3.2. In the figure also species for low-temperature combustion, $C_7H_{15}O_2$, also known as RO_2 is shown in column 1. The intermediate temperature species hydro-peroxide HO_2 and hydrogen peroxide H_2O_2 in column 2 and 3 and the high temperature species hydroxyl radicals OH in column 4, are also shown. It is seen that the PPC engine combustion behavior is very different from the typical HCCI engine combustion behavior and combustion is initiated at a 'preferred' location. RO_2 is formed at the downstream region near the wall and is quickly consumed due to the high ambient temperature and high levels of hydrogen peroxide are found in a much wider region than that of RO_2. At 3 CAD aTDC the RO_2 vanishes except in the wall boundary layer, where the low temperature inhibits further chemical reactions. Intermediate temperature regimes are manifested by the presence of HO_2 and H_2O_2 prior to main-heat release. The fuel from the first two injections undergo chemical reactions in the bowl, in such a way that when the last fuel injection is directed into the bowl, the fuel mixes with the hot temperature reservoirs adjacent to the fuel-jet impingement location, which initiates the high-temperature reactions and the main-stage ignition event. If the reservoirs are too cold, it is likely that the cold fuel from the last injection quenches the combustion process. This makes the control of the interactions between the last injection and the two first injections very important for the combustion process.

Furthermore it is observed that when ignition occurs, H_2O_2 and HO_2 are entirely consumed and OH appears. OH is represented in the high-temperature chemistry regime seen at the high temperature spots in column 5. At TDC it is seen that the first OH sites correspond to the regions where both HO_2 and H_2O_2 are consumed. The ignition and the reaction fronts are thereafter propagating towards the fuel impingement region, and also transported in the azimuthal direction, along with the swirl motion.

The combustion event for the entire engine, starting from low-temperature reactions to the high-temperature reactions, is shown in Fig. 6.3.3 in the Φ-T space. At 10 CAD bTDC mainly the low-temperature chemistry is occurring, below approximately 1000

K (solid red dots) with some HO_2 (bright blue to dark blue color) seen between 800 K and 1000 K. As the temperature of the cylinder, at 5 CAD bTDC HO_2 is extended towards the higher temperature regions around equivalence ratio of 0.5.
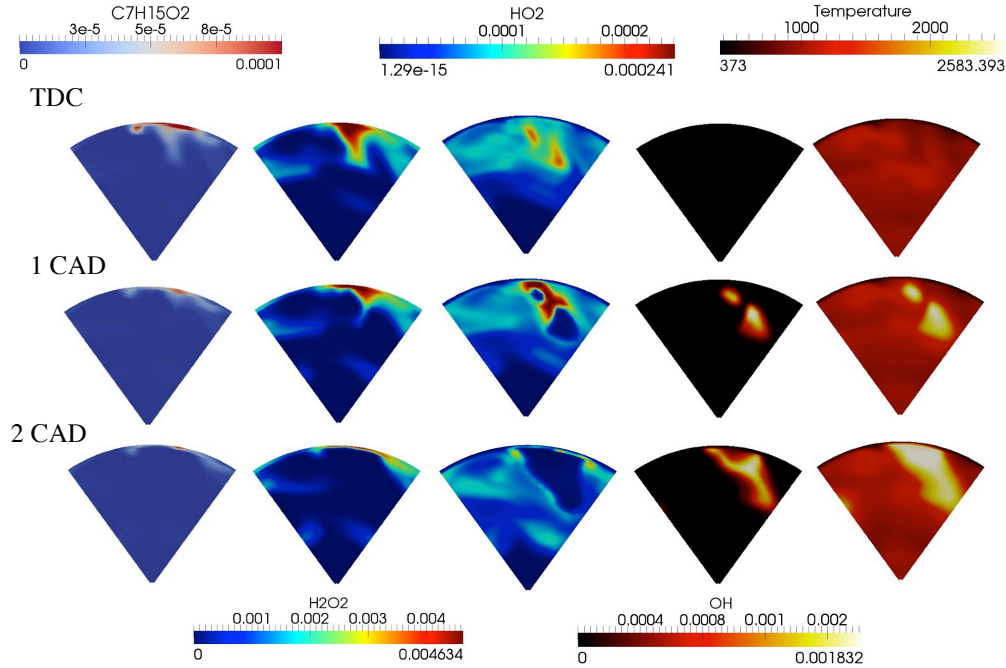

Figure 6.3.2. Instantaneous snapshots of mass fractions of (from the left) RO_2, H_2O_2, HO_2, OH and temperature during an ignition event for the baseline case 1 between TDC to 2 CAD in the horizontal plane 8.6 mm below the cylinder head.

Around TDC at this equivalence ratio, the first indication of high-temperature reactions appears with OH (white to black color) as well as elevated levels of ignition chemistry over a range of equivalence ratio owing to the last injection. Between 5 CAD and 10 CAD, the main-stage heat release occurs under mainly fuel-lean conditions, around equivalence ratio 0.5 and 1.0, but also in the slightly fuel-rich mixtures, with the highest mass fraction of OH at equivalence ratio about 0.8 and temperature 2700 K. The entire main-combustion event under the current conditions is approximately 15

CAD, as also seen in the pressure trace in Fig. 6.3.1.
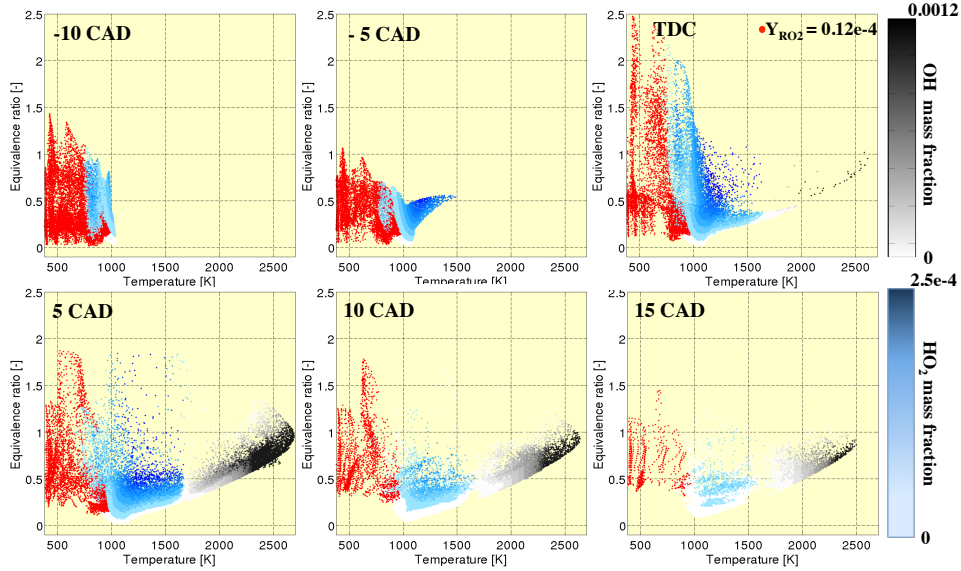
Figure 6.3.3. Three species typical for the low, intermediate and high temperature combustion chemistry regimes plotted in the equivalence ratio and T phase space, from -10 to 15 CAD for the baseline case 1. An active low-temperature chemistry event is indicated by RO_2 until 5 CAD; thereafter ignition is initiated at higher temperatures. The main-stage heat-release is found to start between TDC and 5 CAD and lasts until 10 CAD to 15 CAD.

Overall, the sequential combustion event for the light-duty PPC engine is shown to be controlled by the mixing process, between the ambient air and the fuel from the first two injections, and the low- and intermediate temperature reactions of the partially premixed mixture. The mixture undergoes an ignition event in the recirculation zone at a location with a mixture more prone to reactions, adjacent to the fuel jet-wall impingement region of the final injection. The fuel from the last injection is shown to mix with the hot gas and to initiate the main stage ignition event. More details on the baseline case are presented in Paper IX.

To investigate the sensitivity of the PPC combustion process to the injection strategy three modified injection strategies are considered. The three additional cases, cf. Table 6.3.1, are case 2 with a postponed second injection timing, case 3 with the second injection fuel mass being divided and put into the first and last injection, and case 4

with the second injection at an earlier timing. The predicted pressure traces for the three cases are compared with the predicted pressure trace for the baseline case 1, Figs. 6.3.4. It is seen that the peak pressure of case 2 is lower than that in case 1, unless the intake temperature is increased. In this case, an increase of the initial temperature of 15 K at 25 CAD bTDC gives a pressure-rise-rate closer to that of case 1. For case 3 without any adjustment of the initial temperature the pressure trace shows a poor ignition, nearly a misfire. After increasing the temperature by 15 K, and 30 K, the maximum pressure is still lower than that in case 1. For case 4 with an earlier second injection, a misfire is predicted even after the initial temperature is increased by 30 K.
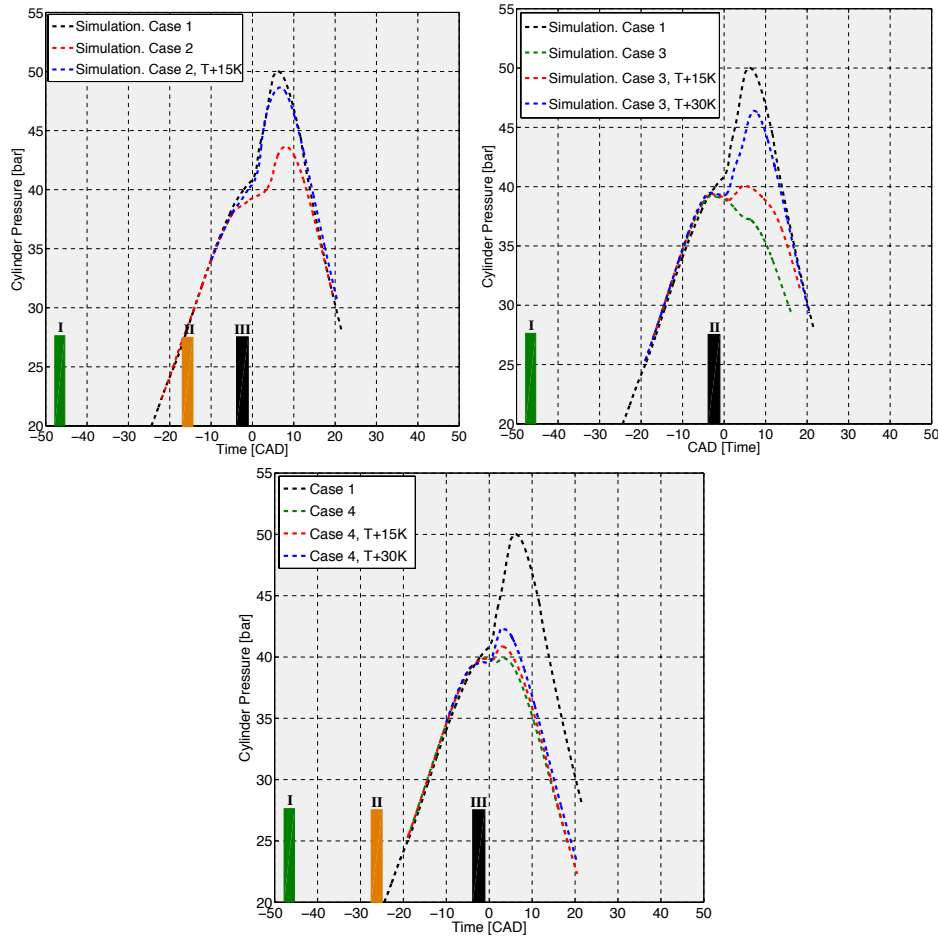
Figure 6.3.4. Predicted pressure traces for cases 1-4 at various adjusted initial temperatures.

As a summary, it appears that the PPC process is very sensitive to the injection strategy. The effect of the fuel injection strategy on the heat-release rate (HRR) is plotted in Fig. 6.3.5, for mixtures at various ranges of equivalence ratio. In Fig. 6.3.6 the corresponding mass of the fuel in the various ranges of equivalence ratio is shown. The heat-release rate is calculated for the fuel mass inside a certain Φ-range, normalized with the total energy that is delivered by the fuel mass. The delivered fuel energy is calculated by multiplying the fuel mass with the fuel heating value. The heating value for the PRF69 fuel is approximately 44.83 MJ/kg and the total injected fuel is 1.56 mg. This yields approximately a total of 70 J energy input. Note that the unit for the y-axis in Fig. 6.3.6 is in 1/s.

It is seen that HRR for the mixtures within $0 < \Phi < 0.2$ is rather low (as compared with the other mixtures, cf. Fig. 6.3.5a and 6.3.5b) and it is seen that almost 50% of the fuel mixtures are within this range for all cases. Between the four cases, case 1 exhibits the lowest percentage of fuel mass in this range. The highest HRR is found for case 3 and 4, which have high amounts of fuel in this region.

Shown in Figs. 6.3.5b and 6.3.6b are the HRR and fuel mass in the interval $0.2 < \Phi < 0.7$. This is the mixture containing the second largest amount of fuel. Around TDC, case 1 has the highest amount of fuel within the given Φ-range. Significant HRR before TDC is only found in case 1 and case 2. Case 3 exhibits an abrupt HRR starting around 2 CAD aTDC, thereafter the heat release reaches similar values as for case 1 and 2. Since the fuel mass of case 3 is the lowest in this range of equivalence ratio, the overall contribution of the mixture in this range to the total heat release rate is low, which explains the difficulty of ignition of case 3 as shown earlier. For case 4 both HRR and the fuel mass are rather low in this range of equivalence, which is the reason of misfire for case 4.
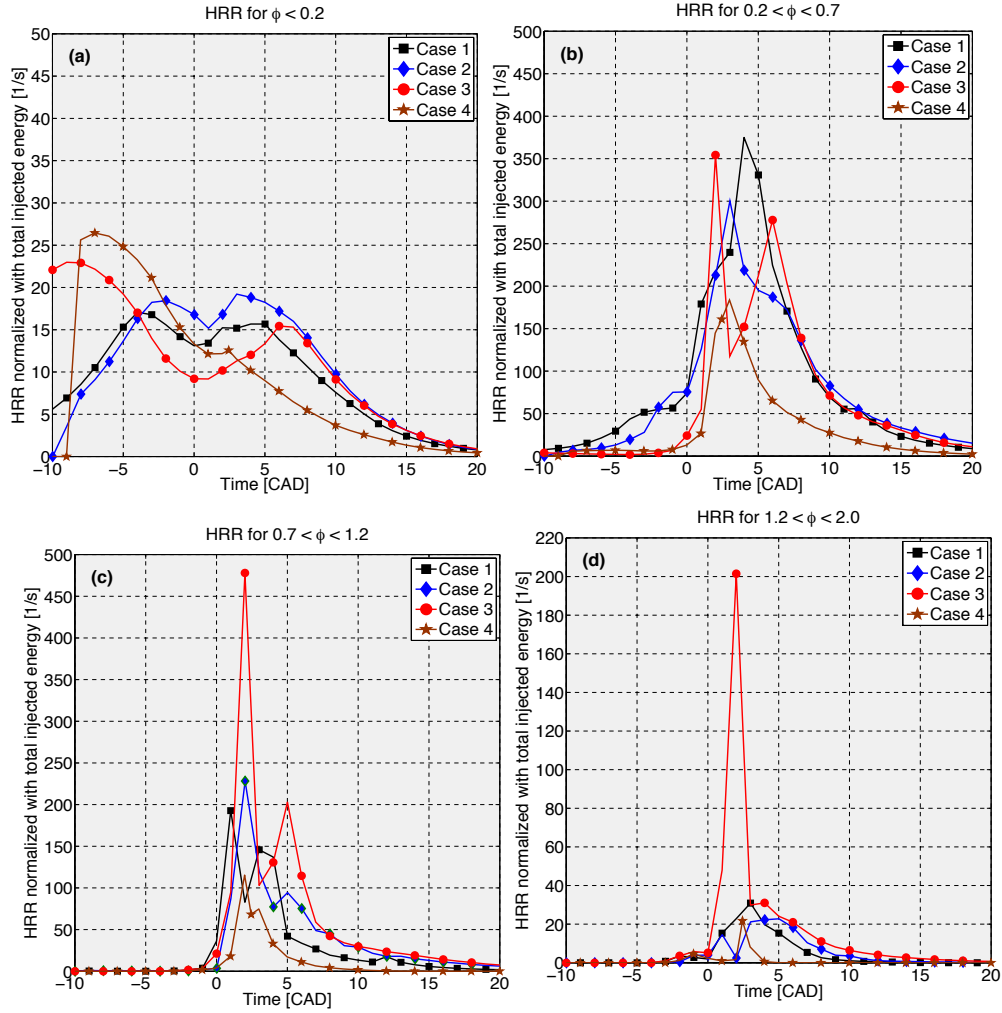
Figure 6.3.5. Normalized heat-release rate from the mixtures at various ranges of equivalence ratio. The HRR is normalized with the total energy input. The adjusted initial temperatures are: case 2: 15K; case 3: 30 K; case 4: 30K.

Figures 6.3.5c and 6.3.6c show the HRR and fuel mass in the range of equivalence ratio $0.7 < \Phi < 1.2$. Compared with the baseline case 1, case 2 with a later second injection results in higher amount of fuel-rich mixture in the later stage (later than TDC), and as such a higher HRR around TDC. Since the fuel mass in this equivalence ratio range is significantly lower than that in the fuel-lean mixtures the overall contribution of the fuel mass in this fuel-richer mixtures to total heat release and pressure-rise rate is low. As expected, case 3 without the second injection yields the highest amount fuel mass in the $0.7 < \Phi < 1.2$ range, which gives rise to the highest HRR among all cases in the equivalence ratio range. Similar to case 2, the fuel mass for case 3 in the equivalence ratio range of $0.7 < \Phi < 1.2$ is so low that its contribution to the total HRR is low. Case 4 with an earlier second injection shows the opposite behavior to case 2, with lower fuel mass and lower HRR in the equivalence ratio range of $0.7 < \Phi < 1.2$.

For the equivalence ranges $\Phi > 1.2$ the behavior is similar to that of $0.7 < \Phi < 1.2$. The above analysis indicates two important factors affecting the fuel/air mixing and HRR,
- the injection timing;
- the injection direction and piston bowl position.

It is clear that if the fuel injection is early, e.g., case 4, there will be longer mixing time and more fuel mass in the fuel-lean mixtures. If the fuel is injected later, e.g., case 2, the fuel injection is directed to the bowl and much faster mixing of fuel and air will occur, resulting also a larger amount of fuel in the fuel-lean mixture.

In summary, in this work the sensitivity of LES results to the initial turbulence and initial temperature was investigated. It was shown that satisfactory agreement with the experimental pressure trace can be achieved for different initial turbulence field by adjusting the initial temperature field. This allows us to further investigate the sensitivity of the PPC engine combustion process to injection strategies. Based on the LES results the following concluding remarks are given:
- Depending on the equivalence ratio the stratified mixtures behave differently. Fuel-lean mixtures ($\Phi < 0.2$) ignite earlier but their overall heat release is low. The main effect of fuel-lean mixtures is to assist the ignition of the fuel-richer mixtures. Mixtures in the equivalence ratio range of $0.2 < \Phi < 0.7$ have the highest heat release rate. In the present PPC engine most of the fuel lies in these mixtures, thus, optimization of the engine performance is largely depending on the mixtures in the equivalence ratio range of $0.2 < \Phi < 0.7$. The

92

mixtures in the equivalence ratio range of $0.7 < \Phi < 1.2$ give also high heat release rate but they also give rise to high CO and NO emissions. Mixtures in the equivalence ratio range of $\Phi > 1.2$ gives rise to the emissions of unburned fuel, CO and soot.

- The performance of PPC engines is very sensitive to the injection strategies. Multiple injection of fuel generates stratified fuel/air mixture. Too early injection would result in a fuel-lean mixture, e.g. in the equivalence ratio range of $\Phi < 0.2$; higher initial temperature is required to ignite such mixture and the pressure-rise rate will be high, similar to that in HCCI engines. Too late injections would result in fuel-rich mixtures similar to diesel engines.

- The performance of PPC engines is also sensitive to the orientation of the injection. The injected fuel stream interacts with the piston bowl. If the fuel is injected directly to the bowl the mixing would be fast and fuel-lean mixtures would be generated. In the present study it is seen that too late second injection would yield a direct injection of the fuel to the bowl.
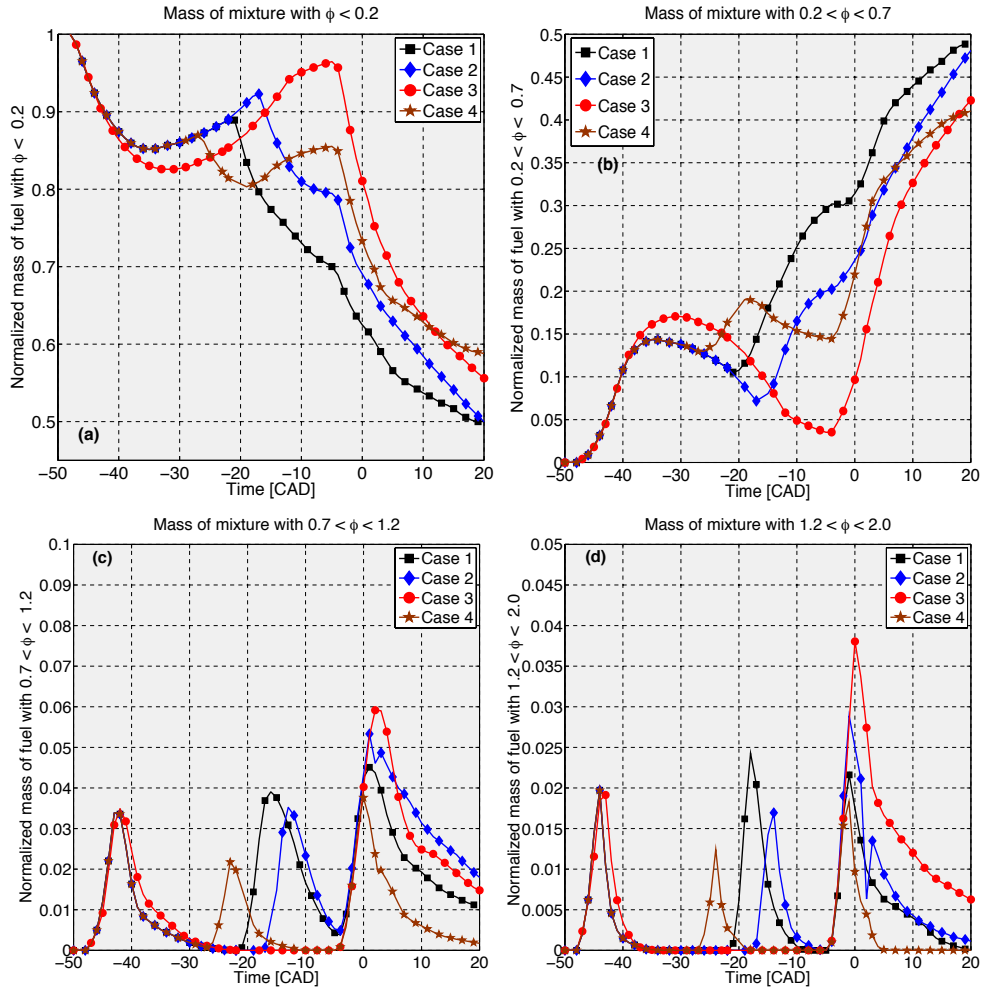
93

Figure 6.3.6. Normalized mass of fuel from the mixtures at various ranges of equivalence ratio. The fuel mass is normalized with the total fuel mass injected to the cylinder, i.e., 1.56 mg. The adjusted initial temperatures are: case 2: 15K; case 3: 30 K; case 4: 30K.

94

6.4 List of publications and author's contribution

The thesis work is carried out by Rickard Solsjö. Prof. Xue-Song Bai is the main supervisor, Dr. Mehdi Jangi and Prof. Bengt Johansson are co-supervisors. The thesis is made up of the following papers published. Division of the work is given below.

Paper I
Rickard Solsjö, Xue-Song Bai
Division of Fluid Mechanics, Lund University, Sweden
SAE Technical Paper 2011-24-0041

This first paper dealt with testing and validating spray-related parameters in the OpenFOAM LES-LPT framework. The tested parameters were the number of injected Lagrangian particles, the droplet size range and cell resolution. The conditions of the spray experimental rig were those later to come under the name spray A, in the international ECN collaboration launched by Sandia. Secondary breakup model was chosen to represent the fuel-spray, based on the argument that primary breakup is very fast with a small liquid core close to the nozzle. The general results from the simulations were a consistently over-predicted liquid-length, but with a good agreement in the vapor phase fuel penetration for all cases. The azimuthal and radial vapor-phase fuel distributions were found to compare well with the experimentally measured distributions, except for the case with fewer injected Lagrangian particles near the nozzle, where the radial fuel distribution was under predicted.

I carried out the simulations and the paper was written together with Xue-Song Bai. The comparison with experimental data was provided from Lyle Pickett at Sandia. The experimental data is now found on the ECN homepage.

Paper II
Mehdi Jangi, Rickard Solsjö, Bengt Johansson , Xue-Song Bai
Division of Fluid Mechanics, Lund University, Sweden
Division of Internal Combustion Engines, Lund University, Sweden
Submitted to International Journal of Heat and Fluid Flow

This paper evaluated the effect of the stochastic particle dispersion and spray-induced turbulence models presented in Chapter 4. LES of spray models and grid sensitivity

was first performed in constant-volume chamber and compard with experimental data, thereafter the modes were used to perform LES in a VOLVO D5 light-duty engine with a triple injection strategy to investigate the model effect on liquid fuel and vapor fuel and air mixing. The results showed a greater sensitivity to the stochastic particle dispersion model compared with an almost negligible effect on the spray-induced turbulence model.

Mehdi Jangi carried out the constant-volume chamber simulations and wrote most of the paper. I carried out the engine-simulations and analyzed the data and wrote the engine-section of the paper. Xue-Song Bai helped to write the paper. The engine-simulations were based on the experimental work by Bengt Johansson and his students.

Paper III
Rickard Solsjö, Mehdi Jangi, Clement Chartier, Öivind Andersson, Xue-Song Bai
Division of Fluid Mechanics, Lund University, Sweden
Division of Internal Combustion Engines, Lund University, Sweden
Proceedings of the Combustion Institute Volume 34, Issue 2, 2013, Pages 3031–3038

OH chemiluminescence imaging and large eddy simulations were carried out to analyze the lift-off length and the flame stabilization mechanisms in a direct injection heavy-duty diesel engine. Two different nozzle configurations were studied with 45°, 90° and 135° inter-jet angle at the same ambient conditions. The local ambient temperature adjacent to the lift-off position increased with decreasing inter-jet angle, indicating an effect from the transport of hot products from neighboring jets on the lift-off and flame stabilization. Both low and high temperature ignition reactions were found to be ongoing in the stoichiometric and rich mixtures upstream of the lift-off position, which together with the complex interaction between the ambient swirl flow and jet-jet interaction leads to a shorter lift-off length than the predictions from a theory developed from a single fuel jet. The present LES captured the difference in lift-off length on the different sides of the jets, with the trends agreeing well with the experimental results.

I carried out the simulations and analyzed the data. The experimental work was performed by Clement Chartier and Ulf Aronsson from the Division of Internal Combustion Engines, under the supervision of Öivind Andersson. I wrote the paper with Xue-Song Bai and Mehdi Jangi, with discussion and input from Öivind Andersson.

96

Paper IV
Rickard Solsjö, Mehdi Jangi, Xue-Song Bai
Division of Fluid Mechanics, Lund University, Sweden
The International Symposium on Diagnostics and Modeling of Combustion in Internal Combustion Engines (COMODIA), 2012, Japan Society of Mechanical Engineering August 4, 2012

This paper was a contemporary paper with paper III with more emphasize on the structure of the auto-ignition process and the differences between the reacting jets.

I carried out the simulations and analyzed the data and I wrote the paper with Xue-Song Bai and Mehdi Jangi. The experimental conditions were those of Paper III, but strictly a simulation paper.

Paper V
Rickard Solsjö, Mehdi Jangi, Xue-Song Bai
Division of Fluid Mechanics, Lund University, Sweden
Eighth Mediterranean Combustion Symposium, Çeşme, Izmir, Turkey, September 8-13, 2013

This paper was focused on the effect of spray inter-jet angle on auto-ignition in a heavy-duty diesel engine. The injection system was the same as in paper III and VI but only employing the case with two inter-jet angles, 45° and 135°. The results showed that due to retarded low-temperature combustion events in the upstream region close to the nozzle, the onset of auto-ignition is found at a downstream position for all jets. The ignition is relatively delayed in the downswirl jet as compared with the other jets. In the equivalence ratio - temperature space the distribution of intermediate species and high-temperature combustion species from the three jets exhibits a complete overlap. This suggested that the retarded ignition event in the downswirl jet was due to the cooling effect from the upstream jets and the swirling motion.

I carried out the simulations and analyzed the data. I wrote the paper with Xue-Song Bai and Mehdi Jangi. The experimental conditions were those of Paper III, but strictly a simulation paper.

Paper VI
Rickard Solsjö, Mehdi Jangi, C. Chartier, Ö. Andersson, Xue-Song Bai
Division of Fluid Mechanics, Lund University, Sweden
Division of Internal Combustion Engines, Lund University, Sweden
SAE Technical Paper 2014-01-1127

The paper presents a large eddy simulation investigation on the effect of fuel injection pressure on mixing, in an optical heavy-duty diesel engine. The investigation is focused on the impinging wall jets at constant-volume and quiescent conditions. The results exhibited augmented air entrainment in wall jets with increasing injection pressure, when compared with a free jet. The increased mixing rates were explained as owing to enhanced turbulence and vortex formation in the jet-tip in the recirculation zone. A recent investigation carried out in an optical heavy-duty diesel engine indicated however a negligible effect of injection pressure on the mixing in the engine environment. The effect of enhanced turbulence and vortex formation of the jet-tip in the recirculation zone is believed weaker than the effect of engine confinement, due to the presence of fuel from adjacent jets limiting the mixing the fuel with the ambient gas. The aims of this paper are to investigate this issue and to look into more details about the nature of the mixing process in diesel engines. Two fuel injection pressures, 2000 bar and 2500 bar for a constant swirl level of 0.5 and inter-jet angles 45° and 135° were employed. The results exhibit the same trend found in the optical experiments. It was shown that increasing the mass flow rate by increasing injection velocity resulted in augmented turbulence levels in the recirculation zone; however, nearly injection pressure independent equivalence ratio was exhibited during quasi-stationary flow conditions.

I carried out the simulations and analyzed the data. The experimental work was performed by Clement Chartier, from the Division of Internal Combustion Engines, and Johan Sjöholm and Elias Kristensson, from the division of Combustion Physics, under the supervision of Öivind Andersson and Mattias Richter. I wrote the paper with Xue-Song Bai and Mehdi Jangi, with discussion and input from Öivind Andersson. Scania provided the injector fuel mass-flow rates.

Paper VII
Rickard Solsjö, Mehdi Jangi, Martin Tuner, Xue-Song Bai
Division of Fluid Mechanics, Lund University, Sweden
Division of Internal Combustion Engines, Lund University, Sweden
SAE Technical Paper 2012-01-0139

This was the first engine-related paper reporting a simulation of a heavy-duty PPC Scania D13 engine operating with ethanol fuel. Three cases were considered with varying swirl level, a multiple and single injection strategy and with different amounts of fuel. In the cases of split injection, liquid fuel impinged the wall due to the low ambient gas density. With sufficient time between the pilot injection and the main injection, the fuel distribution becomes more homogeneous in the presence of swirl compared with that of non-swirling case and the combustion efficiency increased with a higher swirl level, seen from the peak pressure and lower levels of unburned ethanol later during the expansion cycle, compared with the other two cases. It was suggested that swirl may be important for PPC engines working with high-octane number fuel and spray-induced turbulence alone could not oxidize all of the injected fuel.

I carried out the simulations and wrote the paper with and Xue-Song Bai and Mehdi Jangi. Martin Tuner and Helgi Fridriksson helped me to get boundary and initial conditions for the fuel mass-flow rate and wall-temperatures, based on the work of Vittorio Manente.

Paper VIII
Rickard Solsjö, Mehdi Jangi, Bengt Johansson, Xue-Song Bai
Division of Fluid Mechanics, Lund University, Sweden
Division of Internal Combustion Engines, Lund University, Sweden
6th European Combustion Meeting, Lund, Sweden, June 20, 2013

The paper deals with a numerical investigation on the effect of fuel injection on mixing in a light duty partially premixed combustion (PPC) engine. The advanced injection strategy, utilizing a standard nozzle setup of 5 holes, consisted of three direct injections prior to onset of combustion at constant swirl conditions. Two cases, employing different direct injection umbrella angles, 120 and 140 degrees, were compared with each other.. Results from this work indicated that with a small umbrella angle, an overly fuel lean mixture distribution is found in the squish region and an overly fuel rich mixture distribution is found in the bowl region, compared with the results when

utilizing a large umbrella angle, which may explain the experimentally observed emission trends.

I carried out the simulations and analyzed the data. I wrote the paper with Xue-Song Bai and Mehdi Jangi. The experimental conditions were provided from Patrick Borgqvist and Bengt Johansson from the Division of Internal Combustion Engines at Lund University.

Paper IX
Rickard Solsjö, Mehdi Jangi, Bengt Johansson, Xue-Song Bai
Division of Fluid Mechanics, Lund University, Sweden
Division of Internal Combustion Engines, Lund University, Sweden
- Manuscript prepared for submission to Combustion and Flame

This paper presents a numerical investigation of the ignition and combustion process of a primary reference fuel in a PPC light-duty optical engine. Large eddy simulations are employed utilizing a skeletal chemical kinetic mechanism for primary reference fuel capable of capturing the low-temperature ignition and the high temperature combustion. The LES results are compared with experiments in the engine. The results indicate that the first ignition sites are in the bowl region where the temperature is relatively higher and the reaction fronts thereafter propagate in the swirl direction and towards the centerline of the cylinder. The charge from the first two injections initially undergoes low-temperature reactions and thereafter high-temperature reservoirs are formed in the bowl region. The main heat-release is initiated in the engine when the fuel from the third injection reaches the high- temperature reservoirs. By variation of the injection strategy, two trends are identified: (1) by removing the second injection a higher intake temperature is required to enable the ignition of the charge, and (2) by retarding second injection, a longer ignition delay is identified. Both can be explained by the stratification of fuel and air mixture, and the resulting reactivity in various equivalence ratio and temperature ranges. The LES results reveal the details of the charge stratification and the subsequent heat release process. The present results indicate a rather high sensitivity of partially premixed combustion process to the injection strategies.

I carried out the simulations and analyzed the data. I wrote the paper with Xue-Song Bai and Mehdi Jangi. The experimental conditions were provided from Patrick Borgqvist and Bengt Johansson from the Division of Internal Combustion Engines at Lund University.

Chapter 7
Conclusions and Future Work

7.1 Conclusions

Large eddy simulations have been employed to simulate the fuel and air mixing processes and combustion processes in direct injection partially premixed combustion engines and in conventional direct injection diesel combustion engines. The simulations have been performed with the flow-solver libraries in the open source CFD software OpenFOAM. The liquid fuel spray was modeled with a Lagrangian particle tracking (LPT) approach and a finite-rate chemistry approach together with an accelerated chemistry integration algorithm.

The first part of thesis evaluated the feasibility of the LES-LPT modeling approach of the fuel spray injection process. Two models that account for the spray-induced turbulence (SIT) and the stochastic turbulence dispersion (STD) were investigated. The results were compared with the constant-volume spray-A conditions, provided by ECN. The results show that including the STD model is crucial to predict the vapor-phase fuel distribution and vapor-phase fuel penetration as well as the liquid length. In the case of excluding the STD model, the exchange rates between the liquid phase and gas phase were under-predicted, resulting in an erroneous prediction of the spray behavior. The same conclusions were drawn in the studies of a light-duty PPC engine, operating with a multiple injection strategy. Excluding the STD model showed enhanced wall-wetting and different vapor-phase fuel distribution compared with the case that STD was included. This is believed to influence the combustion phasing under reacting case IC engine simulations. The effect of SIT was found nearly negligible for all the studied conditions. The LES-LPT modeling approach was thus used for simulating the turbulent mixing and combustion processes of direct injection diesel engine combustion and partially premixed engine combustion.

Numerical simulations to investigate the effect of jet-jet and jet-wall interactions in the presence of swirling flow were carried out for a conventional heavy-duty DI diesel engine. Overall the inter-jet angle spacing was found to influence the onset of ignition,

lift-off length and the fuel and air mixing process in the recirculation zone close to the cylinder wall. A shorter lift-off length was found with narrower inter-jet angle, due to the entrainment of ambient air containing hot burned products from the adjacent jets. This effect was found to diminish as the inter-jet angle distance was increased. In the same engine configuration, the LES showed that the fuel leaning-out process in the recirculation zones close to the cylinder wall was seems to be more affected by the inter-jet angle configuration than the injection pressure. This may influence the soot oxidation process, as the availability to oxygen diminishes with a narrow inter-jet angle.

The effect of swirl, injection timing and injection strategies were examined in a heavy-duty and a light-duty PPC engine. Employing a triple-injection strategy with PRF70 fuel in a light-duty PPC engine, the first two pilot injections were found to generate a stratified mixture that undergoes low-temperature reactions in the recirculation zones of the impinging jets. The main heat-release is initiated in the engine when the fuel from the third injection reaches the high- temperature reservoirs. By variation of the injection strategy, two trends are identified: by removing the second injection a higher intake temperature is required to enable the ignition of the charge, and a longer ignition delay is seen when the second injection is retarded. Both can be explained by the stratification of fuel and air mixture, and the resulting reactivity in various equivalence ratio and temperature ranges. The LES results reveal the details of the charge stratification and the subsequent heat release process. The present results indicate a rather high sensitivity of partially premixed combustion process to the injection strategies.

7.2 Future work

The modeling of the combustion processes of DI diesel combustion engines and PPC engines can be improved with the following works.

The results from the conventional diesel combustion engine showed that the present model under-predicted the lift-off length, which might be an outcome from the sub-models for the various interplaying processes in the engine, such as the spray vaporization, auto-ignition and flame-stabilization along with the transport from the ambient swirl. To remedy this, a computationally efficient turbulence-chemistry interaction model is needed to improve the predictive power of the numerical

simulations. An improved model to capture the competition between the auto-ignition and flame-front propagation is needed to improve the prediction of the lift-off length.

The onset of ignition in a PPC engine is controlled by ignition chemistry, however, after the ignition, thin reactions front similar to flames can be found. This has been evidenced in the DNS work carried out recently [159]. For this a turbulence and chemistry interaction model is needed both for ignition and flame propagation.

This work has mainly been focused on spray-controlled mixing and combustion and has neglected the impact of more realistic larger-scale background flow structures such as the tumble and swirl motion as well as the turbulence generated from the intake manifold. To include this would give a more complete picture of the combustion-flow interplay in a PPC engine. At the same time, the author believes that assuming a solid-body rotational structure as initial conditions for spray controlled diesel engines is a reasonable approach as the combustion process is mainly driven by spray induced turbulence.

Overall, the entire PPC combustion event was found to be sensitive to the intake temperature and injection strategy. The piston is made of quartz glass and is known to have, e.g., different conductivity compared with metal. The author believes that both researches in the experimental and numerical simulations would benefit from more cylinder wall temperature measurements for case specific studies. To measure the fuel mass-flow profiles for the very short injection pulses that is employed in the light-duty PPC engine is probably difficult but would be useful. To the author's knowledge, the injector current to control the needle lift does not necessarily give the expected mass-flow rate behavior at short current durations. Furthermore, to measure the fuel rate-shape in a test rig at low ambient pressures might be difficult. One solution to this could be numerical modeling of both the internal nozzle flow and the fuel discharge into the surrounding ambient air. Lastly, to perform quantitative optical diagnostics, such as the PLIF measurements, to obtain the fuel and species concentrations (OH, CH_2O, HO_2) in different planes of the optical PPC engines would be useful for the validation of the numerical simulations.

103

Acknowledgements

Bibliography

[1] R. D. Reitz, "Directions in IC engines research," *Combustion and Flame,* vol. 160, pp. 1-8, 2013.

[2] P.C. Miles, L.M. Pickett M.P.B Musclus, "Conceptual models for partially premixed low-temperature diesel combustion," *Prog. Ener. Comb. Science*, pp. 246-283 , 2013.

[3] Swedish Energy Agency. http://www.energimyndigheten.se/en/.

[4] http://www.energimyndigheten.se/Statistik/Slutlig-anvandning/Transport/.

[5] J. C. Tannehill, D. A. Anderson, R. H. Pletcher, *Computational Fluid Mechanics and Heat Transfer*.: Taylor Francis Inc, 1997.

[6] http://www.openfoam.com Open source CFD libraries.

[7] ECN, at SANDIA National Laboratories Engine Combustion Network. http://www.sandia.gov/ecn/.

[8] J.E. Dec, "A conceptual model of D.I. diesel combustion based on laser-sheet imaging," in *SAE Transactions 1997:106(3)*, pp. 1319-48.

[9] J.E. Dec, C. Espey, "Chemiluminescence imaging of auto-ignition in a D.I. diesel engine," in *SAE Transactions 1998:107(3)*, pp. 2230-54.

[10] D.L. Siebers, "Recent Developments on Diesel Fuel Jets under Quiescent Conditions," in *Flow and Combustion in Reciprocating Engines*.: Springer-Verlag Berlin-Heidelberg, 2009.

[11] C. Pauls, G. Grünefeld, S. Vogel, N. Peters, "Combined Simulations and OH-Chemiluminescence Measurements of the Combustion Process using Different Fuels under Diesel-Engine like Conditions," in *SAE Paper 2007-01-0020*, 2007.

[12] C. Gong, M. Jangi, X.S. Bai, "Large eddy simulation of n-Dodecane spray combustion in a high pressure combustion vessel," *Applied Energy*, vol. 135, pp. 373-381, 2014.

[13] L.M. Pickett, S. Kook, H. Persson, Ö. Andersson, "Diesel fuel jet lift-off stabilization of laser-induced plasma ignition," in *Proc. Combust. Inst.*, vol. 2, 2009, pp. 2793-2800.

[14] D.L. Siebers, "Scaling Liquid-Phase Fuel Penetration in Diesel Sprays based on Mixing-Limited Vaporization," in *SAE Paper 1999-01-0528*, 1999.

[15] D.L Siebers, B. Higgins, "Flame Lift-Off on Direct-Injection Diesel Sprays Under Quiescent Conditions," in *SAE Paper 2001-01-0530*.

[16] D.L. Siebers, "Liquid-Phase Fuel Penetration in Diesel Sprays," in *SAE Paper 980809*.

[17] J.D. Naber, D.L. Siebers, "Effect of Gas Density and Vaporization on Penetration and Dispersion of Diesel Sprays," in *SAE Paper 960034*.

[18] L.M. Pickett, D.L. Siebers, C.A. Idicheria, "Relationship between ignition process and

the lift-off length of diesel fuel jets," in *SAE Paper 2005-01-3843*.

[19] B.S. Higgins, C.J. Mueller, D.L. Siebers, "Measurements of Fuel Effects on Liquid-Phase Penetration in DI Sprays," in *SAE Paper 1999-01-0159*, 1999.

[20] S. Kook, L.M. Pickett, M.P.B Musculus, "nfluence of Diesel Injection Parameters on End-of-Injection Liquid Length Recession," in *SAE Paper 2009-01-1356*.

[21] F. Payri, V. Bermúdez, R. Payri, F.J. Salvador, "The influence of cavitation on the internal flow and the spray characteristics in diesel injection nozzles," *Fuel*, vol. 83, pp. 419:431.

[22] M. Jangi, T. Lucchini, G. D'Errico, X.S. Bai, "Effects of EGR on the structure and emissions of diesel combustion," in *Proc. Combust. Inst*, vol. 34, 2013.

[23] T. Lucchini, G. D'Ericco, G. Ferrari, "Numerical investigation of Non-Reacting and Reacting Diesel Sprays in Constant-Volume Vessels," in *SAE Paper 2009-01-1971*, 2009.

[24] U. Aronsson, C. Chartier, Ö. Andersson, R. Egnell, J. Sjöholm, M. Richter, M. Aldén, "Analysis of the Correlation Between Engine-Out Particulates and Local Φ in the Lift-Off Region of a Heavy-Duty Diesel Engine Using Raman Spectroscopy," in *SAE Paper 2009-01-1357*.

[25] U. Aronsson, Ö. Andersson, R. Egnell, P.C. Miles, I.W. Ekoto, "Influence of Spray-Target and Squish Height on Sources of CO and UHC in a HSDI diesel engine during PPCI Low-Temperature Combustion," in *SAE Paper 2009-01-2810*.

[26] U. Aronsson, C. Chartier, Ö. Andersson, B. Johansson, J. Sjöholm, R. Wellander, M. Richter, M. Aldén, P.C. Miles, "Analysis of EGR Effects on the Soot Distribution in a Heavy-Duty Diesel Engine using Time-Resolved Laser Induced Incandescence," in *SAE 2010-01-2104*, 2010.

[27] C. Chartier, U. Aronsson, Ö. Andersson, R. Egnell, R. Collin, H. Seyfried, M. Richter, M. Alden, "Analysis of Smokeless Spray Combustion in a Heavy-Duty Diesel Engine by Combined Simultaneous Optical Diagnostics," in *SAE Paper 2009-01-1353*.

[28] C. Chartier, Ö. Andersson, B. Johansson, M.K Bobba, M.P.B Musculus, "Effects of Post-Injection Strategies on Near-Injector Over-Lean Mixtures and Unburned Hydrocarbon Emissions in a Heavy-Duty Optical Diesel Engine," in *SAE Int. J. Eng. 2011 4:1978-1992*.

[29] M.K. Bobba, C. Chartier, B. Johansson, Ö. Andersson, M.P.B Musculus, "Planar Laser-Diagnostics of Soot and OH with Post-Injections in a Heavy-Duty LTC Diesel Engine", ," in *THIESEL 2010, Conference on Thermo- and Fluid Dynamic Processes in Diesel Engines, Valencia, Spain, September 14-17 2010*. , 2010..

[30] C. Chartier, U. Aronsson, Ö. Andersson, R. Egnell, B. Johansson, "Influence of Jet-Jet Interactions on the Lift-Off Length in an Optical Heavy-Duty DI Diesel Engine," *Fuel*, vol. 112, pp. 311-318.

[31] C. Chartier, J. Sjöholm, E. Kristensson, Y. Gallo, Ö. Andersson, M. Richter, M. Aldén, B. Johansson, "Air Entrainment in Wall-Jets using SLIPI in a Heavy-Duty Diesel

Engine," *SAE Paper 2012-01-1718* .

[32] G. Lequien, E. Berrocal, Y. Gallo, A. Themudo, Ö. Andersson, B. Johansson, "Effect of Jet-Jet Interactions on the Liquid Fuel Jet Penetration in an Optical Heavy-Duty DI Diesel Engine," *SAE Paper 2013-01-1615*.

[33] M.P.B. Musculus, "Multiple Simultaneous Optical Diagnostic Imaging of Early-Injection Low-Temperature, Combustion in a Heavy-Duty Diesel Engine," *SAE Paper 2006-01-0079*.

[34] M.P.B. Musculus, "Effect of the In-Cylinder Environment on Diffusion Flame Lift-Off in a Diesel Engine," *SAE Paper 2003-01-0074*.

[35] L.M. Pickett, J. Lopez, "Jet-Wall Interaction Effects on Diesel Combustion and Soot Formation," *SAE Paper 2005-01-01-09-21* .

[36] G. Bruneaux, "Mixing Process in High Pressure Diesel Jets by Normalized Laser Induced Fluorescence Part II: Wall Impinging Versus Free Jet", ," *SAE Paper 2005-01-2097*.

[37] Z. Li, Ö. Andersson, M. Richter G. Lequien, "Lift-off Length in an Optical Heavy-Duty Diesel Engine," *submitted to SAE World Congress Detroit 2015, 15PFL-0739*.

[38] G. Lequien, Ö. Andersson, P. Tunestal, M. Lewander, "A Correlation Analysis of the Roles of Soot Formation and Oxidation in a Heavy-Duty Diesel Engine," *SAE Paper 2013-01-2535*.

[39] https://www.dieselnet.com/tech/engine_design.php#evol.

[40] www.dieselnet.com.

[41] J.B. Heywood, *Internal Combustion Engine Fundamentals*. New York, US: McGraw-Hill Book Co, 1988.

[42] Y. Wakisaka, A. Azetsu, "Effects of Fuel Injection Rate Shaping on Combustion and Emission Formation in Intermittent Spray," *SAE Paper 2002-01-1159*, 2002.

[43] R. Egnell, "A Theoretical Study of the Potential of NOx Reduction by Fuel Rate Shaping in a DI Diesel Engine," in *SAE Paper 2000-01-2935*.

[44] D.R. Tree, K. I. Svensson, "Soot processes in compression ignition engines," *Prog. Energ. Comb. Science* , vol. 33, pp. 272-309, 2008.

[45] http://energy.gov/eere/vehicles/vehicle-technologies-office-advanced-combustion-engines.

[46] S. Onishi, S.H. Jo, K. Shoda, P.D. Jo, S. Kato, "Active Thermo-Atmosphere Combustion (ATAC) – A new Combustion Process for Internal Combustion Engines," in *SAE 790501*.

[47] J.E. Dec, M. Sjöberg, "A Parametric Study of HCCI Combustion – the Sources of Emissions at Low-loads and the Effects of GDI Fuel Injection," in *SAE 2003-01-0752* , 2003.

[48] S.M. Aceves, D. L. Flowers, F. Espinosa-Loza, R.W. Dibble, M. Christensen, B. Johansson, R.P. Hessel, "Piston-Liner Crevice Geomtry Effect on HCCI Combustion by Multi-Zone Analysis," in *SAE 2002-01-2869*, 2002.

[49] M. Christensen, B. Johansson, P. Amneus, F. Mauss, "Supercharged Homogeneous Charge Compression Ignition," in *SAE 980787*.

[50] M. Christensen, B. Johansson, "Influence of Mixture Quality on Homogeneous Charge Compression Ignition," in *SAE Paper 982454*.

[51] M. Christensen, A. Hultqvist, B. Johansson, "Demonstrating the Multi Fuel Capability of a Homogeneous Charge Compression Ignition Engine with Variable Compression Ratio," in *SAE 1999-01-3679*, 1999.

[52] M. Christensen, B. Johansson, "Supercharged Homogeneous Charge Compression Ignition (HCCI) with Exhaust Gas Recirculation and Pilot Fuel," in *SAE Paper 2000-01-1835*, 2000.

[53] J.O. Olsson, G. Haraldsson, B. Johansson, "A Turbo Charged Dual Fuel HCCI Engine," in *SAE Paper 2001-01-1896* , 2001.

[54] J.O. Olsson, P. Tunestål, B. Johansson, "Closed-loop Control of an HCCI Engine," in *SAE Paper 2001-01-1031*.

[55] D. Law, D. Kemp, J. Allen, G. Kirkpatrick, T. Copland, "Controlled Combustion in an IC-engine with a Fully Variable Valve Train," in *SAE Paper 2001-01-0251*.

[56] N.B. Kaahaaina, A.J. Simon, P.A. Caton, C.F. Edwards, "Use of Dynamic Valving to Achieve Residual-Affected Combustion," in *SAE Paper 2001-01-0549*, 2001.

[57] G. Haraldsson, P. Tunestål, B. Johansson, "HCCI Combustion Phasing in a Multi Cylinder Engine Using Variable Compression Ratio," in *SAE Paper 2002-01-2858*.

[58] J.O. Olsson, P. Tunestål, J. Ulfvik, B. Johansson, "The Effect of Cooled EGR on Emissions and Performance of a Turbocharged HCCI engine," in *SAE Paper 2003-01-0743*.

[59] A. Hultqvist, M. Christensen, B. Johansson, A. Franke, M. Richter, M. Aldén, "A Study of the Homogeneous Charge Compression Ignition Combustion Process by Chemiluminescence Imaging," in *SAE Paper 1999-01-3680*, 3680.

[60] A. Hultqvist, M. Christensen, B. Johansson, M. Richter, J. Nygren, J. Hult, M. Aldén, "The HCCI Combustion Process in a Single Cycle – Speed Fuel Tracer LIF and Chemiluminescence Imaging," in *SAE Paper 2002-01-0424*, 2002.

[61] R. Collin, J. Nygren, M. Richter, M. Aldén, L. Hildingsson, B. Johansson, "Simultaneous OH- and Formaldehyde-LIF Measurements in an HCCI Engine," in *SAE Paper 2003-01-3218*.

[62] H. Nordgren, A. Hultqvist, B. Johansson, "Start of Injection Strategies for HCCI Combustion," in *SAE Paper 2004-01-2990* , 2004.

[63] R. Collin, J. Nygren, M. Richter, M. Aldén, L. Hildingsson, B. Johansson, "The effect of Fuel Volatility on HCCI using Simultaneous Formaldehyde and OH PLIF," in *SAE Paper 2004-01-2948*, 2004.

[64] L. Hildingsson, H. Persson, B. Johansson, R. Collin, J. Nygren, M. Richter, M. Aldén, R. Hasegawa, H. Yanagihara, "Optical Diagnostics of HCCI and Low-Temperature Diesel

using Simultaneous 2-D PLIF of OH and Formaldehyde," in *SAE Paper 2004-01-2949* , 2004.

[65]   J.E. Dec, W. Hwang, M. Sjöberg, "An Investigation of Thermal Stratification in HCCI Engines using Chemiluminescence Imaging," in *SAE Paper 2006-01-1518*.

[66]   R. Yu, X.S. Bai, H. Lehtiniemi, S.S. Ahmed, F. Mauss, M. Richter, M. Aldén, L. Hildingsson, B. Johansson, A. Hultqvist, ", "Effect of Turbulence and Initial Temperature Inhomogeneity on Homogeneous Charge Compression Ignition Combustion," in *SAE Paper 2006-01-3318*, 2006.

[67]   R. Yu, X.S. Bai, L. Hildingsson, A. Hultqvist, B. Johansson, P. Miles, "Numerical and Experimental Investigation of Turbulent Flows in a Diesel Engine," in *SAE Paper 2006-01-3436* , 2006.

[68]   R. Yu, X.S. Bai, A. Vressner, A. Hultqvist, B. Johansson, J. Olofsson, H. Seyfried, J. Sjöholm, M. Richter, M. Aldén, "Effect of Turbulence on HCCI Combustion," in *SAE Paper 2007-01-0183*, 2007.

[69]   L. Koopmans, O. Backlund, I. Denbratt, "Cycle-to-cycle Vartiations: Their Influence on Cycle Resolved Gas Temperature and Unburned Hydrocarbons from a Camless Gasoline Compression Ignition Engine," in *SAE Paper 2002-01-0110*.

[70]   W. Hwang, J.E. Dec, M. Sjöberg, "Fuel Stratification for Low-Load HCCI Combustion: Performance and Fuel-PLIF Measurements," in *SAE Paper 2007-01-4130*, 2007.

[71]   M. Sjöberg, J.E. Dec, "Combined Effects of Fuel-Type and Engine Speed on Intake Temperature Requirements and Completeness of Bulk-Gas Reactions for HCCI Combustion," in *SAE Paper 2003-01-3173* , 2003.

[72]   J.O. Olsson, P. Tunestål, B. Johansson, S. Fiveland, R. Agama, M. Willi D. Assanis, "Compression Ratio Influence on Maximum Load of a Natural Gas Fueled HCCI Engine," in *SAE Paper 2002-01-0111*, 2002.

[73]   J.O. Olsson, O. Erlandsson, B. Johansson, "Experiments and Simulations of a Six-Cylinder Homogeneous Charge Compression Ignition (HCCI) Engine," in *SAE Paper 2000-01-2867*, 2000.

[74]   M. Christensen, B. Johansson, A. Hultqvist, "The Effect of Combustion Chamber Geometry on HCCI Operation," in *SAE Paper 2002-01-0425* , 2002.

[75]   M. Christensen, B. Johansson, "The Effect of In-Cylinder Flow and Turbulence on HCCI Operation," in *SAE Paper 2002-01-2864*, 2002.

[76]   J.E. Dec, M. Sjöberg, "Isolating the Effects of Fuel Chemistry on Combustion Phasing in an HCCI Engine and the Potential of Fuel Stratification for Ignition Control," in *SAE Paper 2004-01-0557*, 2004.

[77]   M. Sjöberg, J.E. Dec, "Potential of Thermal Stratification and Combustion Retard for Reducing Pressure-Rise Rates in HCCI Engines, Based on Multi-Zone Modeling and Experiments," in *SAE Paper 2005-01-0113*.

[78]   R. Yu, T. Joelsson, X.S. Bai, B. Johansson, "Effect of Temperature Stratification on the

110

Auto-Ignition of Lean Ethanol/Air Mixture in HCCI engine," in *SAE Paper 2008-01-1669* , 2008.

[79] J.E. Dec, "Advanced compression-ignition engines – understanding the in-cylinder processes," in *Proc. Combust. Inst.*, vol. 32, 2009, pp. 2727-2742.

[80] M. Sjöberg, J.E. Dec, "Smoothing HCCI Heat-Release Rates using Partial Fuel Stratification with Two-Stage Ignition Fuels," in *SAE Paper 2006-01-0629*.

[81] S. Kimura, O. Aoki, H. Ogawa, S. Muranaka, et al, "New Combustion Concept for Ultra Clean and High-Efficiency Small DI Diesel Engines," in *SAE Paper 1999-01-3681*.

[82] H. Yanihagara, Y. Sato, J. Minuta, "A simultaneous reduction in NOx and soot in diesel engines under a new combustion system (Uniform Bulky Combustion System – UNIBUS)," in *17th International Vienna Motor Symposium*, 1996.

[83] M.P.B Musclus, P.C. Miles, L.M. Pickett, "Conceptual models for partially premixed low-temperature diesel combustion," in *Prog. Ener. Comb. Science Science*, vol. 39, 2013.

[84] C. Noehre, M.Andersson, B. Johansson, A. Hultqvist, "Characterization of Partially Premixed Combustion," in *SAE Paper 2006-01-3412*, 2006.

[85] G. Kalghatgi, P. Riseberg, H. Ångström, "Advantages of Fuels with High Resistance to Auto-Ignition in Late-Injection, Low-temperature, Compression Ignition Engines," in *SAE Paper 2006-01-3385*, 2006.

[86] A. E. Klingbeil, H. Juneja, Y. Ra, R. D. Reitz, "Premixed Diesel Combustion Analysis in a Heavy–Duty Diesel Engine," in *SAE Paper 2003-01-0341* , 2003.

[87] M. Lewander, K. Ekholm, B. Johansson, P. Tunestål, N. Milovanovic, N. Keeler, T. Harcombe, P. Bergstrand, "Investigation of the Combustion Characteristics with Focus on Partially Premixed Combustion in a Heavy Duty Engine," in *SAE Paper 2008-01-1658* , 2008.

[88] G. Kalghatgi, P. Risberg, H. Ångström, "Partially Pre-Mixed Auto-Ignition of Gasoline to Attain Low Smoke and Low NOx at High-load in a Compression Ignition Engine and Comparison with Diesel Fuel," in *SAE Paper 2007-01-0006* , 2007.

[89] V. Manente, B. Johansson, P. Tunestal, W. Cannella, "Effects of Different Type of Gasoline Fuels on Heavy Duty Partially Premixed Combustion," in *SAE. Int. J. Engine 2(2)*, 2010.

[90] V. Manente, C. Zander, B. Johansson, P. Tunestal, et al., "SAE Paper 2010-01-2198 ," in *An Advanced Internal Combustion Engine Concept for Low Emissions and High Efficiency from Idle to Max Load Using Gasoline Partially Premixed Combustion*, 2010.

[91] V. Manente, B. Johansson, P. Tunestal, "Gasoline partially premixed combustion: high efficiency, low NOx and low soot by using an advanced combustion strategy and a compression ignition engine," in *nt. J. Vehicle Design*, vol. 59, 2012.

[92] L. Hildingsson, G. Kalghatgi, N. Tait, B. Johansson, A Harrison, "Fuel Octane Effects in the Partially Premixed Combustion Regime in Compression Ignition Engines," in *SAE*

Paper 2009-01-2648.

[93]   H. Solaka, Impact of Fuel Properties on Partially Premixed Combustion, 2014.

[94]   P. Borgqvist, M. Tuner, A. Mello, P. Tunestål, B. Johansson, "The Usefulness of Negative Valve Overlap for Gasoline Partially Premixed Combustion, PPC," in *SAE Paper 2012-01-1578*, 2012.

[95]   P. Borgqvist, Ö. Andersson, P. Tunestål, B. Johansson, "The Low-load Limit of Gasoline Partially Premixed Combustion using Negative Valve Overlap," in *ICEF 2012-92069* , 2012.

[96]   M. C. Sellnau, J. Sinnamon, K. Hoyer, H. Husted, "Full-Time Gasoline Direct-Injection Compression Ignition (GDCI) for High Efficiency and Low NOx and PM," in *SAE Paper 2012-01-0384*, 2012.

[97]   J. Sinnamon, K. Hoyer, J. Kim, M. Cavotta, H. Husted M.C. Sellnau, "Part-Load Operation of Gasoline Direct-Injection Compression Ignition (GDCI) Engine," in *SAE Paper 2013-01-0272*, 2013.

[98]   S.B. Pope, *Turbulent Flows*.: Cambridge University Press, 2000.

[99]   N. Peters, *Turbulent Combustion*.: Cambridge University Press, 4th Printing, 2006.

[100] H. Carlsson, R. Yu, X.S. Bai, "Direct Numerical Simulation of Lean Premixed CH4/Air and H2/Air Flames at High Karlovitz Numbers," *Int. J. Hydrogen Energy, DOI: 10.1016/j.ijhydene.2014.09.173*, 2013.

[101] H. Carlsson, R. Yu, X.S. Bai, "Flame Structure Analysis for Categorization of Lean Premixed CH4/Air and H2/Air Flames at High Karlovitz Numbers: Direct Numerical Simulation Studies," in *Proc. Combust. Inst., DOI: 10.1016/j.proci.2014.09.002*, 2014.

[102] E. Mastorakos, "Ignition of turbulent non-premixed flames," *Prog. Ener. Combust. Science*, vol. 35, no. 1, pp. 57-97, 2009.

[103] S.P. Burke, T.E.W. Schumann, "Diffusion Flames," *Industrial and Engineering Chemistry*, vol. 20, no. 10, pp. 998-1004, 1928.

[104] S.R.Turns, *An introduction to combustion, concepts and applications*.: Editions McGraw-Hill 2nd Edition, 2000.

[105] C.K. Westbrook, "Chemical Kinetics of Hydrocarbon Ignition in Practical Combustion - Systems," in *Proc. Comb. Inst., 28,* 2000, pp. 1563-1577.

[106] Y. Liu, M. Jia, M.Z. Xie, B. Pang, "Enhancement on a Skeletal Kinetic Model for Primary Reference Fuel Oxidation by Using a Semi-decoupling Methodology," in *Energy Fuels*, vol. 26, 2012, pp. 7069–7086.

[107] U. Maas, R.W. Dibble J. Warnatz, *Combustion – Physical and Chemical Fundamentals, Modeling and Simulation, Experiments, Pollutant Formation*.: Springer-Verlag Berlin Heidelberg 4th Edition, 2006.

[108] F. Battin-Leclerc, "Detailed chemical kinetic models for the low-temperature combustion of hydrocarbons with application to gasoline and diesel fuel surrogates," *Prog. Ener.*

112

Combust. Science, vol. 34, no. 4, pp. 440–498, 2008.

[109] H. Jasak, Z. Tukovic, "Automatic mesh motion for the unstructured finite volume method," in *Transaction of FAMENA*, vol. 30, 2007.

[110] T. Lucchini, G. D'Errico, H. Jasak, X., Z. Zekovic, "Automatic Mesh Motion with Topological Changes for Engine Simulations," in *SAE Paper 2007-01-0170* , 2007.

[111] W.P. Jones and B.E. Launder, "The prediction of laminarization with a two-equation model of turbulence," *Int. J. Heat Mass Transfer*, 1972.

[112] S. Richard, O. Colin, O. Vermorel, A. Benkenida, D. Veynante Angelberg., , "Towards large eddy simulation of combustion in spark ignition engines," in *Proc. Combust. Inst*, vol. 31, 2007, pp. 3059-3066.

[113] O. Vermorel, S. Richard, O. Colin, C. Angelberger, A. Benkenida, D. Veynante, "Towards the understanding of cyclic variability in a spark ignited engine using multi-cycle LES," *Combust. Flame*, vol. 156, no. 8, pp. 1525-1541, 2009.

[114] T. Joelsson, R. Yu, X.S. Bai, "Large eddy simulations of ingition and reaction front propagation in a spark-assisted HCCI engine," *Combust. Science. Tech*, vol. 184, pp. 1051-1065, 2012.

[115] R. Solsjö, M. Jangi, C. Chartier, Ö. Andersson, X.S. Bai, "Lift-off and stabilization of n-heptane combustion in a diesel engine with a multiple-nozzle injection," in *Proc. Combust. Inst.*, vol. 34, 2013, pp. 3031–3038.

[116] D.C. Haworth, K. Jansen, "Large-eddy simulation on unstructured deforming meshes: Towards reciprocating IC engines," *Comp. Fluids*, vol. 29, pp. 493-524, 2000.

[117] C.J Rutland, "Large-eddy simulations for internal combution engines - A review," *Int. J. Eng. Research*, vol. 12, pp. 421-451, 2011.

[118] S. Menon, "Subgrid combustion modeling for large-eddy simulations," *Int. J. Engine Res. 1(2)*, pp. 209-227, 2000.

[119] N. Bharadwaj, C.J. Rutland, S. Chang, "Large eddy simulation modeling of spray-induced turbulence effects," *Int. J. Engine Res. 10(2)*, pp. 97-119, 2000.

[120] A. Fath, C. Fettes, A. Leipertz, "Investigation of diesel spray breakup close to the nozzle at different injection conditions," in *4th Int. Symp. COMODIA 98*, 1998, pp. 429–434.

[121] R. Wirth, A. Fath, A. Leipertz C. Badock, "Investigation of cavitation in real size diesel injection nozzles," in *Int. J. Heat. Fluid Flow* , vol. 20, 1999, pp. 538-544.

[122] V. Vuorinen, M. Larmi, L. Fuchs, "Large eddy simulation on the effect of droplet size distribution on mixing of passive scalar in a spray," in *SAE Paper 2008-01-0933* , 2008.

[123] G.M Faeth, L.-P Hsiang, P.-K Wu, "Structure and breakup properties of sprays," *Int. J. Multiphase Flow*, vol. 21, pp. 99-127, 1995.

[124] R.D. Reitz, F.V. Bracco, "Mechanisms of breakup of round liquid jets," in *The Encyclopedia of Fluid Mechanics*, vol. 3, 1986, pp. 233-249.

[125] F.V. Bracco, R.D. Reitz, "Mechanisms of atomization of a liquid jet," *Phys. Fluids.*, vol.

25, pp. 730-1742, 1982.

[126] R. Solsjö, X-S. Bai, "Injection of Fuel at High Pressure Conditions: LES study," in *SAE Paper 2011-24-0041*.

[127] M. Jangi, X-S. Bai, "On large eddy simulation of evaporating diesel sprays," in *8th Med. Symp. Combust*, Izmir, 2013.

[128] P. O'Rourke, "Statistical properties and numerical implementation of a model for droplet dispersion in a turbulent gas," *J. Computat. Physics*, pp. 345-360.

[129] M. Jangi, R. Solsjö, X.S. Bai, B. Johansson, "On large eddy simulation of diesel spray for internal combustion engines," *submitted to Int. J. Heat and Fluid*, 2014.

[130] G. D'Errico, T. Lucchini, F. Contino, M. Jangi, X.S. Bai, "Comparison of well-mixed and multiple representative interactive flamelet approaches for diesel spray combustion modelling," *Combust. Theor. Model.*, vol. 18, pp. 65-88, 2013.

[131] Y..J. Pei, E.R Hawkes,, S. Kook, "A comprehensive study of the effecs of mixing and chemical kinetic models on prediction of n-heptane jet igntions with the PDF method," *Flow. Turb. Combust*, vol. 90, pp. 249-280, 2013.

[132] S. Bhattacharjee, D.C. Haworth, "Simulations of transient n-heptane and n-dodecane spray flame flames nder engine-relevant conditions using a transported PDF method," *Combust. Flame*, vol. 160, pp. 2083-2012, 2013.

[133] K.J. Nogenmyr, C. Fureby, X.S. Bai, P. Peterson, R. Collin, M. Linne, "Large eddy simulation and laser diagnostic using a transported PDF method," *Combust. Flame*, vol. 156, pp. 25-36, 2009.

[134] I.S. Ertesvåg, B.F. Magnussen, "The eddy dissipation energy cascade model," *Combust. Flame*, vol. 159, pp. 213-235, 2000.

[135] J. Chomiak, A. Karlsson, "Flame liftoff in diesel sprays," *Int. Symposium. Combust*, vol. 26, pp. 83-96, 1996.

[136] V. Sabelnikov, C. Fureby, "LES combustion modeling for high Re flames using a multi-phase analogy," *Combust. Flame*, vol. 160, pp. 83-96, 2013.

[137] O. Colin, A. Benkenida, "The 3-Zones Extended coherent Flame mode (Ecfm3z) for computing Premixed/DIffusion Combustion, Oil & Gas," *Science. Tech - Rev. IFP*, vol. 59, pp. 593-609, 2004.

[138] S-C. Kong, R.D. Reitz, "Application of detailed chemistry and CFD for predicting direct injection HCCI engine combustion and emissions," in *Proc. Combust. Inst*, vol. 29, 2002, pp. 663-669.

[139] D.B. Spalding, "Mixing and chemical reaction in steady confined turbulent flames," in *Thirteenth symposium (International) on Combustion*, vol. 13, 1971, pp. 649–657.

[140] B.H. Hjertager B.F. Magnussen, "On mathematical modeling of turbulent combustion with special emphasis on soot formation and combustion," in *Symposium (International) on Combustion*, vol. 16, 1977, pp. 719–729.

[141] H. Carlsson, E. Nordström, A. Bohlin, P. Peterssonb, Y. Wu, R Collin, M Aldén, P.E. Bengtsson, X.S Bai, "Large eddy simulations and rotational CARS/PIV/PLIF measurements of a lean premixed low swirl stabilized flame," *Combustion and Flame*, vol. 161, no. 10, pp. 2539–2551, 2014.

[142] T.D. Butler, P.J. O'Rourke, "A numerical method for two dimensional unsteady reacting flows," in *Symposium (International) on Combustion*, vol. 16, 1977, pp. 503–1515.

[143] F. Charlettea, C. Meneveau, D. Veynante, "A power-law flame wrinkling model for LES of premixed turbulent combustion Part I: non-dynamic formulation and initial tests," *Combustion and Flame*, vol. 131, pp. 159-180.

[144] H.J. Curran, W.J. Pitz, C. K. Westbrook, C.V. Callahan, F.L. Dryer, "Oxidation of Automotive Primary Reference Fuels at Elevated Pressures," in *Proc. Combust. Inst.*, vol. 27, 1998, pp. 379-387.

[145] M. Sjoberg, J.E. Dec, "An Investigation into Lowest Acceptable Combustion Temperatures for Hydrocarbon Fuel in HCCI Engines," in *Proc. Combust. Inst.*, vol. 30, 2004, pp. 2719-2726.

[146] M. D. Smooke, *Reduced Kinetic Mechanisms and Asymptotic Approximations for Methane-Air Flames*.: Lecture Notes in Physics, Springer-Verlag, 1991, 1991.

[147] F. Contino, T. Lucchini, G.D'Errico, C. Duynslaegher, et al., "Simulations of Advanced Combustion Modes Using Detailed Chemistry Combined with Tabulation and Mechanism Reduction Techniques," *SAE Int. J. Engines 5(2):1*, pp. 85-196.

[148] T. Rente, V.I. Golovitchev, I. Denbratt, "Effect of Injection Parameters on Auto-Ignition and Soot Formation in Diesel Sprays," in *SAE Paper 2001-01-3687* , 2001.

[149] H.J. Curran P. Gaffuri, W.J. Pitz, C.K. Westbrook, "A Comprehensive Modeling Study of n-Heptane Oxidation," *Combustion and Flame*, vol. 114, 1998.

[150] M. Jangi, R. Yu, X.S. Bai, "A multi-zone chemistry mapping approach for direct numerical simulation of auto-ignition and flame propagation in a constant volume enclosure," *Combust. Theor. Model.* , vol. 16, pp. 221-249, 2011.

[151] M. Jangi, R. Yu, X.S. Bai, "Multidimensional chemistry coordinate mapping approach for combustion modeling with finite-rate chemistry," *Combust. Theor. Model.*, vol. 6, pp. 1109-1132.

[152] M. Jangi, R. Yu, X.S. Bai, "Development of Chemistry Coordinate Mapping Approach for Turbulent Partially Premixed Conditions," *Flow. Turb. Combust.*, vol. 90, pp. 285-299 , 2013.

[153] X. Zhao, D. C. Haworth, X.S Bai M. Jangi, "Stabilization and liftoff length of a non-premixed methane/air jet flame discharging into a high-temperature environment: An accelerated transported PDF method, In Press," *Combust. Flame*, 2014.

[154] www.artofillusion.org.

[155] Y. Wu, Large Eddy Simulation of Turbulent Swirling Flows in Combustor Related Geometries, 2013.

[156] R.I. Issa, "Solution of the implicitly discretised fluid flow equations by operator-splitting," *J. Comp. Phys.*, vol. 62, pp. 40-65, 1986.

[157] C. Schulz, V. Sick, "Tracer-LIF diagnostics: quantitative measurement of fuel concentration, temperature and fuel/air ratio in practical combustion systems," *Prog. Ener. Combust. Science*, vol. 31, 2005.

[158] E. Kristensson, Structured Laser Illumination Planar Imaging SLIPI Applications for Spray Diagnostics, 2012.

[159] F. Zhang, R. Yu, X.S. Bai, "Direct numerical simulation of PRF70/air partially premixed combustion under IC engine conditions," in *Proc. Combust. Inst, In Press*, 2014.